

**UNRAVELING THE FUNCTIONS OF SYNAPTOTAGMIN AND MUNC13 IN  
NEUROTRANSMITTER RELEASE**

APPROVED BY SUPERVISORY COMMITTEE

Jose Rizo-Rey, Ph.D., Advisor

---

Michael K. Rosen, Ph.D., Committee Chair

---

Joseph Albanesi, Ph.D.

---

Qiu-Xing Jiang, Ph.D.

---

To my most loved ones!

**UNRAVELING THE FUNCTIONS OF SYNAPTOTAGMIN AND MUNC13 IN  
NEUROTRANSMITTER RELEASE**

by

ALPAY BURAK SEVEN

DISSERTATION

Presented to the Faculty of the Graduate School of Biomedical Sciences

The University of Texas Southwestern Medical Center at Dallas

In Partial Fulfillment of the Requirements

For the Degree of

DOCTOR OF PHILOSOPHY

The University of Texas Southwestern Medical Center

Dallas, Texas

May, 2015

Copyright

by

ALPAY BURAK SEVEN, 2015

All Rights Reserved

**UNRAVELING THE FUNCTIONS OF SYNAPTOTAGMIN AND MUNC13 IN  
NEUROTRANSMITTER RELEASE**

Publication No. \_\_\_\_\_

Alpay Burak Seven, Ph.D.

The University of Texas Southwestern Medical Center at Dallas, 2014

Supervising Professor: Jose Rizo-Rey, Ph.D.

Neurotransmitter release is a central event in interneuronal communication. The release machinery includes three SNAREs (soluble N-ethylmaleimide sensitive factor adaptor protein receptor) and Munc18-1 as core components. Munc13, synaptotagmin and complexin underlie the exquisitely tight regulation of synaptic exocytosis. The SNAREs form the SNARE complex that brings synaptic vesicles and plasma membrane together. This complex is disassembled by NSF/ $\alpha$ -SNAP (soluble N-ethylmaleimide sensitive fusion protein/NSF attachment protein). Munc18 binds to syntaxin, which keeps syntaxin in its closed confirmation and prevents to form the SNARE complex. Interactions between Munc13, Munc18, and syntaxin perform a vital role in regulation of the SNARE complex formation.

Tight regulation of the release machinery requires other factors such as  $\text{Ca}^{2+}$  sensor Synaptotagmin-1 and negatively charged lipids. Synaptotagmin interacts with the SNARE complex and the negatively charged lipids, and initiates the synchronous fast release by sensing the  $\text{Ca}^{2+}$  influx.

It is crucial to investigate functions of individual proteins to understand the mechanism of membrane fusion and neurotransmitter release. Therefore, we investigated the mechanism of membrane bridging by synaptotagmin. Our cryo-electron microscopy (cryo-EM) images showed that a majority of synaptotagmin fragment containing both  $\text{C}_2\text{A}$  and  $\text{C}_2\text{B}$  domains ( $\text{C}_2\text{AB}$ ) molecules bridge membranes directly. Fluorescence spectroscopy demonstrates that the bottom of the  $\text{C}_2\text{B}$  domain contacts the membrane in a substantial population of membrane-bound synaptotagmin fragments. NMR analysis of  $\text{C}_2\text{AB}$ -nanodiscs shows that a fraction of  $\text{C}_2\text{AB}$  molecules binds to membranes with antiparallel orientations of the  $\text{C}_2$  domains. Together with previous studies, these results show that direct bridging constitutes the prevalent mechanism of membrane bridging by synaptotagmin, suggesting that this mechanism underlies the function of synaptotagmin-1 in neurotransmitter release.

We have also discovered that Munc13-1 can bridge membranes in a  $\text{Ca}^{2+}$ -independent manner, which shed light to the docking activity of Munc13-1. We also showed that Munc13-1 can cause efficient lipid mixing and slow content mixing together with Munc18-1 in the absence of synaptotagmin-1. Addition of synaptotagmin facilitates the fusion pore formation in content mixing assays. Recently, we were able to reconstitute key components of the release machinery. We are further investigating our observations with cryo-electron microscopy to understand the mechanism of membrane fusion.

## **Acknowledgements**

I would like to thank Jose Rizo-Rey for being a wonderful mentor for six wonderful years. He embraces many hard to find and admirable traits, which profoundly influenced my personality and enthusiasm about science. There are many other great people who contributed to who I am today, such as seminar speakers who often left me mesmerized and amused about their scientific envisions. I thank all of you for your teachings that made me passionate about science.

I would especially like to thank Xiaoxia Li. She is a very talented scientist and an important part of this work; this project would not have been possible without her. I am also grateful to Yi Xu for another important part of this thesis. I also wish to thank Cong Ma and Shae Padrick for long and fruitful discussions; Kyle Brewer, Victoria Esser, Lijing Su and other lab members for their support; my dear friends for making me happy in graduate school; Liang Shi and Hui Zheng for constantly helping me with electron microscopy.

Additionally, I would like to acknowledge my thesis committee members Michael K. Rosen, Joseph Albanesi, and Qiu-Xing Jiang. I greatly appreciate all of your insightful guidance throughout my graduate career as I transitioned to the scientist I am today.

Last but not least, I would like to thank my family. My wife, Nigar Isiklar Seven enriched my life with her love and wisdom, while constantly supporting me in every step along this incredible journey. Together my wife, my precious son Mazhar Y. Seven, my mother Havva Seven, my father Nevzat Seven, and my sister Arife Seven are the most wonderful family that a person can be blessed to enjoy life with each and every day. I would like to thank all of you for everything, which I will always be eternally grateful for.

## TABLE OF CONTENTS

1	GENERAL INTRODUCTION.....	1
1.1	Membrane Fusion.....	1
1.2	SNARE Proteins.....	4
1.2.1	SNAREs, NSF and $\alpha$ -SNAP .....	10
1.2.2	Energy of Fusion and SNAREs .....	11
1.3	SM Proteins .....	15
1.4	Munc13s.....	17
1.5	Synaptotagmins .....	23
1.5.1	Architecture.....	24
1.5.2	Functional Studies.....	31
1.5.3	Ca <sup>2+</sup> Independent Synaptotagmin Functions .....	32
1.6	Complexins.....	32
2	MEMBRANE BRIDGING AND HEMIFUSION BY DENATURATED MUNC18-1	37
2.1	Introduction .....	37
2.2	Results .....	41
2.2.1	sMunc18-1 can cluster liposomes.....	41
2.2.2	Denaturation of sMunc18-1 induces clustering of liposomes.....	54
2.2.3	Visualization of clustering and hemifusion of liposomes induced by sMunc18-1 Using Cryo-EM.....	57
2.3	Discussion .....	62
2.4	Materials and Methods.....	67

2.4.1	Recombinant Proteins and Protein Purification .....	67
2.4.2	Preparation of Liposomes and Reconstitution of the SNAREs .....	68
2.4.3	Lipid Mixing Assays.....	69
2.4.4	Dynamic Light Scattering.....	69
2.4.5	NMR Spectroscopy.....	70
2.4.6	Circular Dichroism.....	70
2.4.7	Cryo-Electron Microscopy.....	71
3	PREVALENT MECHANISM OF MEMBRANE BRIDGING BY SYNAPTOTAGMIN-1 .....	72
3.1	Introduction .....	72
3.2	Results .....	77
3.2.1	Do synaptotagmin-1 fragments behave differently?.....	77
3.2.2	Direct membrane bridging by $\ln C_2AB$ is the prevalent model for liposome clustering.....	88
3.2.3	The bottom of the $C_2B$ domain contacts the phospholipid membranes.....	97
3.2.4	Substantial populations of antiparallel orientations of the two $C_2$ domains on nanodiscs.....	101
3.3	Discussion .....	110
3.4	Materials and Methods.....	119
3.4.1	Recombinant Proteins .....	119
3.4.2	Preparation of Phospholipid Vesicles .....	122
3.4.3	Fluorescence Experiments .....	123

3.4.4	Turbidity .....	123
3.4.5	Cryo-EM .....	123
3.4.6	Nanodisc Preparation .....	124
3.4.7	Spin Labeling of Synaptotagmin-1 .....	125
3.4.8	NMR Spectroscopy .....	126
4	MUNC13-1 DOCKS THE VESICLES AND SYNAPTOTAGMIN-1 OPENS THE FUSION PORE .....	127
4.1	Introduction .....	127
4.2	Results .....	128
4.2.1	Munc13-1 clusters liposomes and facilitates lipid mixing between liposomes. 128	
4.2.2	Ca <sup>2+</sup> -dependent lipid mixing enhancement by C <sub>1</sub> C <sub>2</sub> BMUN and Munc18-1 ..	138
4.2.3	Synaptotagmin-1 helps with the fusion pore opening.....	144
4.3	Discussion .....	150
4.4	Materials and Methods .....	156
4.4.1	Recombinant Proteins and Protein Purification .....	156
4.4.2	Preparation of Phospholipid Vesicles .....	161
4.4.3	Reconstitution of SNAREs .....	162
4.4.4	Lipid mixing assays .....	164
4.4.5	Content Mixing Assays.....	164
4.4.6	Co-Floatation Assays .....	165
4.4.7	Dynamic Light Scattering .....	165

5	References:.....	167
---	------------------	-----

## PRIOR PUBLICATIONS

- **Seven AB**, Brewer KD, Shi L, Jiang QX, Rizo J.

Prevalent mechanism of membrane bridging by synaptotagmin-1.

*Proc Natl Acad Sci U S A.* 2013 Aug 20;110(34):E3243-52.

- Ma C, Su L, **Seven AB**, Xu Y, Rizo J.

Reconstitution of the Vital Functions of Munc18 and Munc13 in Neurotransmitter Release.

*Science.* 2013 Jan 25;339(6118):421-5.

- Xu Y\*, **Seven AB\***, Su L, Jiang QX, Rizo J.

Membrane bridging and hemifusion by denaturated Munc18.

*PLoS One.* 2011;6(7):e22012.

\*: These authors contributed equally to this work.

- Pan YR, Lou YC, **Seven AB**, Rizo J, Chen C.

NMR structure and calcium-binding properties of the tellurite resistance protein TerD from *Klebsiella pneumoniae*.

*J Mol Biol.* 2011 Feb 4;405(5):1188-201.

## LIST OF FIGURES

Figure 1.1: The stalk model of fusion of two lipid bilayers.....	3
Figure 1.2: Architecture of the SNAREs, Munc18-1, and their complexes. ....	5
Figure 1.3: Models of SNARE function. ....	7
Figure 1.4: Model of synaptic vesicle fusion machinery.....	12
Figure 1.5: Model of the neuronal SNARE complex inserted in a bilayer.....	14
Figure 1.6: Structure and function of Munc13s.....	20
Figure 1.7: Syntaptotagmin-1 and its coupling to SNAREs and membranes.....	26
Figure 1.8: Comparison of the architecture of mouse synaptotagmins. ....	28
Figure 1.9: Sequence Alignment for synaptotagmins encoded in the mouse genome. ....	29
Figure 1.10: Complexins and their interplay with the SNARE complex and synaptotagmin-1...	35
Figure 2.1: sMunc18-1 can induce SNARE-independent increases in the apparent NBD fluorescence intensity in lipid mixing assays.....	43
Figure 2.2: Liposome clustering activity of sMunc18-1.....	49
Figure 2.3: Liposome clustering induced by sMunc18-1 is reversed by trypsinolysis.....	50
Figure 2.4: Time-dependent binding of sMunc18-1 to lipids.....	53
Figure 2.5: sMunc18-1 is less stable than rMunc18-1.....	56

Figure 2.6: Glycerol hinders the liposome clustering activity of sMunc18-1. ....	58
Figure 2.7: Cryo-EM analysis of liposome clusters induced by sMunc18-1.....	59
Figure 2.8: Proposed model of how a denatured protein can induce membrane hemifusion without proceeding through a stalk intermediate.....	61
Figure 3.1: Two models of membrane bridging by synaptotagmin-1. ....	74
Figure 3.2: <sup>1</sup> H NMR spectrum of C2AB.....	80
Figure 3.3: Ca <sup>2+</sup> -bound lnC2AB yields high-quality NMR data.....	81
Figure 3.4: Impurities promote aggregation of lnC2AB in solution.....	85
Figure 3.5: Peaks 1 and 2 in the gel filtration profile of Fig. 3A correspond to table species.....	86
Figure 3.6: Cryo-EM analysis of liposome clustering by lnC2AB.....	92
Figure 3.7: Slight underestimation of intermembrane distance due to cryoEM projection.....	94
Figure 3.8: Increased fluorescence of NBD probes placed at the bottom of the C2B domain upon membrane binding. ....	99
Figure 3.9: NMR analysis of C2AB on nanodiscs.....	104
Figure 3.10: Analysis of PBEs within C2AB bound to nanodiscs. ....	108
Figure 3.11: Mechanistic implications of the direct bridging and oligomerization models. ....	117
Figure 4.1: Munc13-1 enhances lipid mixing.....	131
Figure 4.2: Munc13-1 clusters of liposomes.....	135

Figure 4.3: Munc13-1 lipid mixing enhancement depends on the SNARE complex formation	137
Figure 4.4: Munc13 lipid mixing enhancement depends on DAG and PIP2.....	142
Figure 4.5: Synaptotagmin-1 helps opening the fusion pore .....	146
Figure 4.6: Leakiness of the synaptobrevin liposomes with C1C2BMUN .....	149
Figure 4.7: Lipid mixing with freshly purified NSF and $\alpha$ -SNAP .....	155

## LIST OF TABLES

Table 1.1: Affinities of Munc13-1 interactions .....	22
Table 1.2: Isoforms and Localization of Synaptotagmins .....	31
Table 2.1: Liposome clustering activity of sMunc18-1 under different conditions measured by DLS .....	48

## LIST OF DEFINITIONS

VAMP	vesicle associated membrane protein
$\mu\text{M}$	micromolar
1D	one dimensional
ApoA1	apolipoprotein A1
ATP	adenosine triphosphate
<i>C. elegans</i>	caenorhabditis elegans
$\text{CaCl}_2$	calcium chloride
CD	circular dichroism
Ch	cholesterol
Cryo-EM	cryo-electron microscopy
$\text{D}_2\text{O}$	deuterium oxide
DiD	1,1'-Dioctadecyl-3,3,3',3'-Tetramethylindodicarbocyanine Perchlorate
DLS	dynamic light scattering
DNA	deoxyribonucleic acid
DOPS	1,2-dioleoyl-sn-glycero-3-phospho-L-serine
DTT	dithiothreitol
EGTA	ethylene glycol tetraacetic acid
EPR	electron paramagnetic resonance
<i>g</i>	gravitational force
GST	glutathione S-transferase

H <sub>2</sub> O	hydrogen oxide
HCl	hydrogen chloride
HEPES	4-(2-hydroxyethyl)-1-piperazineethanesulfonic acid
HMQC	heteronuclear multiple quantum coherence
HSQC	heteronuclear single quantum coherence
IANBD amide	N,N'-dimethyl-N-(iodoacetyl)-N'-(7-nitrobenz-2-oxa-1,3-diazol-4-yl)ethylenediamine
ILV	isoleucine, leucine and valine
IPTG	isopropyl β-D-1-thiogalactopyranoside
k <sub>B</sub> T	boltzmann constant, k, and the temperature, T.
KCl	potassium chloride
kDa	kilodalton
LB	Lennox L Broth
lnC <sub>2</sub> AB	longer fragment of C <sub>2</sub> AB
mA	milliamper
mg	milligram
MgCl <sub>2</sub>	magnesium chloride
ml	milliliter
mM	millimolar
MTSL	(1-oxyl-2,2,5,5-tetramethyl-3-pyrroline-3-methyl) methanethiosulfonate
NaCl	sodium chloride

NaOAc	sodium acetate
NBD	7-nitrobenz-2-oxa-1,3-diazole
NBD-PE	N-NBD-1,2-dipalmitoyl-sn-glycero-3-phosphatidylethanolamine
nm	nanometer
NMR	nuclear magnetic resonance
NSF	N-ethylmaleimide sensitive fusion protein
OD	optical density
PBE	paramagnetic broadening effect
PBS	phosphate buffered saline
PI	phosphatidylinositol
PIP <sub>2</sub>	phosphatidylinositol-4,5-bisphosphate
PIPs	phosphatidylinositolphosphates
POPC	1-palmitoyl-2-oleoyl-sn-glycero-3-phosphatidylcholine
POPE	palmitoyl-2-oleoyl-sn-glycero-3-phosphoethanolamine
PS	phosphotidylserine
Rho-PE	N-(lissamine rhodamine B sulfonyl)-1,2-dipalmitoyl-sn-glycero-3-phosphatidylethanolamine
rMunc18-1	rat Munc18-1
SM proteins	Sec1/Munc18-like proteins
SMR	the strongest methyl resonance
sMunc18-1	squid Munc18-1
SNAP-25	synaptosomal-associated protein-25

SNARE	soluble N-ethylmaleimide sensitive factor adaptor protein receptor
TB	terrific broth
TCEP	tris(2-carboxyethyl)phosphine
Tris	2-amino-2-hydroxymethyl-propane-1,3-diol
TROSY	transverse relaxation-optimized spectroscopy
t-SNAREs	target membrane associated SNAREs
v-SNAREs	vesicle associated SNAREs
$\alpha$ -SNAP	alpha-soluble NSF attachment protein
$\beta$ -OG	octyl-beta-glucoside
$\mu$ M	micromolar

## CHAPTER 1

# 1 GENERAL INTRODUCTION

### *1.1 Membrane Fusion*

Many vital processes in life require a fundamental membrane fusion step. Some examples of the very diverse processes where fusion of two membranes plays a vital role are the fertilization of an egg by a sperm, neuronal communication, protein or hormone secretion to the extracellular space, virus entry to host cell, protein trafficking, autophagy, and development [1-10]. These diverse reactions take place on various different time scales, involve different sizes of membranes, and are controlled by different protein and lipid molecules [11]. Despite the diversity in the membrane fusion processes, some of the basic underlying mechanistic properties are widely conserved. Contact of two membranes, merging of the membranes, and formation of a fusion pore are the fundamental steps that are shared by various membrane fusion processes.

Protein free membranes that contain physiological lipid compositions are very stable and do not fuse with each other even at long time scales [11]. However, small molecules such as polyethylene glycol and certain lipids such as the cone shaped phosphatidylethanolamine can promote fusion of membranes [12]. Early characterization of the protein free membrane fusion events revealed two fundamental fusion intermediates, hemifusion and fusion pore formation (Figure 1.1) [13, 14]. Merging of only the outer leaflets of two bilayers leads to a

hemifusion structure and inner leaflets continue to stay intact. This state represents the lipid mixing between two merging membranes without any content mixing. This state can be followed by merging of inner leaflets and the formation of a fusion pore that leads to complete fusion of two apposing membranes [14, 15].

Membrane fusion in the cell is carried out with the help of various proteins in a multi-step process. The first step is bringing two membranes close to each other within a few nanometers. Second, membranes are brought into a very close contact state where the apposing membranes are partially dehydrated and electrostatic repulsion of counter membranes is overcome. The third step is the destabilization and re-localization of the lipid molecules in the contact points of apposing membranes to merge the outer leaflets of the bilayers. This step leads to non-bilayer intermediates such as the hemifusion diaphragm. The lipid components of the two separate bilayers can mix at this step. Further rearrangement of the lipid molecules in the non-bilayer interfaces merges inner leaflets and results in fusion pore formation. Efficient content mixing can occur only after fusion pore formation and growth of the fusion pore. All transitions and rearrangements (membrane clustering, dehydration and destabilization of membranes, etc.) during membrane fusion require energy, which is provided by proteins and facilitated by various lipid molecules. Different models have been postulated about the mechanism of membrane fusion, sharing most of the intermediate states explained above and varying generally in the intermediate steps. According to the commonly accepted stalk model of membrane fusion, a non-bilayer intermediate state involves highly curved membrane contact where the outer leaflet is fused and inner leaflet is not fused (Figure 1.1) [11, 16-18].

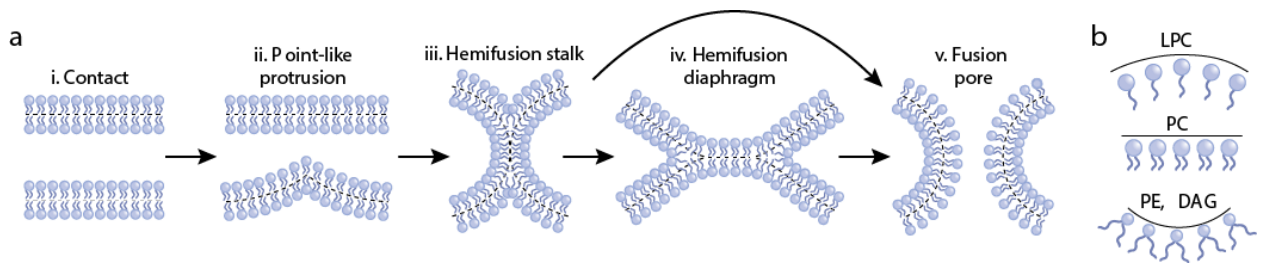


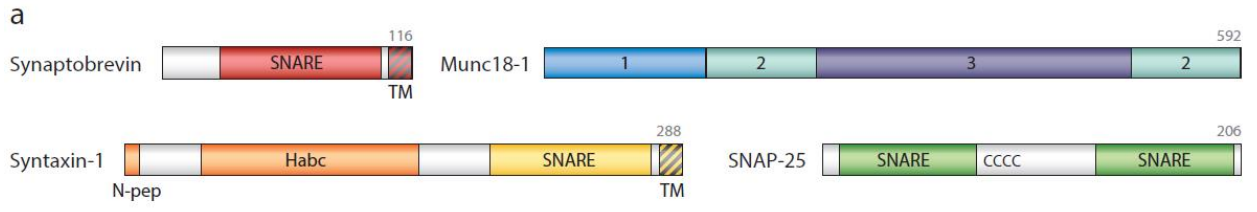
**Figure 1.1: The stalk model of fusion of two lipid bilayers.**

(a) (i) Initial membrane approach before fusion. (ii) Some of the lipid molecules protrude to minimize the initial contact surface and decreases the energy required for dehydration of the outer leaflets. (iii) A hemifusion stalk intermediate forms where the outer leaflets are fused and inner leaflets remains unfused (iv) Expansion of stalk intermediate leads to hemifusion diaphragm. (v) Fusion pore formation occurs either through hemifusion diaphragm or directly from hemifusion stalk intermediate.

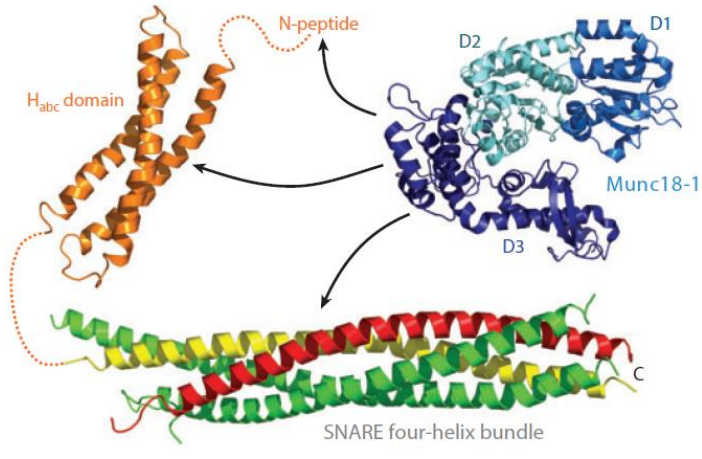
(b) Different lipid molecules promote distinct membrane curvatures. Diacylglycerol (DAG) and phosphatidylethanolamine (PE) are cone-shaped lipids due to their small head-head groups and promotes monolayers to bend towards the head-groups. Lysophosphatidylcholine (LPC) is an inverted cone-shaped lipid and promotes monolayers to bend towards acyl chains. Phosphatidylcholine (PC) is cylindrical and promotes monolayers to be flat.

## ***1.2 SNARE Proteins***

Neurotransmitter release and most types of intracellular membrane fusion are facilitated by highly conserved SNARE proteins. The SNARE proteins that are responsible for neurotransmitter release are syntaxin-1, SNAP25, and synaptobrevin (also called VAMP). Different isoforms and homologs of these proteins govern almost all the intracellular membrane fusion machineries. SNARE proteins were first discovered as substrates for clostridial neurotoxins [19-22]. SNARE proteins consist of characteristic SNARE motif(s) composed of 60-70 residues. SNARE motifs are intrinsically disordered polypeptides that have the tendency to form coiled-coil structures with other SNARE motifs. Many SNARE proteins contain only one SNARE motif, as that seen in synaptobrevin and syntaxin, on the other hand SNAP25 and some of its homologs contain two SNARE motifs. Synaptobrevin is bound to a synaptic vesicle by its C-terminal transmembrane region. Syntaxin also contains a C-terminal transmembrane region and is located at the plasma membrane. SNAP-25 does not have any transmembrane region but it is anchored to the plasma membrane through its palmitoylated cysteine residues located at the region that links the two SNARE motifs of SNAP25 (Figure 1.2). These four SNARE motifs from three different SNARE proteins and 2 separate membranes form a very stable 4 parallel  $\alpha$ -helical coiled coil structure called the SNARE complex, which brings the plasma membrane and synaptic vesicles into close proximity [23-26] (Figure 1.2 B and Figure 3).



**b** Munc18-1/SNARE complex assembly



**c** Munc18-1/closed syntaxin-1 complex

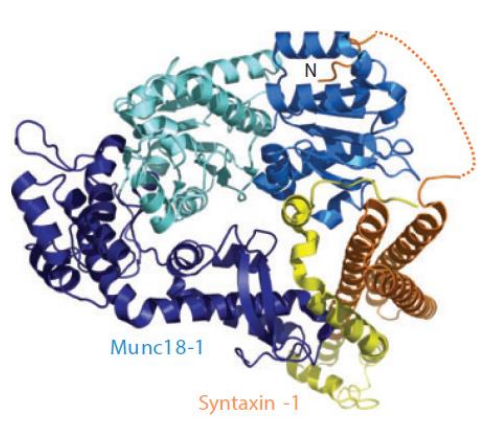


**Figure 1.2: Architecture of the SNAREs, Munc18-1, and their complexes.**

(a) Domain architectures of Munc18-1, and the neuronal SNAREs; synaptobrevin, syntaxin-1, and SNAP-25. SNARE motifs are marked as SNARE and N-pep represents the N-peptide of syntaxin-1. CCCC represents the cysteine-rich motif of SNAP-25 that is palmitoylated and anchored to the plasma membrane. The numbers on the bar that represents Munc18-1 show three distinct domains. Domain-2 is separated in the protein sequence. The numbers above the bars shows the length of the protein sequences.

(b) Ribbon diagrams of the structures of the four-helix bundle of the SNARE complex [27], Habc domain of syntaxin-1 [28] and Munc18-1 from the Munc18-1/syntaxin-1 structure [29]. Two dashed orange lines represent the N-peptide and the linker between the Habc domain and the SNARE motif of syntaxin-1. C-terminus of the four-SNARE motifs in the SNARE complex is labeled with the letter “C”. D1–D3 indicates the three domains of Munc18-1. The interactions of Munc18-1 with the SNARE complex, N-peptide and Habc domain of syntaxin-1 are illustrated with black arrows.

(c) Ribbon diagram of the Munc18-1/syntaxin-1 complex [29]. N-terminus of syntaxin-1 is labeled with the letter “N”. N-peptide of the syntaxin-1 interacts with Munc18-1 and forms a short helix in this structure. The linker between Habc domain and the N peptide is shown as the dashed orange line.

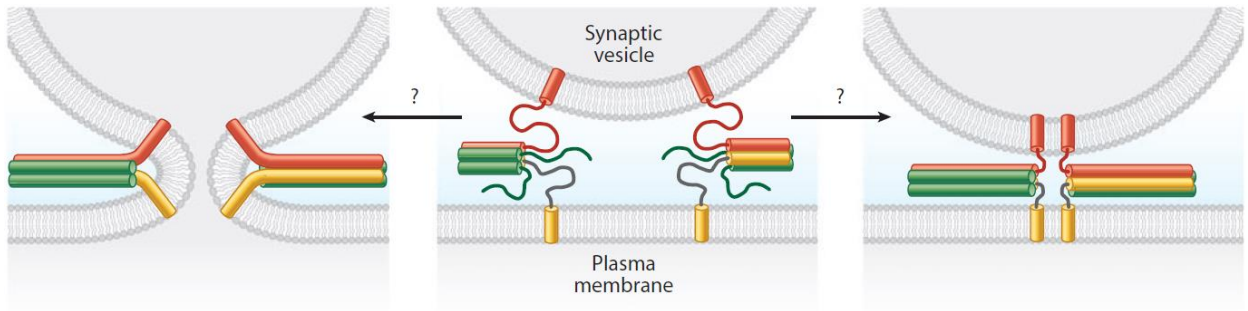


**Figure 1.3: Models of SNARE function.**

Models demonstrating how the plasma membrane and a synaptic vesicle are brought to close proximity with the formation of the four-helix bundle from SNARE motifs. Synaptobrevin is shown in red, SNAP-25 in green and syntaxin-1 in yellow. Formation of the SNARE complex could lead to membrane fusion (left panel) or helix formation may not be continuous due to flexibility of the linker between the trans-membrane regions and the SNARE motifs of synaptobrevin and syntaxin-1, in which the SNARE complex formation cannot lead to membrane fusion (right panel). Habc domain of the syntaxin-1 is not represented in this figure for simplicity.

The coiled coil structure of the SNARE complex is governed by multiple hydrophobic interactions of the side chains and a polar layer located in the middle of each SNARE motif. This polar layer is composed of three glutamine residues, two of which are provided by SNAP-25 and another by syntaxin-1, and an arginine residue provided by synaptobrevin [30]. Sequence analysis revealed that the polar layer is a conserved property throughout the SNARE protein family and SNARE proteins can be classified into Q<sub>a</sub>, Q<sub>b</sub>, Q<sub>c</sub> and R-SNAREs according to the central polar layer residue and the localization of Q-SNAREs in the SNARE complex (e.g., [30, 31]). Another commonly used classification of the SNAREs depends on the localization of the SNAREs on membranes. Vesicle associated SNAREs are called v-SNAREs (as for synaptobrevin) and target membrane associated SNAREs are called t-SNAREs (as for syntaxin-1 and SNAP-25). This classification does not involve any structural similarity among t-SNAREs or v-SNAREs [32].

The observation of the parallel interaction of synaptobrevin and syntaxin-1 in the SNARE complex and the fact that the SNARE motifs of synaptobrevin and syntaxin-1 are close to their transmembrane regions suggested that SNARE complex formation brings synaptic vesicles and plasma membrane into close proximity, which may also fuel the energy required for fusion of those membranes [23] (Figure 1.1 and 1.3). Initial studies with *in vitro* liposome reconstitution studies using the neuronal SNARE proteins claimed that SNARE proteins are sufficient to cause membrane fusion between liposomes (Figure 1.3) [33]. However, the relevance of these results and the question of whether the energy released during the SNARE complex formation can be transferred directly to actual fusion of the membranes have been highly debated [34]. Nevertheless, it has been undoubtedly accepted that SNARE proteins

have a vital role in synaptic vesicle exocytosis and intracellular membrane fusion in general [35-37] and *in vitro* reconstitution assays became a valuable tool to understand the function of many proteins involved in intracellular membrane fusion machineries. The SNARE complex is a very stable coiled coil structure and, therefore, disassembly of the SNARE complex and recycling of SNAREs for another round of membrane fusion requires NSF,  $\alpha$ -SNAP, and ATP [38, 39]. Some SNARE proteins contain sequences other than SNARE motif and transmembrane region, which regulate the formation of the SNARE complex. The H<sub>abc</sub> domain located at the N-terminus of syntaxin-1 is a three helix bundle that is autonomously folded and interacts with the SNARE motif of the syntaxin-1 to keep syntaxin-1 in the so called closed conformation state. The closed conformation of syntaxin-1 prevents syntaxin-1 from interacting with other SNAREs, and thus inhibits formation of the SNARE complex [40-42] (Figure 1.2 A and C). The closed conformation of syntaxin-1 plays an important role in synaptic vesicle exocytosis, which will be discussed in following sections. The closed conformation of syntaxin-1 is not conserved through all syntaxin-1 family members; however, the H<sub>abc</sub> domain is conserved through entire syntaxin family [43-47]. Other regulatory domains are adopted by some SNAREs from other SNARE families and some of these domains may also participate in inhibition of SNARE complex formation, but not all [48-51]. Additionally, a small region called N-peptide located in the very N-terminus of most of the proteins in the syntaxin family is also responsible for another layer of regulation on membrane fusion [43, 44, 47, 52-57]. All of these observations reveal that SNAREs possess very critical functions within membrane fusion machineries. Some of the

features of SNARE proteins are well conserved in most of these machineries and others are tailored to meet the specialized functions of the particular fusion machineries.

### **1.2.1 SNAREs, NSF and $\alpha$ -SNAP**

SNAREs are very promiscuous proteins and many SNAREs are interchangeable during the SNARE complex formation. This notion becomes a problem for membrane trafficking specificity since the SNAREs are conserved in many intracellular membrane fusion machineries [58]. Therefore, the specificity of membrane fusion is provided mostly by other proteins, including tethering factors, Rab GTPases and partly by the SNARE proteins [59-61]. The promiscuity of the syntaxin-1 and SNAP-25 SNARE motifs results in formation of various alternative helical complexes in addition to the SNARE complex and those complexes are hypothesized to compete with the actual SNARE complex formation [62-64] (Figure 1.4). These alternative coiled-coil complexes are non-productive for neurotransmitter release and are also observed in yeast vacuolar fusion [65]. These nonproductive complexes in yeast vacuoles are disassembled by homologs of NSF and  $\alpha$ -SNAP, which then allows fusion to proceed in a proper way [65]. Additionally, NSF and  $\alpha$ -SNAP were shown to disassemble similar complexes in an *in vitro* reconstitution assay where neuronal SNAREs, Munc18-1, Synaptotagmin-1, and Munc13-1 altogether can precede membrane fusion in the presence of NSF and  $\alpha$ -SNAP [66] (Figure 1.4). In synapses, reformation of these nonproductive complexes is prevented by the closed conformation state of syntaxin-1 and its interaction with Munc18-1 together with disassembly of various SNARE complexes by NSF and  $\alpha$ -SNAP [66].

### 1.2.2 Energy of Fusion and SNAREs

A considerable amount of energy is required to carry out each intermediate step of membrane fusion [37, 67]. Certain lipid molecules dictate a higher requirement of energy by providing different curvature to lipid bilayer during the intermediate fusion steps [68]. Theoretical calculations estimate that the overall free energy for complete fusion is between 50-100  $k_B T$  [69]. Experimental studies showed that a single SNARE complex formation can provide 23-35  $k_B T$  [70, 71] or 65  $k_B T$  [72] free energy. If all the energy yielded by the formation of a SNARE complex can be transferred to membrane fusion, one to three SNARE complexes should be sufficient to cause membrane fusion according to theoretical calculations and the experimental data. Indeed, a recent study reported that two SNARE complexes can provide sufficient energy for synchronous release in synapses and three in chromaffin cells [73, 74]. The correlation of *in vivo* results with the theoretical energy calculations should be carefully interpreted, since the energy released from SNARE complex formation may not be directly transferred to fusion of membranes.

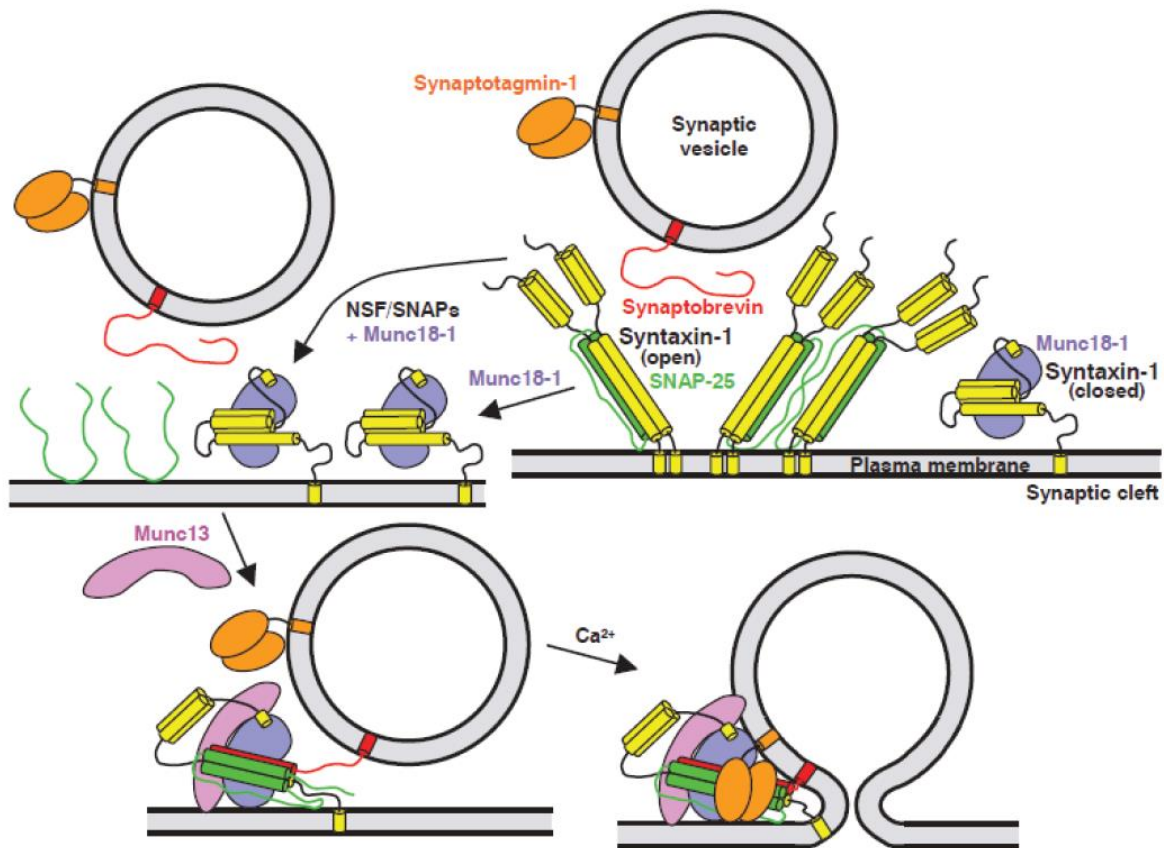


**Figure 1.4: Model of synaptic vesicle fusion machinery.**

A closed conformation of syntaxin-1/Munc18-1 complex and open conformation of syntaxin-1/SNAP-25 heterodimers are shown in the top right panel. Syntaxin-1/SNAP-25 heterodimers are shown to be disassembled by NSF and  $\alpha$ -SNAP, and Munc18-1 keeps syntaxin-1 in its closed conformation (top left panel). Munc13-1 triggers the opening of the syntaxin-1 closed conformation. Munc13-1 together with Munc18-1 helps SNAREs to form the trans-SNARE complex, which is bound to Munc18-1 and Munc13-1. NSF and  $\alpha$ -SNAP cannot disassemble the trans-SNARE complex at this state (bottom left panel). Synaptotagmin-1 together with  $\text{Ca}^{2+}$  leads to fast synaptic vesicle fusion (bottom right panel).

The arrangement of the proteins is not well characterized, and synaptotagmin-1 may be involved in the earlier steps of the process.

One of the early models of membrane fusion claiming that SNAREs are sufficient to cause membrane fusion depends on the formation of continuous helices between SNARE motifs and the transmembrane regions of both syntaxin-1 and synaptobrevin [75, 76]. In this model, zippering from the N-terminus to the C-terminus of the SNARE motifs extends to the transmembrane regions of both syntaxin-1 and synaptobrevin such that the energy released during the SNARE complex formation can be transferred to induce membrane fusion. A recent crystal structure of the neuronal SNARE complex revealed that the helical structure of the SNARE motifs can indeed extend to the transmembrane regions of both syntaxin-1 and synaptobrevin [77] (Figure 1.5). However, another study reported flexibility between SNARE motifs and transmembrane regions of syntaxin-1 and synaptobrevin [78]. Energy transfer from the SNARE complex formation to induce membrane fusion can be abolished due to this flexibility [37]. Therefore the free energy of SNARE complex formation measured in previous studies may be utilized only to bring membranes close to each other without inducing fusion [70]. The remaining energy released upon the formation of a helix for the linker region was shown to be  $8 k_B T$  by a recent study [72], which is alone not sufficient to fuse membranes. The crystal structure of the SNARE complex mentioned above may represent the structure of the SNARE complex after fusion of membranes the linker between the SNARE motifs and the transmembrane regions of SNAREs is flexible. The remaining energy released upon the formation of a helix for the transmembrane regions of the SNAREs has not been exclusively studied.

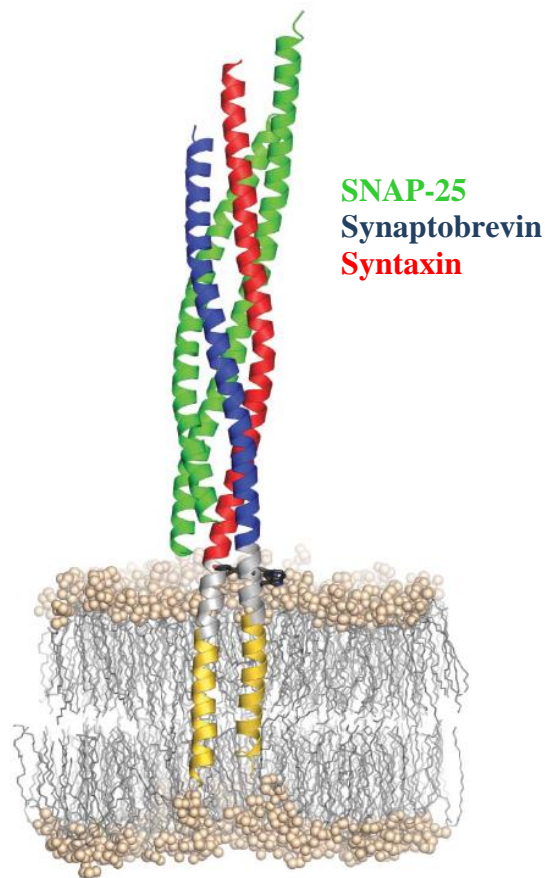


**Figure 1.5: Model of the neuronal SNARE complex inserted in a bilayer.**

Aromatic residues are shown as black stick model within the linker region, which is shown as grey ribbon diagram. SNAP-25 is shown in green, the syntaxin-1 SNARE motif in red, the synaptobrevin SNARE motif in blue and trans-membrane regions of syntaxin-1 and synaptobrevin are shown in yellow. Head groups of POPEs shown as balls and their carbon chains as sticks. The relative position of the SNARE complex within the POPE bilayer was estimated by molecular dynamic simulations. (POPE is a cone shaped lipid and promotes membrane bending as shown in Figure 1.1, usage of POPE alone might give rise to non-physiological features on lipid bilayers that are simulated in this study).

### ***1.3 SM Proteins***

All intracellular membrane fusion processes governed by the SNARE proteins also involve SM proteins. Lack of SM proteins was reported to abrogate membrane fusion [79-81]. For example, knocking out the SM protein, Munc18-1, from mice abolishes synaptic vesicle exocytosis in neurons [82]. Despite the fact that SM proteins play a very important role in membrane fusion, their fundamental functions have not been well understood in membrane fusion. There are at least two reasons behind this important functional enigma of SM proteins. First, lipid mixing was observed between SNARE reconstituted liposomes in the absence of SM proteins [33]; however the functional relevance of this observation has been debated over a decade and this observation strongly depends on the conditions of the *in vitro* reconstitution assays. It is important to show that the observed lipid mixing meets the actual physiological requirements of membrane fusion to reliably draw any functional conclusions from these assays. More importantly, the multiple binding modes of SM proteins and SNAREs/SNARE complexes most likely play multiple roles on membrane fusion. Therefore, it was difficult to reconcile Munc18-1 with a simple model [41]. Recently, Munc18-1 was shown to keep syntaxin-1 in its closed conformation and orchestrate trans-SNARE complex formation, which is the primed state and the substrate for synaptotagmin-1 to trigger release upon  $\text{Ca}^{2+}$  influx (Figure 1.4) [66]. This important study provided key evidence to explain functional importance of Munc18-1 in neurotransmitter release. However, it is still unclear whether SM proteins are directly involved in the fusion of membranes like SNAREs or they are just regulators of trans-SNARE complex formation.

Munc18-1 was first characterized as a tight interacting partner of syntaxin-1 [83]. Munc18-1 was the first SM protein found to be involved in membrane fusion through this interaction. Characterization of this interaction revealed that Munc18-1 forms an arch shaped structure by three distinct domains and a central cavity in the middle of those domains (Figure 1.2 C) [42]. Syntaxin-1 binds to this central cavity in its closed conformation, which seemed incompatible with or inhibitory to SNARE complex formation. Another study showed that the yeast SM protein, Sec1p does not interact with Sso1p, a member of the syntaxin family; however, Sec1p was reported to interact with the cognate SNARE complex which is responsible for exocytosis in yeast [84]. In other studies, SM proteins in other intracellular membrane fusion machineries have been shown to interact with their cognate syntaxin through the N-terminal peptide of the cognate syntaxins and these interactions do not involve the closed conformation of the syntaxins or any other domain like H<sub>abc</sub> [43, 47, 52]. Additional studies in these intracellular membrane fusion machineries also reported interaction between SM protein and their cognate SNARE complexes [56, 85-87]. Later, SM protein Munc18-1 was also shown to bind neuronal SNARE complex in addition to syntaxin-1 alone and this binding involves the interaction of N-terminal peptide of syntaxin-1 with Munc18-1 [53, 55, 57]. These studies revealed multiple modes of interaction between SNAREs and SM proteins. Most importantly, the interaction of SM proteins with their cognate SNARE complexes seems to be adopted in most of the intracellular membrane fusion machineries and some of these machineries seem to have evolved to involve interaction of SM proteins with closed conformation of syntaxins to be able to specifically regulate the respective fusion machineries.

## 1.4 *Munc13s*

Munc13 proteins are large proteins containing multiple domains that are responsible for vesicle priming and presynaptic plasticity through protein and lipid interactions [88-91]. Munc13s were first characterized by their abundance at active zones and homology to Unc13 from *C. elegans* [92]. Absence of Munc13s was shown to abolish neurotransmitter release; therefore they are vital for synaptic vesicle exocytosis, which has been associated with their vesicle priming activity [88-91]. Additionally, various studies reported another function called synaptic vesicle docking (upstream of the priming step) for Munc13s with slightly different conclusions [11, 89, 93-95].

Multidomain Munc13s contain a phorbol-ester binding C<sub>1</sub> domain, a MUN domain, three C<sub>2</sub> domains (C<sub>2</sub>A, C<sub>2</sub>B and C<sub>2</sub>C) dispersed throughout the protein, among which C<sub>2</sub>B binds to Ca<sup>2+</sup> ions [96-98], and a central calmodulin binding region [99]. Munc13-1 is involved in neurotransmitter release and its domain architecture is depicted in Figure 1.6. C<sub>2</sub> domains in general are known to interact with other proteins. Additionally, the C<sub>2</sub>B domain is responsible for the Ca<sup>2+</sup> dependent phospholipid (mainly PIP<sub>2</sub>) binding of activity of Munc13-1 [96-98]. The C<sub>2</sub> domains and other motifs of Munc13-1 are responsible for various ways of regulation of synaptic vesicle exocytosis and presynaptic plasticity through lipid-Munc13 interactions, protein-Munc13 interactions by controlling the activity of MUN domain of Munc13, which plays an important role in vesicle priming and the membrane fusion [100-102].

In addition to the dramatic effect of Unc13 knockout in *C. elegans* exocytosis, double knockout of Munc13-1 and Munc13-2 in mice or homologs in *Drosophila melanogaster*

abolished neurotransmitter release (both spontaneous and evoke release) [103]. Expression of the MUN domain in these double knockout mice is sufficient to rescue most of the neurotransmitter release, which shows that the MUN domain is the main functional unit of Munc13 proteins [104]. Additionally, the constitutively open syntaxin-1 LE mutation is sufficient to partially rescue the release in *C. elegans* [105], suggesting an important role for Munc13 in the conformational transition of syntaxin-1 (from closed conformation to open conformation). However, this mutant is not sufficient to rescue release in mice [106]. Therefore Munc13-1 may have another important role in neurotransmitter release beyond regulating the conformational transition of syntaxin-1.

Several studies reported different modes of interaction between the MUN domain of Munc13-1 and syntaxin-1 or different fragments of neuronal SNARE complexes, which is tabulated here. These data provide valuable information towards understanding the function of Munc13 in neurotransmitter release.

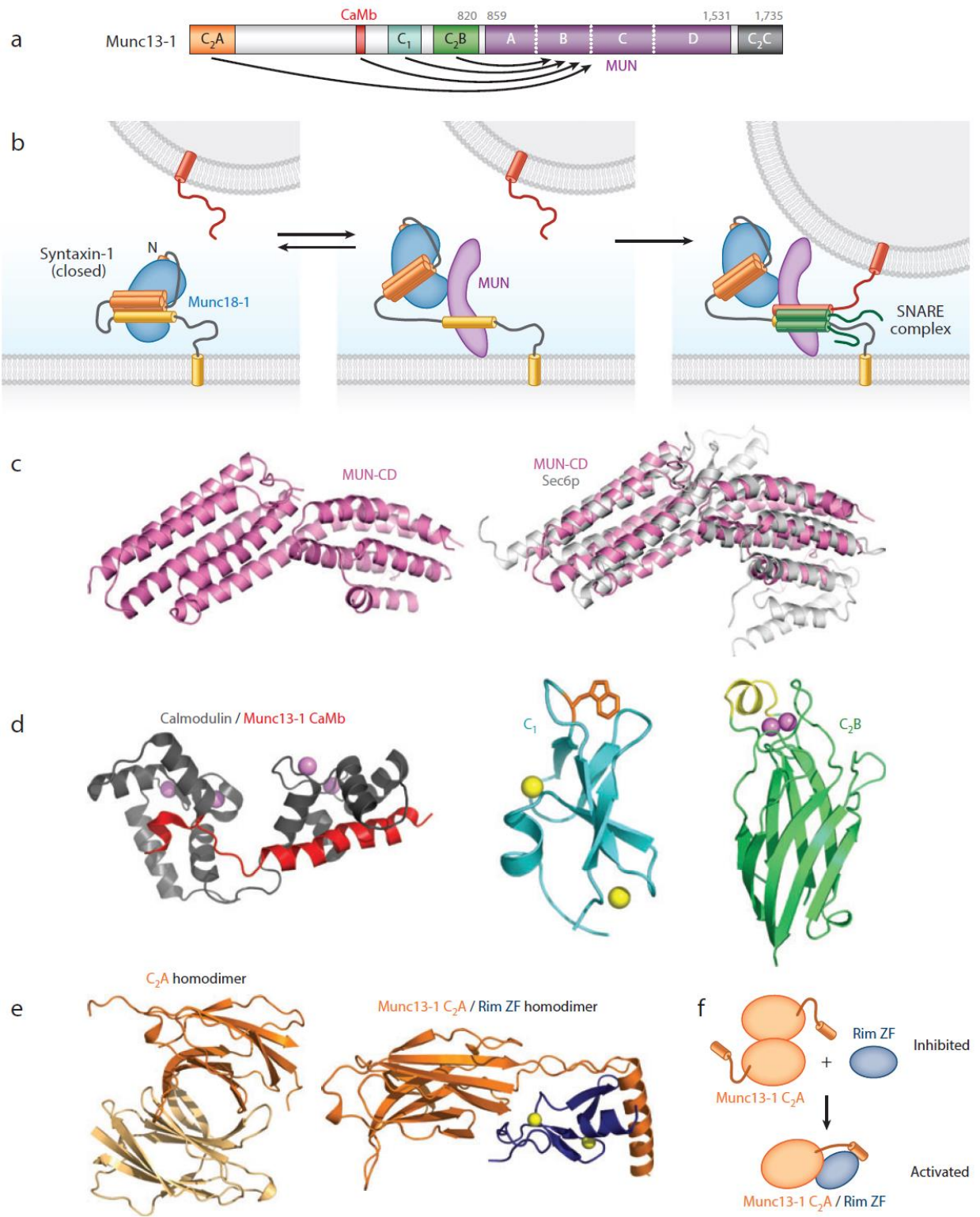


**Figure 1.6: Structure and function of Munc13s.**

(a) Domain architecture of Munc13-1. The letters A through D indicate four subdomains of the MUN domain. The numbers above the bar indicates the residue numbers. The MUN domain priming activity was hypothesized to be regulated by other domains of Munc13-1 during presynaptic plasticity which is depicted by black curved arrows. Calmodulin-binding sequence is denoted as CaMb.

(b) Model of transition from the closed conformation syntaxin-1/Munc18-1 complex to the Munc18-1/SNARE-complex assembly by the MUN domain of Munc13-1 [66]. The syntaxin-1 SNARE motif is extracted from the syntaxin-1/Munc18-1 complex by the MUN domain due to higher affinity of the MUN domain for the SNARE motif in the open conformation. Weak interaction between the MUN domain and Munc18-1 may play a role to stabilize the transient complex shown in the middle panel. This transient complex provides a template for trans-SNARE complex formation and Munc18-1 may translocate from the Habc domain of syntaxin-1 to four-helix bundle (right panel).

(c) Ribbon diagram of the crystal structure of the C-terminal half of the Munc13-1 MUN domain (MUNCD) [107] (left panel). The similarity between the structures of MUNCD (pink) and the exocyst subunit Sec6p (light gray) [108] is shown by superposition of their crystal structures (right panel).

(d) Crystal structures of the calmodulin binding module (CaMb), C<sub>1</sub> [109] and C<sub>2</sub>B [110] domains are shown in the top panel. Calmodulin is shown in dark grey and CaMb in red at left panel [111]. Purple and yellow spheres shows Ca<sup>2+</sup> and Zn<sup>2+</sup> ions respectively. The tryptophan residue that occludes the ligand-binding site is shown as orange stick model in C<sub>1</sub>

domain. The unique  $\alpha$ -helix that is responsible for the phosphatidylinositide phosphate-binding for C<sub>2</sub>B domain is shown in yellow.

(e) Structures of homodimer of Munc13-1 C<sub>2</sub>A domain and heterodimer of Munc13-1 C<sub>2</sub>A domain/ Rab3-interacting molecule (RIM) zinc finger (ZF) domain are shown as ribbon diagrams [112]. C<sub>2</sub>A domain is shown in orange and ZF domain in dark blue.

(f) Activation switch of the Munc13-1 C<sub>2</sub>A domain / RIM ZF-domain heterodimer.

Munc13-1 MUN domain - neuronal SNARE complex	~30 $\mu$ M
Munc13-1 MUN domain - Munc18-1	~150 $\mu$ M
Munc13-1 MUN domain - syntaxin-1 SNARE motif	~45 $\mu$ M
Munc13-1 MUN domain - syntaxin-1 (closed conformation)	~200 $\mu$ M
Munc13-1 MUN domain - syntaxin-1 (N-terminal region)	no detectable binding

**Table 1.1: Affinities of Munc13-1 interactions**

Interestingly, the MUN domain mostly governs weak interactions between Munc13 and syntaxin-1 or the SNARE complex. However, the MUN domain was shown to form tighter interaction with membrane anchored SNARE complex and also syntaxin-1/SNAP25 complex as opposed to soluble ones [113, 114]. Additionally, weak interactions of the MUN domain with the SNARE complex and Munc18-1 cooperate to form a more stable complex to carry out its function [115]. It is important to note that the MUN domain integrates weak protein interactions and its membrane interaction to carry out its function. These studies provide a basis for a model of MUN domain function in which the MUN domain in collaboration with Munc18 and membranes facilitates transition of the syntaxin-1 SNARE motif from the closed conformation to the open conformation so that it can form the SNARE complex with other SNAREs (Figure 1.2 and 1.4). In support of this model, the MUN domain was recently shown to accelerate the transition from the closed conformation of the syntaxin-1/Munc18-1

complex to the formation of the Munc18-1/SNARE complex using FRET and NMR experiments [116].

### ***1.5 Synaptotagmins***

When an axon fires, the action potential migrates towards the active zone of a nerve terminal leading to opening of  $\text{Ca}^{2+}$  channels that initiate synaptic vesicle exocytosis. Therefore, this membrane fusion process leading to neurotransmitter release critically depends on  $\text{Ca}^{2+}$ . The coupling of action potentials and  $\text{Ca}^{2+}$  influx to synaptic vesicle exocytosis was shown by electrophysiological studies [117].  $\text{Ca}^{2+}$  triggered fusion occurs on the millisecond time scale which is comparable to the timescales of  $\text{Ca}^{2+}$  channel gating. This type of release is called evoked neurotransmitter release or synchronous neurotransmitter release. There are two additional types of  $\text{Ca}^{2+}$  dependent release called asynchronous release and spontaneous release [118, 119]. Spontaneous release is claimed to be triggered by fluctuations of  $\text{Ca}^{2+}$ . The physiological relevance of the spontaneous release has been debated over the years; however, it has been observed in many types of neurons, for example in individual excitatory synapses (one release per 2-3 hours) and inhibitory synapses (one release per 3 minutes) of the hippocampal CA1 region [120]. Both synchronous and asynchronous release are induced by action potentials; however, asynchronous release is the slower form of vesicle exocytosis and only manifests itself in most neurons after deletion of synaptotagmin-1 [121-124] Initial binding studies conducted using antibodies described synaptotagmin-1 as a protein associated with synaptic vesicles [125].

### 1.5.1 Architecture

Synaptotagmins belong to the type-1 membrane protein family and are primarily characterized by an N-terminal transmembrane region, followed by a central linker of variable length and two C-terminal C<sub>2</sub> domains called C<sub>2</sub>A and C<sub>2</sub>B [126] (Figure 1.7). There are at least 15 isoforms of synaptotagmin-1 encoded by the mammalian genome [126-128] (Figure 1.8).

C<sub>2</sub> domains are evolutionarily conserved and abundant 130-140 residue protein sequences found in all organisms except plants and unicellular eukaryotes and adopt a conserved 8 stranded  $\beta$ -sandwich structure (Figure 1.7 and 1.8). The C<sub>2</sub> domains of eight of the synaptotagmins (synaptotagmin-1, 2, 3, 5, 6, 7, 9 and 10) bind to several Ca<sup>2+</sup> ions [118, 126, 132, 133]. Previous NMR studies in our lab have revealed that five conserved aspartate residues located on the top loops of both C<sub>2</sub>A and C<sub>2</sub>B domains are exclusively responsible for the Ca<sup>2+</sup> binding activity of synaptotagmin-1 (Figure 1.7). All of the well characterized synaptotagmins that bind to Ca<sup>2+</sup> possess a Ca<sup>2+</sup> binding site of similar architecture.

These conserved aspartate residues are absent in other synaptotagmin isoforms that do not bind Ca<sup>2+</sup>, including both the C<sub>2</sub> domains of synaptotagmin-8, 12, 13, 14, 15 and the C<sub>2</sub>A domain of synaptotagmin-4 and 11 [126, 132, 133] (Figure 1.9). The C<sub>2</sub>B domains of synaptotagmin-4 and 11 possess conserved aspartate residues but fail to form coordination sites for Ca<sup>2+</sup> binding [134, 135] (Figure 1.8). These eight synaptotagmins bind to Ca<sup>2+</sup> ions with widely varying affinities due to the variation in their Ca<sup>2+</sup> coordination sites. Therefore, these synaptotagmins act as a set of proteins that can function at a wide range of Ca<sup>2+</sup>

concentrations to meet the requirements of various  $\text{Ca}^{2+}$ -dependent membrane trafficking and signal transduction processes in a cell [126, 136-141].

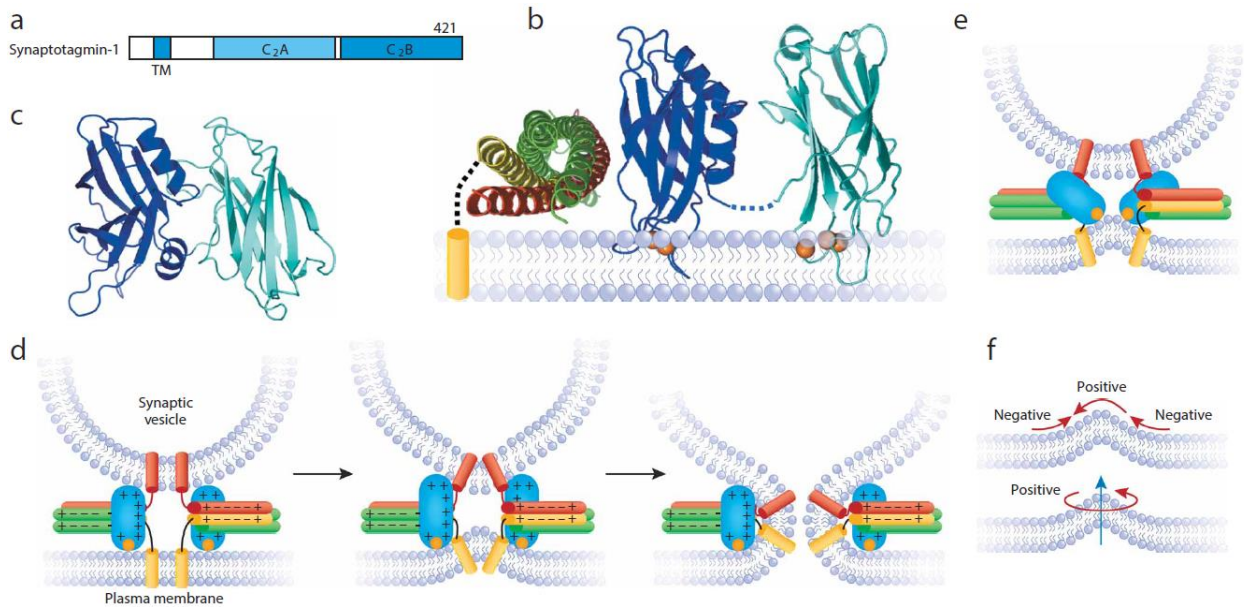


**Figure 1.7: Syntaptotagmin-1 and its coupling to SNAREs and membranes.**

(a) Domain architecture of syntaptotagmin-1. Trans-membrane region is labeled as TM and the polypeptide length is denoted above the bar.

(b) Model of the quaternary complex the SNARE complex, syntaptotagmin-1,  $\text{Ca}^{2+}$  and phospholipid (SSCAP). This model is built from the individual structures of the SNARE complex [27], syntaptotagmin-1  $\text{C}_2$  domains [129, 130] and mutagenesis studies on SSCAP complex [131].  $\text{Ca}^{2+}$  ions are shown as orange spheres; the linker between the syntaxin-1 SNARE motif (yellow) and transmembrane region shown as a dashed black curve. Syntaptotagmin-1  $\text{Ca}^{2+}$ -binding loops may bind to either the plasma membrane or synaptic vesicle membrane.

(c) Ribbon diagram of syntaptotagmin-1 structure without  $\text{Ca}^{2+}$ . Both  $\text{C}_2$  domains contain eight  $\beta$ -strands and  $\text{C}_2\text{B}$  domain contains additional  $\alpha$ -helices.

(d) Model of interplay between the synaptotagmin-1 C<sub>2</sub>B domain and the SNARE complex for inducing membrane fusion upon Ca<sup>2+</sup> influx where C<sub>2</sub>B domain binds both membranes and the SNARE complex. Two Ca<sup>2+</sup> ions are shown as an orange circle. The electrostatic potential of the surface of the C<sub>2</sub>B domain and the SNARE complex is denoted with the + and – signs. The positively charged surface of the C<sub>2</sub>B domain may help to bend the membranes. Binding mode of the C<sub>2</sub>B domain to the SNARE complex may be different and C<sub>2</sub>A domain is not shown in this figure for simplicity but it may play an important role in this process.

(e) The Ca<sup>2+</sup> binding loops of the C<sub>2</sub> domains of synaptotagmin-1 may help to cause positive curvature on the membrane to force membranes to fuse.

(f) Both positive and negative curvature is required to bend membranes.

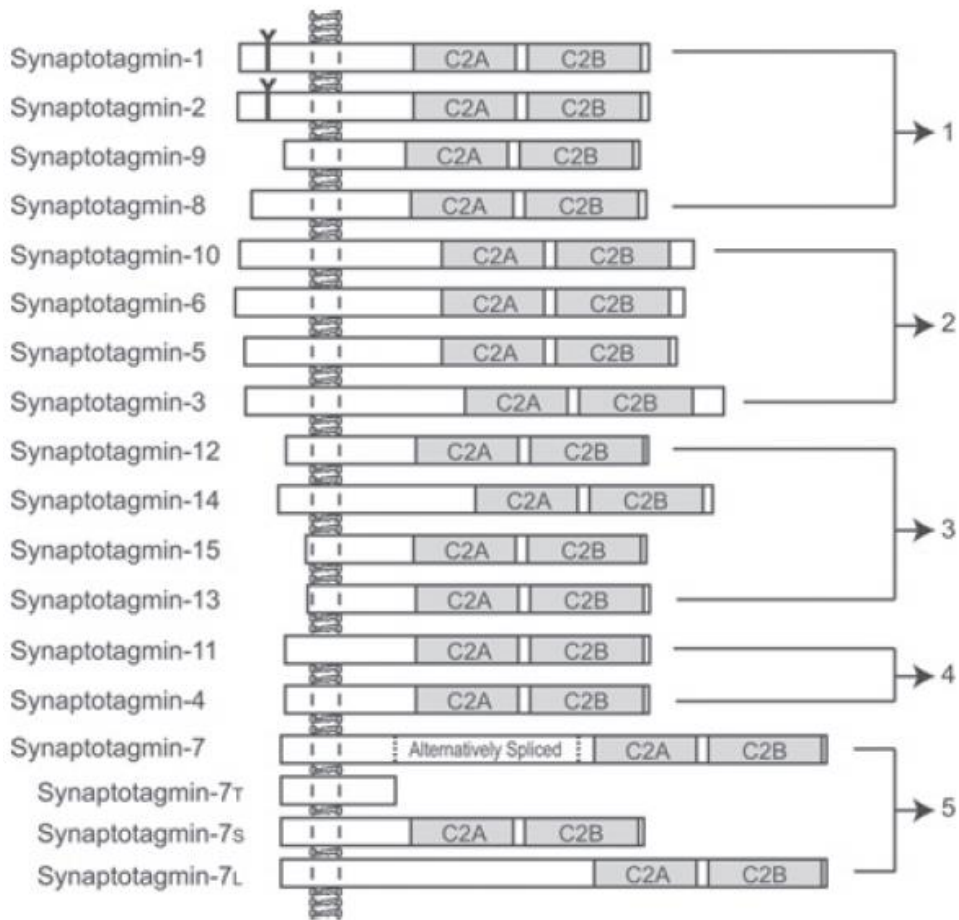


**Figure 1.8: Comparison of the architecture of mouse synaptotagmins.**

All synaptotagmins include N-terminal membrane spanning region, two C<sub>2</sub> domains and a variable length linker between membrane spanning region and C<sub>2</sub> domains. Proteins in this family can be classified in five groups according to their sequence similarities. Two synaptotagmins includes N-terminal glycosylation site denoted with ‘Y’ shape. There are 12 alternatively spliced variant of synaptotagmin-7. The longest, shortest and standard forms of synaptotagmin-7 are shown in group 5.

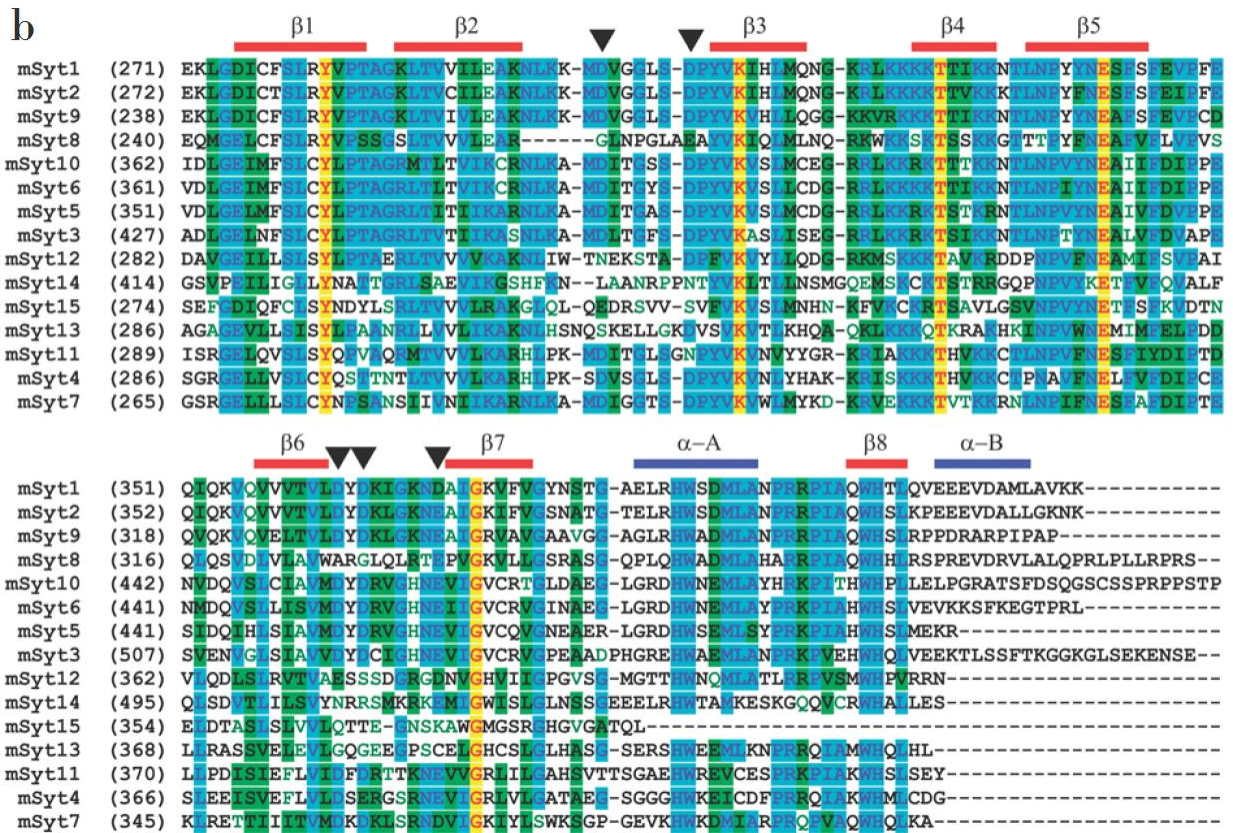
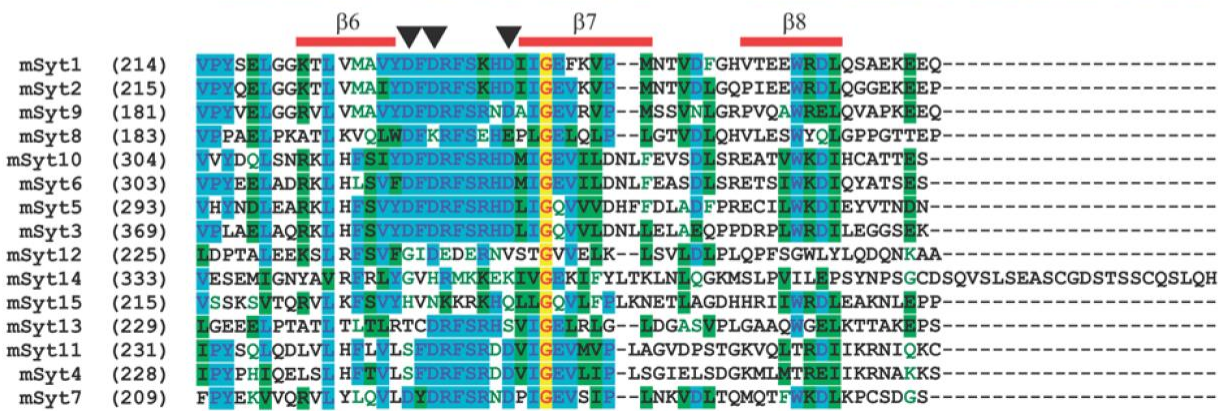
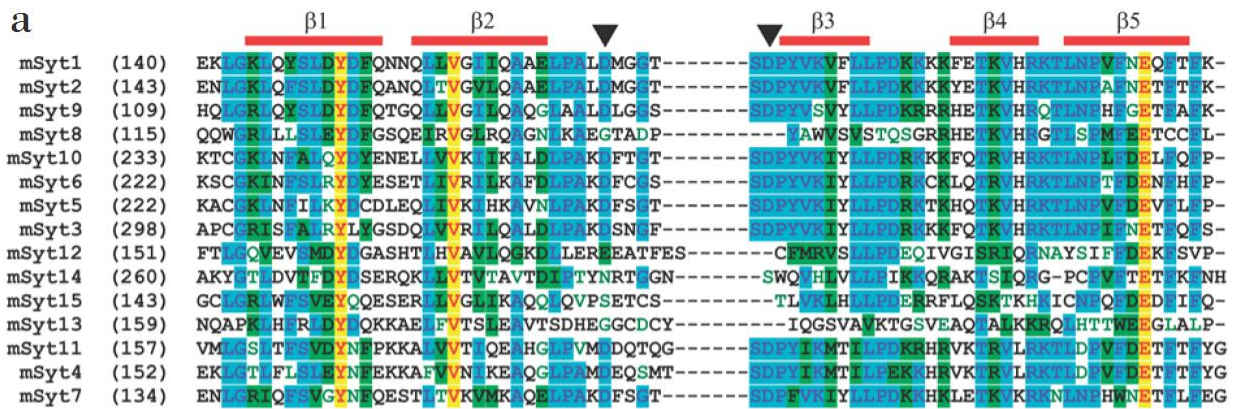


**Figure 1.9: Sequence Alignment for synaptotagmins encoded in the mouse genome.**

Alignments of C<sub>2</sub>A (a) and C<sub>2</sub>B (b) domains of synaptotagmins were generated using the AlignX feature of Vector NTI software (Invitrogen). Red bars illustrate the eight  $\beta$ -strands and labeled as  $\beta$ 1- $\beta$ 8. Blue bars illustrate two  $\alpha$ -helices that are found in the C<sub>2</sub>B domain of some of the synaptotagmins. Inverted black triangles mark the acidic residues that are responsible for Ca<sup>2+</sup> binding. Identical residues are illustrated by blue and yellow highlighting of the letters. Yellow highlighted the residues that are completely conserved and blue highlighted residues that are mostly conserved in synaptotagmins. Aminoacid substitutions with similar chemical properties are illustrated by green highlighting.

Synaptotagmin-1, 2, 9 and 12	Synaptic vesicles, neuroendocrine vesicles [121, 123, 136, 142-146]
Synaptotagmin-7	Plasma membrane, secretory lysosomes, neuroendocrine vesicles [147]
Synaptotagmin-10	Secretory vesicles (olfactory mitral neurons) [148]
Synaptotagmin-4	Synaptic vesicles, trans-Golgi complex, postsynaptic membranes [149]
Other synaptotagmins	Mostly transport vesicles and some enriched in plasma membrane [150]

**Table 1.2: Isoforms and Localization of Synaptotagmins**

Localization of the some of synaptotagmins is poorly understood and not all synaptotagmin containing vesicles are characterized. Therefore, Table 1.2 does not provide comprehensive information of the cellular localization of the synaptotagmins.

### 1.5.2 Functional Studies

Ca<sup>2+</sup> dependent phospholipid interactions of synaptotagmin-1 and binding of synaptotagmin-1 to the SNARE complex were shown in early studies [130, 139, 151-153]. Negatively charged lipids such as PS and PIP<sub>2</sub> are required for Ca<sup>2+</sup> dependent phospholipid interactions of synaptotagmin-1 [154]. Negatively charged lipids increase the apparent affinity of

synaptotagmin-1 for  $\text{Ca}^{2+}$  ions, possibly by providing an additional coordination site for  $\text{Ca}^{2+}$  binding [130, 135]. This effect of phospholipids allows synaptotagmins to function at the required  $\text{Ca}^{2+}$  concentration range (~10-40  $\mu\text{M}$ ) and cooperativity value (~5) that is required for synchronous release. [146, 149, 155-158].

An early study reported that  $\text{Ca}^{2+}$  enhanced the interaction between synaptotagmin-1 and syntaxin-1 [139]. Synaptotagmin-1 was also shown to interact with the neuronal SNARE complex in both a  $\text{Ca}^{2+}$  dependent and an independent manner [154]. These interactions also depend on the ionic strength of the solution. The phospholipid binding activity of synaptotagmin-1 seems to be common for all  $\text{Ca}^{2+}$  binding synaptotagmin isoforms [137, 139, 159, 160] with various affinity regimes [137].

### **1.5.3 $\text{Ca}^{2+}$ Independent Synaptotagmin Functions**

$\text{C}_2$  domains in general are also thought to be involved in protein-protein interactions that do not necessarily depend on  $\text{Ca}^{2+}$  ions. In agreement with this notion, synaptotagmin-12 that does not bind to  $\text{Ca}^{2+}$  ions was shown to form a tight complex with synaptotagmin-1 in synaptic vesicles [161]. However, other synaptotagmin isoforms that does not bind to  $\text{Ca}^{2+}$  ions have not been biochemically well characterized.

## **1.6 *Complexins***

Complexins are evolutionary conserved soluble proteins that were named after characterization of their interaction with the SNARE complex [162]. Complexins together with synaptotagmins are found in all animals. Complexins are composed of about 120

residues and are intrinsically disordered in solution [163]. However, a crystallization study showed that complexin-1 binds to the groove between the SNARE motifs of syntaxin and synaptobrevin in the membrane proximal region of the SNARE complex and the central ~20 residues of complexin form an  $\alpha$ -helical structure (called central helix) that is anti-parallel to the SNARE proteins in the complex [164] (Figure 1.10). The crystal structure of the complexin-1/SNARE complex revealed that a short sequence in the amino terminal region of complexin-1 also forms an  $\alpha$ -helical structure called accessory helix but does not interact with the SNARE complex [164]. The extreme terminal sequences of complexin-1 have not been reported to form any secondary structure elements.

The mammalian genome encodes four isoforms of complexins. complexin-1 and complexin-2 are abundantly expressed in the brain [162]. Complexin-3 and Complexin-4 are likely to be localized to plasma membrane through a C-terminal isoprenylation site that is specific to these isoforms and specialized for retinal cells [165].

Complexins function in the neurotransmitter release machinery is coupled to synaptotagmin-1, the SNARE proteins and the SNARE complex. Double knockout of Complexin-1 and Complexin-2 in mice partially abolished synchronous release without significantly affecting asynchronous release [166]. Ensuing studies reported that knockdown of these two isoforms elevated the spontaneous release and changed the  $\text{Ca}^{2+}$  affinity and the cooperativity regime of neurotransmitter release [167, 168]. These effects are similar to the effect of synaptotagmin-1 knockout on neurotransmitter release. However, depletion of complexins also significantly decreased the readily releasable pool of synaptic vesicles, which was not affected by synaptotagmin-1 knockout in neurons [168]. Interpretation of the function of

complexins became harder with the observation of rescue experiments where expression of complexin-1 mutants in complexin-1 and complexin-2 double knockout mice showed that the interaction between complexin-1 and the SNARE complex is necessary for the function of complexins [169]. Rescue of complexin-1 was abrogated by mutations that prevent its interaction with the SNARE complex [169]. However a fragment of complexin-1 lacking the N-terminal 26 residues (Complexin-1 27-134) can still interact with the SNARE complex but cannot rescue synchronous neurotransmitter release [169]. Removal of additional 20 residues (Complexin-1 47-134) was able to partially rescue the release [169]. These results showed that the interplay between complexins and synaptotagmin-1 possesses multiple important roles through the SNARE complex in regulation of synchronous neurotransmitter release.

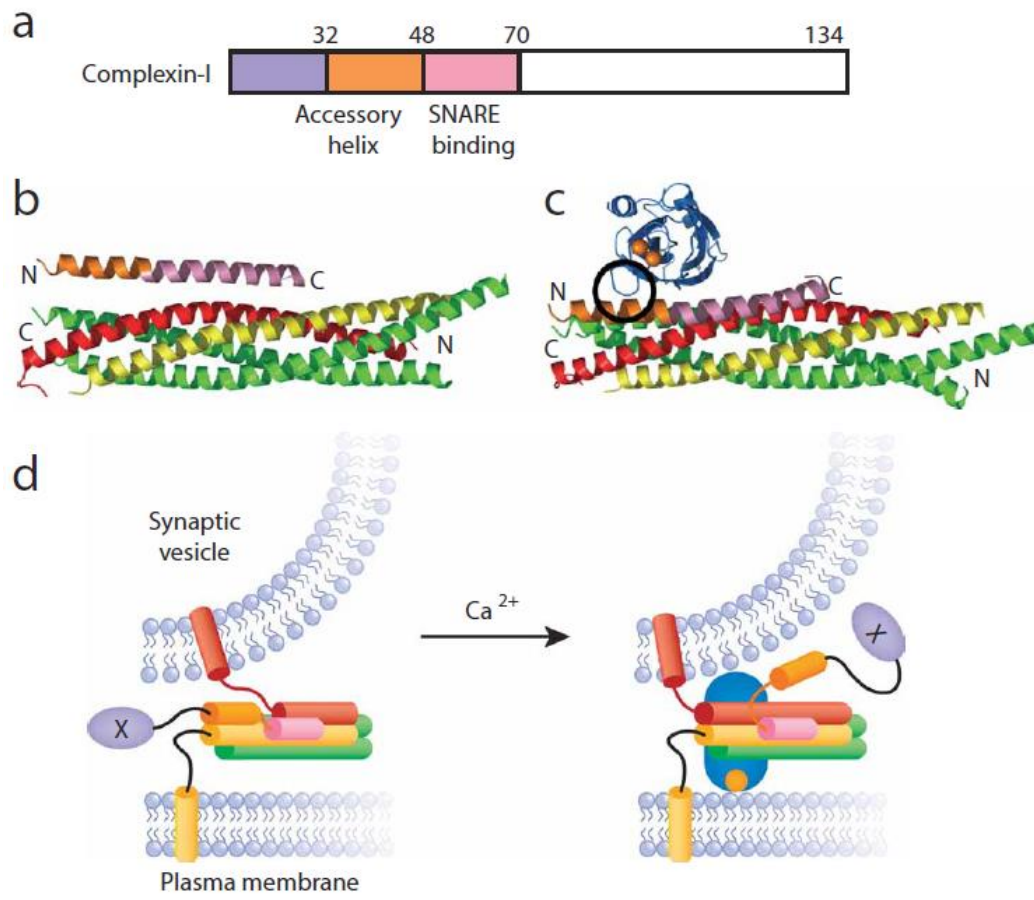


**Figure 1.10: Complexins and their interplay with the SNARE complex and synaptotagmin-1.**

(a) Domain architecture of complexin-1. Numbers above the bar indicate the residue numbers.

(b) Structure of a complexin-1 fragment with the SNARE complex 26. N-terminus and C-terminus of the polypeptides are indicated with the letters “N” and “C”.

(c) The model of SNARE-synaptotagmin- $\text{Ca}^{2+}$ -phospholipid complex [131] (without membrane and  $\text{C}_2\text{A}$  domain of synaptotagmin) is superimposed with the structure of complexin-1 shown in panel b. The overlapping region is shown with a black circle, which includes the accessory helix of complexin-1 and  $\text{C}_2\text{B}$  domain of synaptotagmin-1

(d) Models of inhibition of fusion are shown for the accessory helix binding to the C-terminus of the SNARE complex, which prevents the full SNARE complex formation (left), and how the  $\text{C}_2\text{B}$  domain of synaptotagmin-1 can compete with complexin-1 to release the inhibition of the fusion (right). Purple ellipse with X in the center indicates an N-terminal region that includes important uncharacterized interactions. Orientation of this region is arbitrary in both panels.

## CHAPTER 2

# 2 MEMBRANE BRIDGING AND HEMIFUSION BY DENATURATED MUNC18-1

### *2.1 Introduction*

Many important biological functions such as egg fertilization by sperm, communication of neurons, and secretion and localization of membrane proteins require membrane fusion [1-10]. All the membrane fusion machineries responsible for these critical functions are proposed to follow a common mechanism called the stalk model of membrane fusion. In this model, the outer leaflets of the opposing membranes fuse and form stalk intermediates. This intermediate can either be followed by inner leaflet fusion that leads to fusion pore formation, or expansion of the stalk intermediate, which leads to a hemifusion diaphragm. The stalk model has been proposed as a model of membrane fusion in several different systems with different proteins involved [11, 34, 170, 171]. In all of these studies, membranes appear to have both common and diverse intermediate structures during fusion [172-174].

Intracellular membrane fusion is a very tightly regulated process that involves fusion of two membrane bilayers, such as the plasma membrane and synaptic vesicles during neurotransmitter release in neurons. There are many proteins involved in this fusion process, most of which belong to highly conserved protein families including NSF, SNAPs [173],

SNAREs [5], SM proteins [175] and tethering factors [176]. Proteins from these conserved protein families compose most of the intracellular membrane fusion machinery. For example, SNAREs are a very important group of proteins required for membrane fusion. SNAREs bring two membranes together by forming a highly stable four helix bundle called the SNARE complex [27, 76, 177]. These proteins were initially reconstituted from an *in vitro* membrane fusion model system to study the mechanism of membrane fusion and neurotransmitter release. Initial experiments claimed that SNARE proteins were sufficient to cause lipid mixing between SNARE reconstituted liposomes, which led to the proposal that SNAREs are the minimal machinery required for membrane fusion [33]. Many *in vitro* reconstitution studies followed this study, but very contradictory results have been reported over the years about whether SNAREs alone are sufficient for membrane fusion. One study even claimed that a single SNARE complex formation is sufficient for fusion of two membranes [178]. On the other hand, other studies have shown that membrane fusion by SNAREs alone depend on the reconstitution conditions, such as protein to lipid ratio and proteoliposome preparation method [179-185]. Therefore, there is a controversy about the minimal model of membrane fusion machinery. Additionally, there are other vitally important proteins for intracellular membrane fusion process including the SM protein Munc18-1 and Munc13s. However, *in vitro* reconstitution studies that propose the minimal model of membrane fusion cannot explain the vital dependence of intracellular membrane fusion on these proteins.

SM proteins are a very critical component of the intracellular membrane fusion machinery. Absence of any of the SM proteins was shown to completely abrogate membrane fusion in

different intracellular membrane fusion processes [175, 186, 187]. For example, Munc18-1 knockout mice completely lack neurotransmitter release in synapses [188]. Surprisingly, this is an even more dramatic effect than knocking out any of the individual SNAREs. Despite the very prominent effects of Munc18-1 on membrane fusion, it is quite difficult to explain the function of SM proteins in a simple model since SM proteins seem to possess multiple functions on membrane fusion and interact with SNAREs in different ways [174, 186]. The SM protein Munc18-1 can bind to the closed conformation of neuronal syntaxin-1 [189-191], which seems to prevent SNARE complex formation since the closed conformation of syntaxin-1 is not compatible for interaction with the other SNAREs in order to form the SNARE complex. This interaction suggests that Munc18-1 has an inhibitory role on neurotransmitter release. However, Munc18-1 was also shown to bind to the assembled SNARE complex [192, 193]. Additionally, absence of Munc18-1 results in loss of membrane fusion. These studies added another layer of complexity toward understanding the role of Munc18-1 on neurotransmitter release. It was later shown that all of these interactions require a conserved amino terminus of syntaxin-1 [29, 192-195] and involve the H<sub>abc</sub> domain of syntaxin-1 [28]. Even with this additional knowledge about the functional importance of SM proteins, it is still enigmatic how SM proteins are involved in membrane fusion, why are they important, and which interactions are relevant for regulating membrane fusion. Central to the conserved functional information is undoubtedly that all SM proteins interact with SNARE complexes [174, 186]. This puts SM proteins right in the center of the actual membrane fusion event, and many models postulate this concept. In one model, SM proteins are proposed to be important for keeping membranes at a distance in order to give the SNAREs

enough torque to curve the membranes and cause membrane fusion [34]. Another model proposes that SNARE complex formation causes hemifusion of membranes and that Munc18-1 then alters the curvature of the hemifused membrane, which leads to full membrane fusion [175].

All these studies clearly show that SM proteins are critical for intracellular membrane fusion. This notion is supported also by *in vitro* reconstitution experiments in which Munc18-1 increases lipid mixing between SNARE reconstituted liposomes [192, 196]. Another study showed that Munc18-1 is necessary for the lipid mixing between synaptobrevin reconstituted small vesicles (mimicking synaptic vesicles ~40nm) and syntaxin-1 reconstituted giant vesicles (mimicking plasma membrane) [197]. However, ensuing studies provided contradictory results regarding the sequence requirements for the enhancement of lipid mixing enhancement between SNARE reconstituted liposomes [192, 198, 199]. Even in lieu of these results, the mechanism and functional importance of SM protein – SNARE complex interactions is still a mystery. To shed light on this problem, we have used several biophysical techniques including a commonly applied NBD fluorescence dequenching assay to monitor lipid mixing between membranes [33] and cryo-EM microscopy to visualize structural changes on membranes. Our study led to the surprising results that squid Munc18-1 (sMunc18-1) can cluster liposomes and cause hemifusion without any SNAREs present. Both the clustering and the hemifusion activity by sMunc18-1 result from the denaturation of sMunc18-1 and its following interactions with liposomes. Addition of a commonly used protein stabilizing agent, glycerol, in the sample is sufficient to prevent this activity of sMunc18-1. Heavy clustering of liposomes by sMunc18-1 leads to increased scattering in

lipid mixing assays and is responsible for part of the increased NBD fluorescence intensity, which is normally considered as a direct readout of lipid mixing in this assay. However, these experiments should be interpreted carefully to assess lipid mixing between liposomes because they do not show actual membrane fusion; they only show lipid mixing. Our results showed that increased scattering, hemifusion of membranes and alteration of membrane integrity can be responsible for the increase in NBD fluorescence, which could be mistakenly interpreted as a membrane fusion. Our results also showed that sMunc18-1 alone can cluster liposomes and induce membrane hemifusion. The physiological relevance of these functions of sMunc18-1 is highly enigmatic. However, this study suggests a new mechanism of hemifusion of membranes that does not follow the commonly accepted stalk model of membrane fusion mechanism. Instead, denaturation of sMunc18-1 alters the integrity of the membrane and causes extensive membrane hemifusion interfaces.

## ***2.2 Results***

### **2.2.1 sMunc18-1 can cluster liposomes**

The behavior of sMunc18-1 is better than rMunc18-1, which is used in our lab under physiological conditions. High concentrations of sMunc18-1 can be achieved, but rMunc18-1 precipitates even at low concentration (~20 uM). Additionally, both sMunc18-1 and rMunc18-1 can bind to the mammalian neuronal SNARE complex and syntaxin-1 [200]. Therefore, sMunc18-1 has been used in some of the experiments in this study to elucidate the function of Munc18-1. rMunc18-1 had been suggested to stimulate lipid mixing between synaptobrevin reconstituted liposomes (v-SNARE liposomes) and syntaxin-1/SNAP-25

reconstituted liposomes (t-SNARE liposomes) [192, 196]. We tested whether sMunc18-1 is able to facilitate lipid mixing between t-SNARE and v-SNARE liposomes by a NBD fluorescence dequenching assay. Two sets of liposomes were prepared, one with v-SNAREs and one with t-SNAREs. Lipids individually conjugated to the FRET pair of NBD and rhodamine were included only in the v-SNARE liposomes. The quenched NBD signal would be dequenched upon lipid mixing between v-SNARE and t-SNARE liposomes due to dilution of the FRET pairs [33].

My coworker, Yi Xu, had tested whether both sMunc18-1 and rMunc18-1 facilitate lipid mixing between t-SNARE and v-SNARE liposomes. We observed slight increase in NBD fluorescence signal (NBD dequenching) over time after mixing v-SNARE and t-SNARE liposomes in the absence of any Munc18-1 (Figure 2.1 A). Addition of either sMunc18-1 or rMunc18-1 led to much stronger increase in NBD fluorescence signal (Figure 2.1 A). We consistently observed a larger increase in fluorescence signal with sMunc18-1 than rMunc18-1. The enhancement of NBD dequenching increased progressively with addition of more sMunc18-1. This enhancement became saturated at 7  $\mu$ M sMunc18-1 in the presence of 150  $\mu$ M total lipids (t-SNARE and v-SNARE liposomes) (Figure 2.1 B). Interestingly, sMunc18-1 was also able to lead to an increase in NBD signal in the absence of t-SNARE liposomes (Figure 2.1 C). This increase in the NBD signal cannot not be due to SNARE dependent lipid mixing because there are no t-SNARE liposomes in the experiment and control experiments with only v-SNARE liposomes do not show any increase in the NBD signal without sMunc18-1 (Figure 2.1 C).

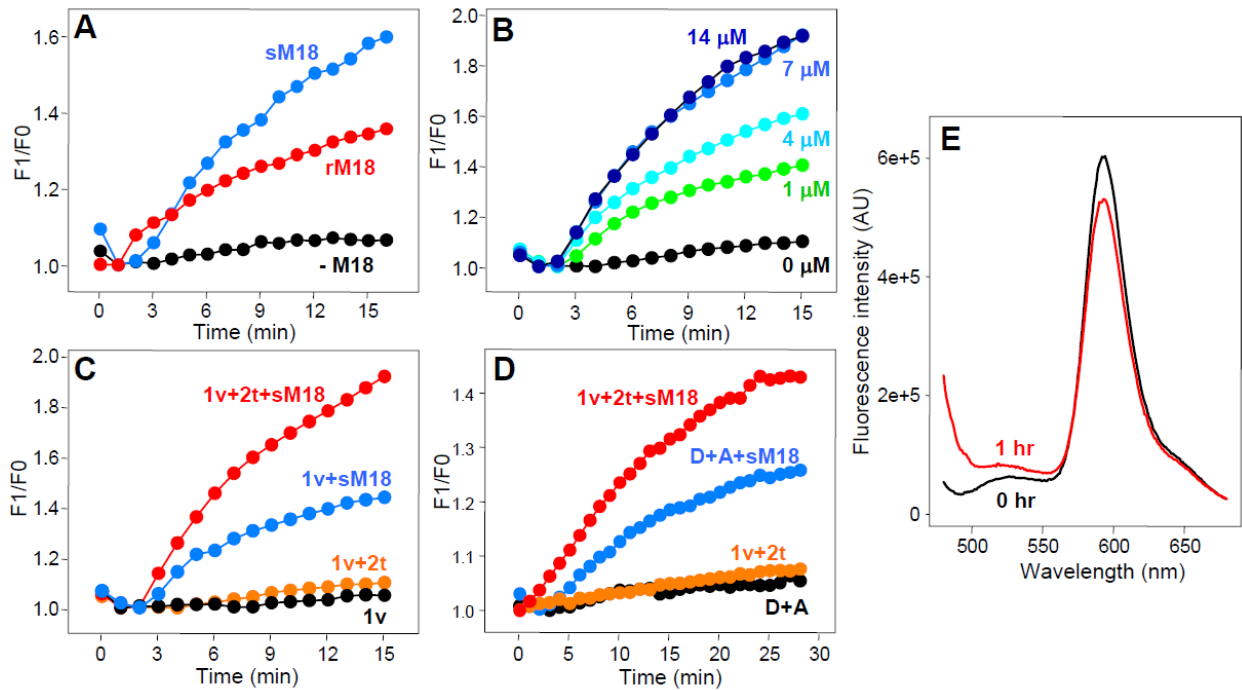


**Figure 2.1: sMunc18-1 can induce SNARE-independent increases in the apparent NBD fluorescence intensity in lipid mixing assays.**

(A-C) Plots of the ratio between observed fluorescence intensity ( $F1$ ) and the initial fluorescence intensity ( $F0$ ) during assays intended to monitor lipid mixing through NBD fluorescence de-quenching. The experiments were performed using proteoliposomes containing synaptobrevin ( $v$ ) or co-expressed syntaxin-1/SNAP-25 ( $t$ ) reconstituted using the standard method with a 1:1000 protein-to-lipid ratio and a lipid composition consisting of POPC:POPE:DOPS:PI:cholesterol 50:20:10:10:10 (molar ratio). In the  $v$ -SNARE liposomes, 3% of POPC was replaced with 1.5% NBD-PE and 1.5% Rho-PE. In (A),  $v$ -SNARE liposomes (50  $\mu$ M lipids) and  $t$ -SNARE liposomes (50  $\mu$ M lipids) were mixed in the absence of Munc18-1 (black circles), or in the presence of 4  $\mu$ M rMunc18-1 (red circles) or 4

$\mu\text{M}$  sMunc18-1 (blue circles). In **(B)**, v-SNARE liposomes ( $50 \mu\text{M}$  lipids) and t-SNARE liposomes ( $100 \mu\text{M}$  lipids) were mixed in the presence of the indicated concentrations of sMunc18-1. In **(C)**, reactions contained v-SNARE liposomes ( $50 \mu\text{M}$  lipids) without (black circles) or with  $7 \mu\text{M}$  sMunc18-1 (blue circles), or v-SNARE liposomes ( $50 \mu\text{M}$  lipids) and t-SNARE liposomes ( $100 \mu\text{M}$  lipids) without (orange circles) or with  $7 \mu\text{M}$  sMunc18-1 (red circles). **(D)** Lipid mixing assays performed similarly to (A-C) but using protein-free donor liposomes “D-Liposomes” ( $50 \mu\text{M}$  lipids) and protein free acceptor liposomes “A-Liposomes” ( $100 \mu\text{M}$  lipids) in the absence (black circles) or presence of  $7 \mu\text{M}$  sMunc18-1 (blue circles), or v-SNARE liposomes ( $50 \mu\text{M}$  lipids) and t-SNARE liposomes ( $100 \mu\text{M}$  lipids) in the absence (orange circles) or presence of  $7 \mu\text{M}$  sMunc18-1 (red circles). For these experiments, the proteoliposomes were prepared with the direct method, using a protein-to-lipid ratio of 1:1000 and a lipid composition consisting of POPC:DOPS 85:15 (molar ratio) (3% of POPC was replaced with 1.5% NBD-PE and 1.5% Rho-PE for donor liposomes and v-SNARE liposomes). All experiments in **(A-D)** were performed at  $37^\circ\text{C}$  monitoring the fluorescence emission intensity at 533 nm (excitation at 460 nm). **(E)** Fluorescence emission spectra of the sample used to perform the experiments with D+A liposomes and  $7 \mu\text{M}$  sMunc18-1 of panel **(D)** (blue circles), at the start of the reaction (black trace) and after 1 hr incubation (red trace). (These experiments were performed by Yi Xu)

There are different methods to reconstitute proteins on liposomes. The above experiments were done with detergent-mediated reconstitution [201], which requires co-solubilization of proteins with phospholipids in the presence of appropriate detergents. The detergents are then removed by various removal steps, in this case dialysis. This is a widely used method to reconstitute proteins in lipid environments; however it is hard to control the size distribution of the liposomes made with this method. Since the size of the liposomes and the curvature of the lipid bilayers have significant effect on membrane fusion, we have repeated some of the key NBD dequenching lipid mixing assays with another reconstitution method called direct incorporation of proteins into preformed liposomes [201]. In this method, plain liposomes are made by extrusion of hydrated lipids through polycarbonate filters with distinct pore sizes. This allows preparation of liposomes with a homogenous size distribution. Proteins solubilized with detergent are then slowly added to the liposome solution and allowed to incorporate. Both t-SNARE and v-SNARE liposomes made with the direct incorporation method gave us time dependent minimal increase in NBD fluorescence signal. Addition of sMunc18-1 to t-SNARE and v-SNARE liposomes again largely increased NBD fluorescence signal (Figure 2.1 D). Surprisingly, addition of sMunc18-1 into the plain liposomes without any SNAREs (same concentration of t-SNARE liposomes without t-SNAREs and v-SNARE liposomes without v-SNARE but including fluorescently labeled lipids) also led to a large increase in NBD fluorescence signal, which is comparable to the addition to t-SNARE and v-SNARE liposomes (Figure 2.1 D). Figures 2.1 A through D show time dependent NBD fluorescence change at a certain wavelength (533 nm). We obtained fluorescence emission scans of plain liposomes immediately after addition of sMunc18-1 and after 1 hour

incubation to show wavelength dependent increase in the fluorescence intensity (Figure 2.1 E). Emission scan experiments showed that there is a strong increase in the fluorescence signal close to excitation wavelength which decays sharply with increasing wavelength. This is a characteristic effect of light scattering, where very strong incident light is scattered by particles that are comparable in size with the excitation wavelength (460 nm) and emission decays sharply with increasing wavelength. When we analyzed these data, we realized that an increase in the fluorescence signal (533 nm) in the lipid mixing assays is a result of increased light scattering instead of dequenching of NBD fluorescence. Increased light scattering should arise from increased size of the macromolecules in our sample. Since there is almost no dequenching of NBD fluorescence, the increase in size should be due to clustering of the liposomes instead of fusion of the liposomes (Figure 2.1 E). Therefore, we hypothesized that sMunc18-1 clusters liposomes and therefore increases light scattering. We tested this hypothesis by adding sMunc18-1 into preformed liposomes made by the extrusion method using 50 nm filters and analyzing with dynamic light scattering (DLS). The DLS results showed that liposomes without sMunc18-1 had distribution of sizes close to 50 nm as expected (Figure 2.2 A, Table 2.1). Addition of s-Munc18-1 at 25 °C did not change the size distribution of the liposomes over 2 hours. Interestingly, the size distribution of the liposomes shifted over 500 nm when we incubated liposomes with sMunc18-1 at 37 °C, which is the temperature at which the NBD fluorescence dequenching experiments had been done (Figure 2.2 B, Table 2.1). Since the size increase in liposomes is massive and we did not observe NBD fluorescence dequenching, this size increase should arise from clustering of liposomes by sMunc18-1. To further test our hypothesis and the reversibility of those

clusters, I performed similar clustering assays and added trypsin to liposomes incubated with sMunc18-1 at 37 °C for 20 minutes. I plotted the auto correlation functions obtained from DLS results for better visualization. After addition of sMunc18-1 into liposomes with a nominal size of 50 nm, the autocorrelation function shifted towards the right, suggesting an increased size with time at 37°C (Figure 2.3 A). Addition of trypsin to the same incubated sample shifted the autocorrelation function back almost exactly to the plain-unclustered liposome state. Investigation of the calculated size distribution of vesicles in multiple experiments revealed that the size of the particles increased from about 50 nm to 500 nm in 15 minutes and more than 90% of the particles returned to their original size of 50 nm after addition of trypsin (Figure 2.3 B,) which is expected to digest sMunc18-1.

Interestingly, small amounts of particles with large size always remained. This observation will be addressed in the following experiments. I also observed the size change with a static light scattering experiment in which I measured scattered light at 350 nm after shining 350 nm light at a right angle to the liposome sample. I observed an increase in scattered light after addition of sMunc18-1 that rapidly returned to almost its original level after trypsinolysis (Figure 2.3 C).

	Temperature(°C)	Time	R <sub>av</sub> (nm)
Liposomes	25/37		55–80
Liposomes+4 μM sMunc18-1	37	5 min	151
Liposomes+4 μM sMunc18-1	37	10 min	>500
Liposomes+4 μM sMunc18-1+1M NaCl	37	10 min	55
Liposomes+4 μM sMunc18-1, after 10 min added 1 M NaCl	37		>500
Liposomes+4 μM sMunc18-1+4 μM Syx	37	10 min	139
Liposomes+4 μM sMunc18-1, after 10 min added 20 μM Syx	37		>500
Liposomes+4 μM sMunc18-1	25	2 hr	60
Liposomes+4 μM sMunc18-1	25	O/N	131

**Table 2.1: Liposome clustering activity of sMunc18-1 under different conditions measured by DLS**

DLS measurements of particle size in samples containing protein-free liposomes (POPC:DOPS 85:15 molar ratio; 30 mM lipids) and the reagents indicated at the left column. The temperature, incubation time and average radius measured (R<sub>av</sub>) are indicated in the other columns.

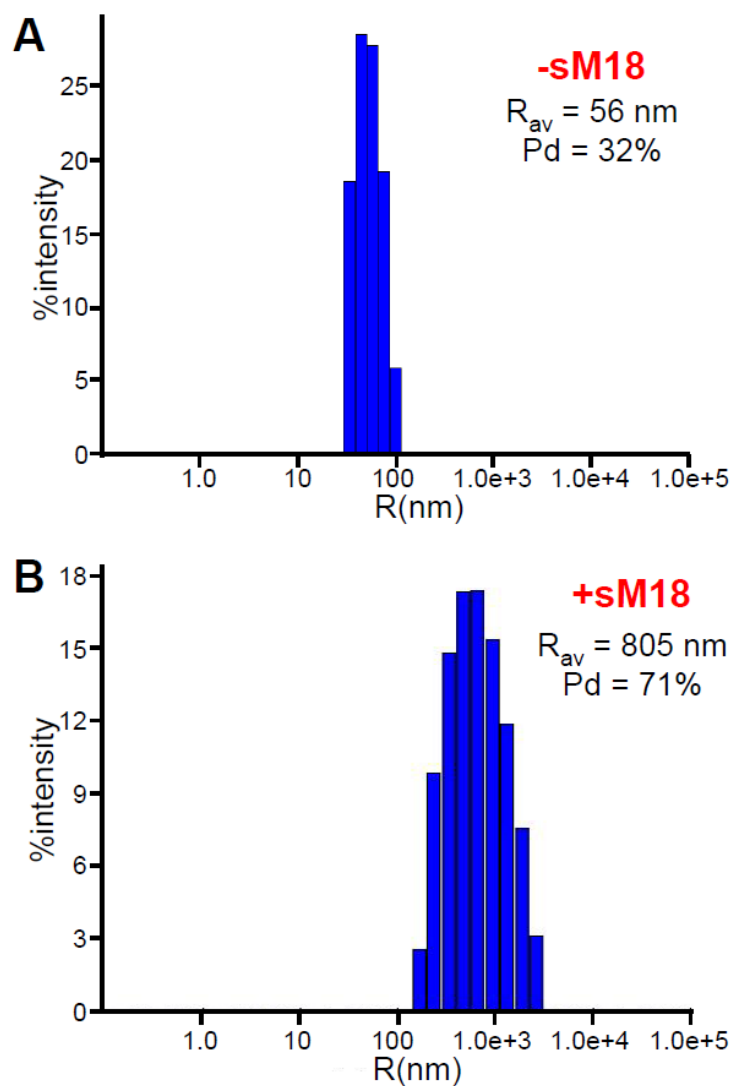


**Figure 2.2: Liposome clustering activity of sMunc18-1.**

(A,B) DLS measurements of particle size in samples containing protein-free liposomes (POPC:DOPS 85:15 molar ratio; 30  $\mu\text{M}$  lipids) in the absence (A) or presence (B) of 4  $\mu\text{M}$  sMunc18-1 after 10 min incubation at 37  $^{\circ}\text{C}$ . The average radius ( $R_{av}$ ) and polydispersity (Pd) are indicated.

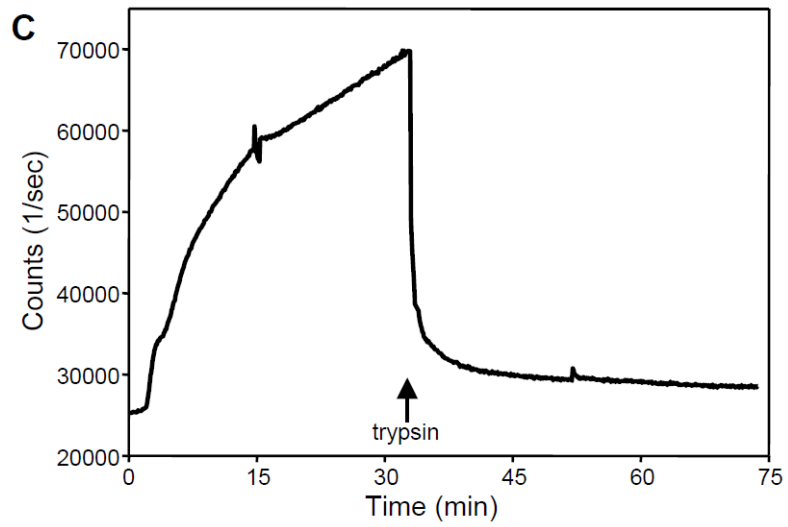
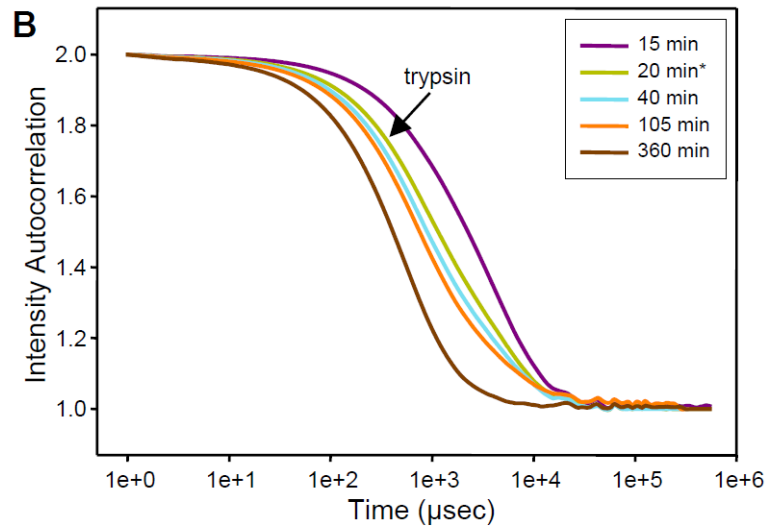
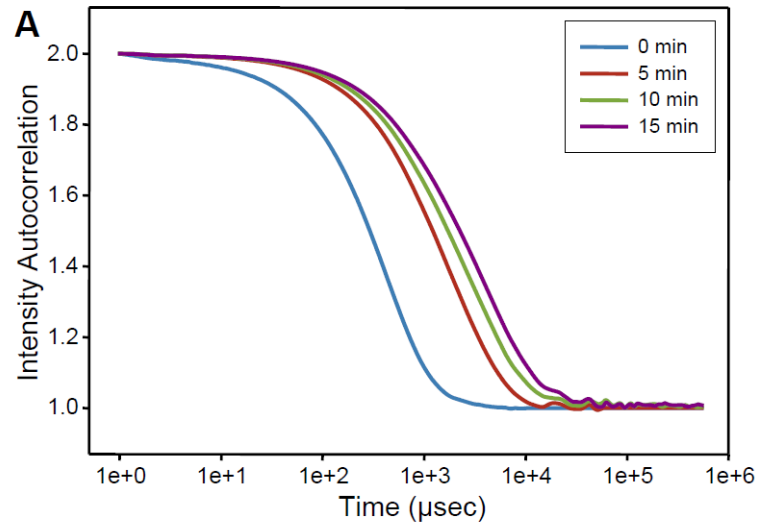


**Figure 2.3: Liposome clustering induced by sMunc18-1 is reversed by trypsinolysis.**

(A,B) Autocorrelation functions obtained by DLS at different time points after mixing protein-free liposomes (POPC:DOPS 85:15 molar ratio; 100  $\mu$ M lipids) with 7  $\mu$ M sMunc18-1 (A), and after adding 0.7  $\mu$ M trypsin at the 20 min time point (B). The insets indicate the color codes for the times at which the data were acquired. Note that the starting point in panel (B) is the same curve as the last point of panel (A), and that the times indicated in panel (B) refer to the beginning of the clustering reaction, rather than the point of trypsin addition. (B) Apparent fluorescence signal intensity at 350 nm (excitation at 350 nm) observed as a function of time after mixing protein-free liposomes (POPC:DOPS 85:15 molar ratio; 100  $\mu$ M lipids) with 7  $\mu$ M sMunc18-1. Trypsin (0.7  $\mu$ M) was added to the reaction at 33 min. All the experiments in panels (A-C) were performed at 37 °C.

These results revealed that sMunc18-1 clusters vesicles under the conditions of the lipid mixing experiments performed, which are physiological ionic strength, temperature and pH. These results were then strongly supported with the cryo-electron microscopy results described in a later section. Liposome clustering by sMunc18-1 resulted in increased light scattering with time because the size of particles became comparable to the excitation wavelength used in the NBD dequenching experiments. Increased light scattering in those experiments interfered with the NBD dequenching results since there is a considerable amount of scattering at the emission wavelength used. Most of the increased light scattering could be reversed upon trypsin digestion of sMunc18-1. DLS of the liposomes showed matching results in which the autocorrelation function shifted to the right with sMunc18-1 incubation and was returned close to the original value upon trypsin digestion. Only <10 % particles remained bigger in these samples (Figure 2.1). All of these results showed that sMunc18-1 would cause limited amount of lipid mixing, fusion, or hemifusion in these experimental conditions. In addition, sMunc18-1 did not cause clustering of liposomes in high salt concentration. This observation can be explained by the following potential reasons. High salt may prevent the initial interaction of sMunc18-1 with phospholipids or may stabilize sMunc18-1 and hinder denaturation of sMunc18-1 with phospholipids. On the other hand, addition of high salt after clustering of liposomes by sMunc18-1 did not reverse the clustering, unlike trypsin digestion. This result suggested that irreversible interaction of sMunc18-1 with liposomes bridges two lipid bilayers, which could be reversed by trypsin digestion of sMunc18-1.

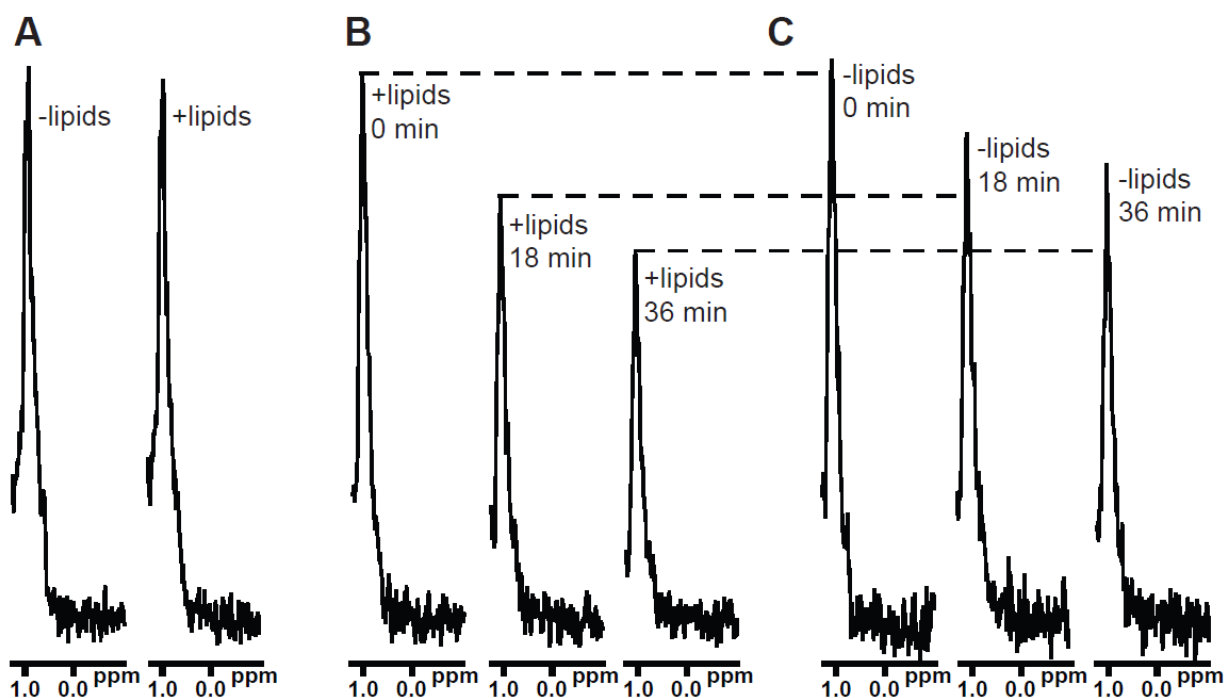


**Figure 2.4: Time-dependent binding of sMunc18-1 to lipids.**

(A) 1D  $^{13}\text{C}$ -edited  $^1\text{H}$ -NMR spectra of  $2\ \mu\text{M}$   $^{13}\text{C}$ -labeled sMunc18-1 in the absence or presence of liposomes (POPC:DOPS 85:15 molar ratio; 1 mM lipids) at  $25\ ^\circ\text{C}$ . (B) 1D  $^{13}\text{C}$ -edited  $^1\text{H}$ -NMR spectra of the same sample containing liposomes in panel (A) acquired as a function of time after the temperature was raised to  $37\ ^\circ\text{C}$ . (C) 1D  $^{13}\text{C}$ -edited  $^1\text{H}$ -NMR spectra of the same sample lacking liposomes in panel (A) acquired as a function of time after raising the temperature to  $37\ ^\circ\text{C}$ . (These experiments were performed by Lijing Su)

### **2.2.2 Denaturation of sMunc18-1 induces clustering of liposomes**

A protein can cause clustering of liposomes if it can interact with 2 membranes simultaneously, such as the case with Synaptotagmin-1 [202]. Co-floatation assays suggested weak binding of Munc18-1 to membranes [113]. To conclusively understand whether Munc18-1 binds to membranes or not, Lijing Su performed NMR experiments to observe the strongest methyl resonance (SMR) of  $^{13}\text{C}$ -labeled Munc18-1 in 1D  $^{13}\text{C}$  edited  $^1\text{H}$ -NMR spectra [203]. In these experiments, the observed SMR from sMunc18-1 will broaden upon binding of to an unlabeled macromolecule due to its increase in size. In the case of Munc18-1 binding to liposomes, the intensity of the Munc18-1 SMR should decrease possibly beyond the detection limit due to the size of the liposomes. However, there was no significant change observed in the intensity of SMR of  $^{13}\text{C}$ -labeled sMunc18-1 after addition of liposomes at 25 °C (Figure 2.4 A), suggesting that there is no interaction between liposomes and sMunc18-1 at 1 mM lipid concentration and 25°C. These experiments were repeated at 37 °C since all the lipid mixing and DLS experiment were performed at this temperature. The SMR intensity of  $^{13}\text{C}$ -labeled sMunc18-1 gradually decreased over time at 37 °C in the presence of liposomes (Figure 2.4 B). The SMR intensity of  $^{13}\text{C}$ -labeled sMunc18-1 also decreased without liposomes but at a much slower rate (Figure 2.4 C). These results can be explained by the following arguments. Slow denaturation of sMunc18-1 can cause aggregation, which leads to the SMR intensity drop. In the presence of liposomes, denaturated sMunc18-1 binds to liposomes and leads to a larger SMR intensity drop. Denaturation of sMunc18-1 leads to binding of its multiple exposed hydrophobic regions with membranes, which causes liposome clustering. Thermal denaturation by circular dichroism (CD) showed that sMunc18-

1 and rMunc18-1 possess very similar and highly cooperative denaturation curves as expected due to their similar structure and fold. However, the midpoint of the sMunc18-1 denaturation curve is shifted 8 °C lower than rMunc18-1 to a value of 43 °C (Figure 2.5). Interestingly, and as expected, sMunc18-1 starts denaturing below 37 °C.

These results also support the idea of clustering by sMunc18-1 denaturation at these conditions. The relative thermal stability of rMunc18-1 over sMunc18-1 correlates with the higher increase caused by sMunc18-1 in the lipid mixing assays (Figure 2.1 A).

We have further tested whether denaturation of sMunc18-1 is responsible for the liposomes clustering. Addition of 15% glycerol, which is a well-known stabilizing agent, prevented the clustering activity of sMunc18-1 (Figure 2.6). Pre-incubation of sMunc18-1 with syntaxin-1 also prevented the clustering activity of sMunc18-1, since the interaction of sMunc18-1 and syntaxin-1 stabilizes both proteins [106, 191]. Additionally, sMunc18-1 failed to cluster liposomes at 25 °C after 2 hours of incubation and a small percentage clustering was observed after overnight at 25 °C (Table 2.1). All of these results strongly suggest that sMunc18-1 denatures and clusters liposomes over time at 37 °C.

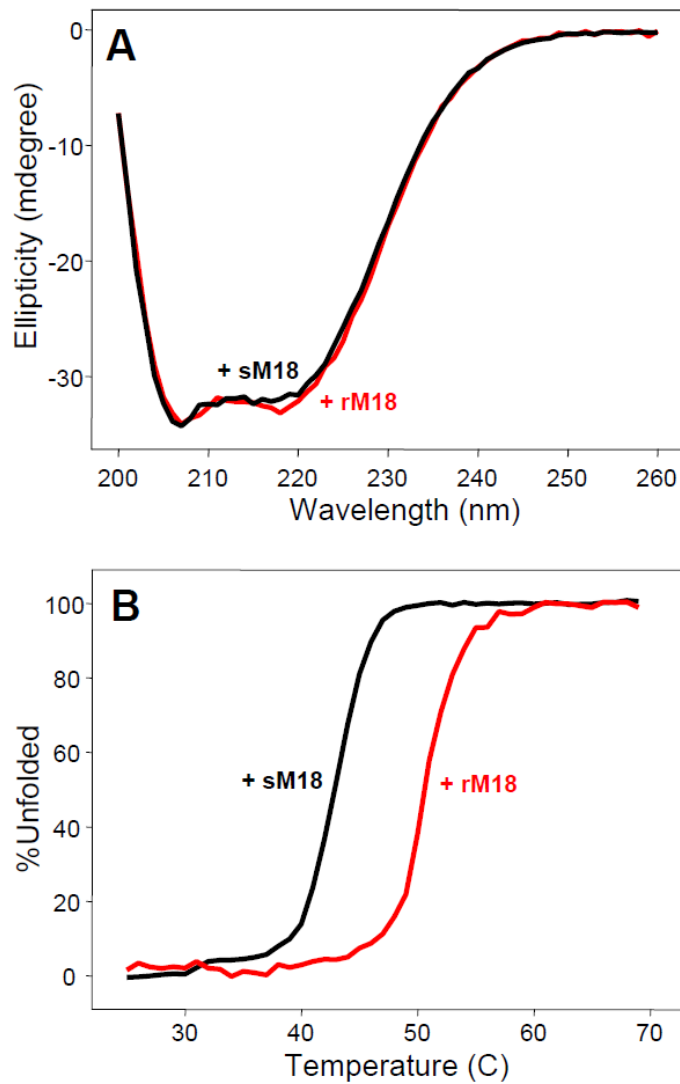


**Figure 2.5: sMunc18-1 is less stable than rMunc18-1.**

(A) CD spectra of sMunc18-1 (black) and rMunc18-1 (red) at 25 °C in phosphate buffer saline (PBS), pH 7.4. (B) Thermal denaturation curves of sMunc18-1 (black) and rMunc18-1 (red) monitored through the CD absorption at 220 nm. The  $T_m$  values calculated for sMunc18-1 and rMunc18-1 are 43 °C and 51 °C, respectively. (These experiments were performed by Yi Xu)

### **2.2.3 Visualization of clustering and hemifusion of liposomes induced by sMunc18-1 Using Cryo-EM**

I used cryo-electron microscopy (cryo-EM) to visualize sMunc-18-1 on liposomes at 37 °C. Liposomes without sMunc18-1 showed homogenously dispersed vesicles without inter-liposome interactions with the expected size and spherical shape. Addition of sMunc18-1 to liposomes at 37 °C led to many large liposomes clusters (Figure 2.7 A) with very short inter-membrane distances (Figure 2.7 A –Yellow Arrows and Figure 2.7 B). The distances between membranes are typically less than 2 nm, which is smaller than a sMunc18-1 molecule whose smallest dimension is 4.5nm according to its crystal structure [204]. Membrane flattening and breaks in the membrane curvature were observed in most of the large inter-membrane interfaces (Figure 2.7 B). Very rare cases of blurring of inter-membrane interfaces were observed, suggesting fusion of the outer leaflet of membranes during fast freezing of the sample (Figure 2.7 C). Many cases of hemifusion of the membranes were also observed (Figure 2.7 A - Red Arrows and Figure 2.7 D).

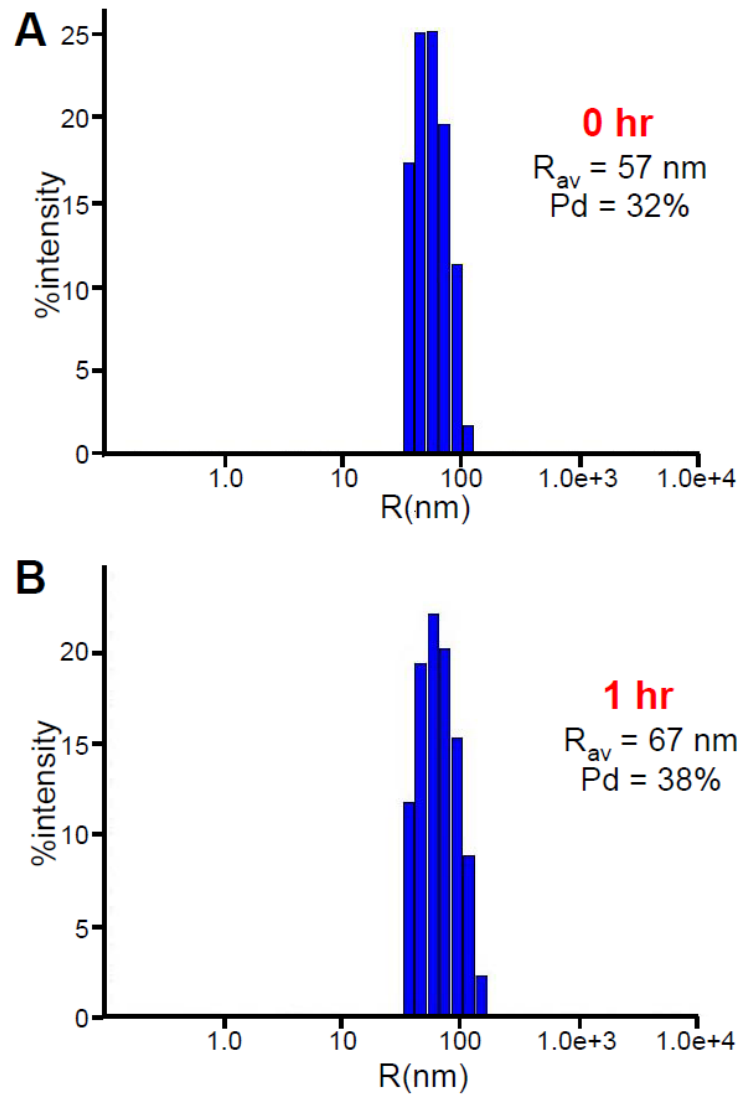


**Figure 2.6: Glycerol hinders the liposome clustering activity of sMunc18-1.**

(**A,B**) DLS measurements of particle size in samples containing 15% glycerol, protein-free liposomes (POPC:DOPS 85:15 molar ratio; 30  $\mu\text{M}$  lipids) and 4  $\mu\text{M}$  sMunc18-1 right after mixing (**A**) and after 1 hr incubation at 37  $^{\circ}\text{C}$  (**B**). The average radius ( $R_{av}$ ) and polydispersity (Pd) are indicated. (These experiments were performed by Yi Xu)

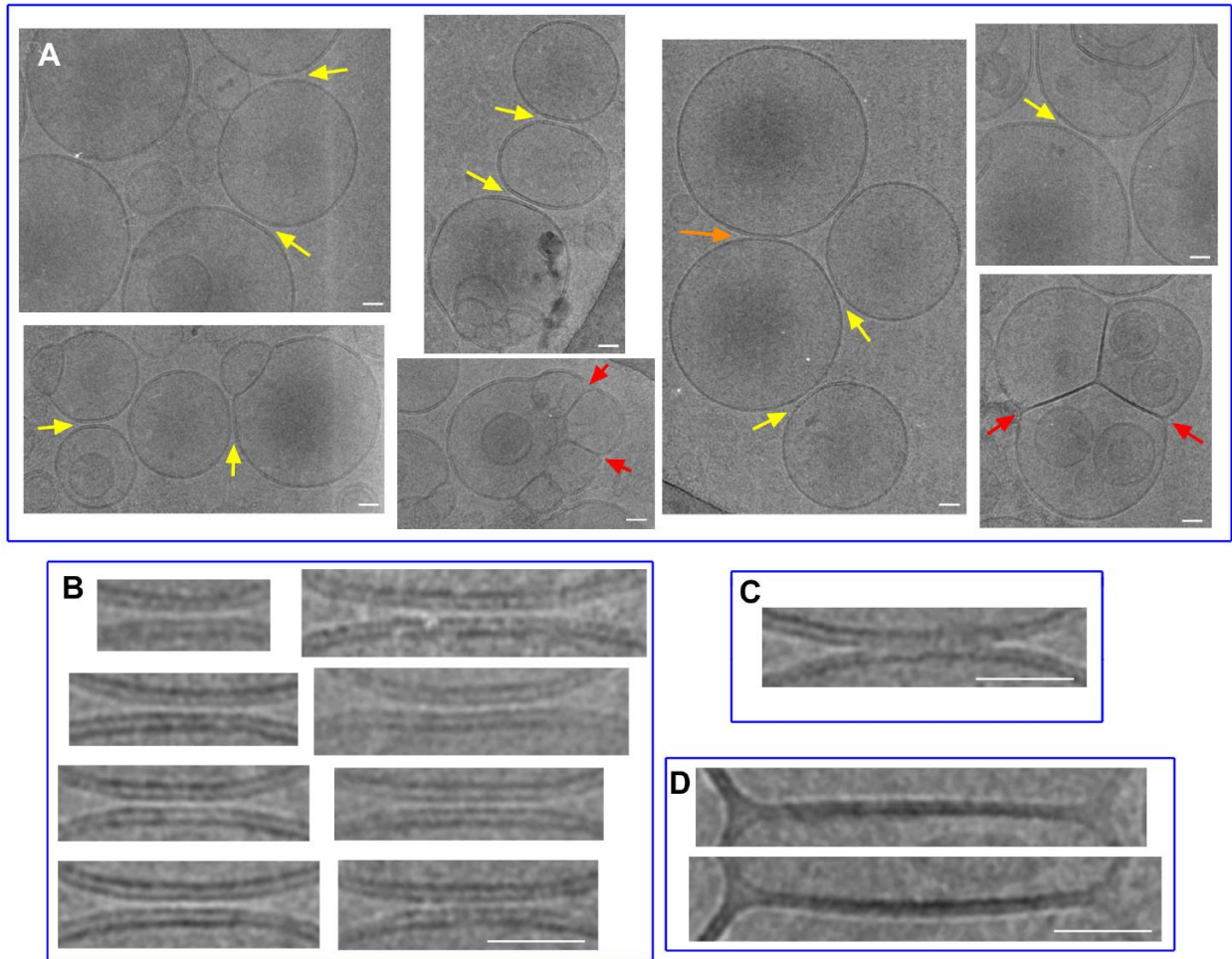


**Figure 2.7: Cryo-EM analysis of liposome clusters induced by sMunc18-1.**

(A) Gallery of cryo-EM images of selected liposome clusters observed in a sample containing sMunc18-1 (30  $\mu$ M) and liposomes (POPC:DOPS 85:15 molar ratio; 2.5 mM lipids). The sample was incubated for 5 min at 37  $^{\circ}$ C after mixing, and was fast-frozen after loading onto the EM grid. (B-D) Expanded views of close interfaces between liposomes (B), of one interface where the bilayers appear to have been mixing at the moment the sample was frozen (C), and of hemifusion diaphragms (D). The three types of liposome interfaces are

indicated with yellow, orange and red arrows, respectively, in panel (A). The scale bars correspond to 20 nm.

All of these results showed that sMunc18-1 can cause liposome clustering and hemifusion, which does not show any of the typical observations of the conventional stalk model of membrane fusion (Figure 2.8). Both the denaturation results and cryo-EM results suggest a model for sMunc18-1 liposomes clustering. sMunc18-1 should penetrate into membranes since the clustered membranes are very close to each other (Figure 2.7 A and B), and denaturation of sMunc18-1 is directly related to its clustering activity. The extended membrane interfaces and breaks in the membrane curvature suggest that multiple sMunc18-1 molecules are responsible for its clustering activity. The size of the membrane interfaces appears to be correlated to the necessity of multiple sMunc18-1 molecules. Lipid mixing can be explained by destabilization of apposing membranes that are bridged by multiple denaturated sMunc18-1 molecules, which eventually results in merging of the outer layers of apposing membranes to form the hemifused state (Figure 2.7 A-D, Figure 2.8). Not all apposing membranes are merged and form hemifusion probably, because merging membranes requires high energy so it is a slow reaction (Figure 2.1 E).

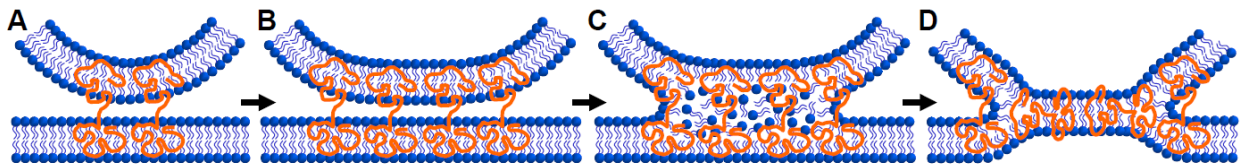


**Figure 2.8: Proposed model of how a denatured protein can induce membrane hemifusion without proceeding through a stalk intermediate.**

The model postulates that denatured proteins (represented as orange randomly shaped curves), and perhaps other amphipathic macromolecules, can induce hemifusion by binding to two membranes (**A**), accumulating at the membrane-membrane interface (**B**), and causing a scrambling of lipid molecules at the interface (**C**) that eventually rearranges into a stable hemifusion diaphragm (**D**). A curved membrane from a vesicle and a flat membrane are used in the drawings, but the mechanism could apply to membranes with diverse curvatures.

### ***2.3 Discussion***

In vitro reconstitution experiments are vital to reveal important mechanistic and functional roles of proteins in membrane fusion assemblies. However, the results obtained in these reconstitution experiments should be well correlated with in vivo studies since they are missing many other components of the studied machineries and the rest depend on the experimental conditions such as protein to lipid ratio and method of liposomes preparation. The lipid composition of the membranes, the method of reconstitution, the protein to lipid ratio, and some other experimental conditions are very important details that may alter the results in many different directions. For example, there have been contradictory models of membrane fusion proposed previously depending on reconstitution assays. Initial studies reported that the neuronal SNAREs are the minimal machinery to fuse membranes [33] but, later, other studies reported very diverse results from similar reconstitution assays with neuronal SNAREs [34]. The notion that the SNAREs constitute a minimal fusion machinery model is contradictory with the vital dependence of synaptic vesicle fusion on Munc18-1 and SM proteins. Therefore, it is very important to unravel the critical function of Munc18-1 in synaptic vesicle fusion. Several models have been proposed about the function of Munc18-1 [34, 175] and some aspects of the reconstitution experiments have supported these models, suggesting that Munc18-1 stimulates SNAREs-driven membrane fusion in general [192, 196, 198] and Munc18-1 is strictly required to initiate the fusion of the membranes used in the reconstitution assays [197]. Even though these studies shed light onto the function of Munc18-1 on synaptic vesicle fusion, these studies did not provide any information about how Munc18-1 works to facilitate or trigger membrane fusion. Munc18-1 might directly be

involved in membrane fusion or merely stimulate or help SNAREs to form the SNARE complex. In this study we showed that membranes can lose their integrity due to denatured sMunc18-1 molecules. sMunc18-1 can bind to two membranes simultaneously and eventually cause hemifusion. Both the clustering and the hemifusion activities of sMunc18-1 require denaturation. Our results also show that NBD dequenching assays should be carefully examined and supplemented with several other types of experiments, especially *in vivo* assays. In addition, hemifusion of membranes by denatured sMunc18-1 shows a novel example of membrane fusion induced by amphipathic macromolecule.

It is very unlikely that the membrane clustering and the hemifusion activities of denatured sMunc18-1 are physiologically relevant for the mechanism of neurotransmitter release because those activities can simply be prevented by addition of glycerol and high salt (Figure 2.6 and Table 2.1) and there is evidence that some other proteins, like  $\alpha$ -lactalbumin, are unrelated to intracellular membrane fusion, but cause membrane fusion induced by denaturation [205]. However, these proteins can only fuse membranes under acidic conditions that also affect the stability of the membranes [205]. On the other hand, sMunc18-1 shows its membrane clustering and hemifusion activity at physiological pH levels. Another notable property of sMunc18-1 is its efficiency. Small denatured fractions of sMunc18-1 can cluster liposomes extensively in 10 minutes (Table 2.1 and Figure 2.2). Even though denaturation of a whole protein and extensive membrane interfaces are unlikely to be physiologically relevant, we should still consider that the actual mechanism of release may involve partial denaturation or a rearrangement of a part of Munc18-1 that exposes some hydrophobic residues to perturb membrane integrity. We should also consider that an

unknown conformational state of sMunc18-1 can also explain the fusogenic activity of sMunc18-1 in our studies. However, a conformational change of a protein in a membrane environment is intrinsically hard to study.

A yeast study assigned a direct role for Sec1p, the SM protein in yeast membrane fusion process. This study showed that Sec1p plays a functional role after SNARE complex assembly [206]. This observation and the results reported in our study suggest that SM proteins may fulfill a direct and vital role on membrane fusion, which involves interaction of SM protein and membranes. Therefore, the potential physiological relevance of the results presented here should not be completely discarded. A speculative model that explains all of these results would be the following. The SNARE complex formation brings two membranes in close proximity and the integrity of the membranes may be destabilized by a conformational change or partial denaturation of SM protein.

Cryo-EM images that are reported here (Figure 2.7) provide compelling evidence for a novel mechanism of how an amphipathic molecule leads to membrane bridging and hemifusion of those membranes without involving a stalk intermediate (Figure 2.8). Physiological relevance of this mechanism is unclear. Formation of extended hemifusion and double-membrane diaphragms (Figure 2.8) do not seem to be compatible with the small size (40 nm) of synaptic vesicles and microsecond time scale of the fusion pore formation in neurotransmitter release [11]. However, it is still possible that an extension of this mechanism in the presence of other proteins involved in neurotransmitter release may account for the actual mechanism of membrane fusion.

Hemifusion of the membranes is obviously not enough for merging of the environment of the two opposing membranes, however; additional factors might help Munc18-1 to cause complete fusion of these opposing membranes. Nevertheless, the observation of extensive membrane interfaces (Figure 2.7 and Figure 2.8) seems to be incompatible with the small size of the synaptic vesicles (about 40 nm in diameter [207]). We should still keep in mind that not all type of membrane fusion are as fast as synchronous neurotransmitter release and additional factors may limit the extension of the membrane interfaces and accordingly hemifusion and the time scale of the whole fusion event. In addition to neurotransmitter release, other membrane fusion events such as homotypic vacuolar fusion, which requires large and flat opposing double membrane ring formation, may show similarities to observations we obtained with the cryo-EM images [208]. This observation from yeast vacuolar fusion *in vivo* provided structural evidence that extended membrane interfaces similar to the ones caused by sMunc18-1 exist in nature.

NBD dequenching assays are very important tools to study lipid mixing between membranes in any membrane fusion machineries. However, as reported in our study and others, NBD dequenching assays should not be over interpreted as complete membrane fusion and they should be complemented with other *in vitro* studies and correlated with *in vivo* results. A study that incorporated complementary DNA fragments to different liposomes also showed very strong lipid mixing about 80% but only limited amount of content mixing about 2% between those liposomes [209]. The results reported here show that simply liposome clustering can increase the fluorescence intensity that is observed and commonly interpreted as lipid mixing or even membrane fusion in NBD dequenching assays. All lipid mixing starts

with bridging membranes and fusion of those membranes does not give rise to massive increase in the size of the liposomes, however clustering of the liposomes without complete fusion increases the apparent size of the liposomes/macromolecules in NBD dequenching assays and increase the observed light scattering due to size difference of the macromolecules interferes with NBD signal observed in these assays. These scenarios affect the interpretation of lipid mixing results and therefore lead to over interpretation of membrane fusion.

The extent of the scattering effect of liposome clustering on NBD dequenching assays is determined by both the magnitude of the clusters and also technical parameters of the NBD dequenching assay, most importantly the excitation and the emission wavelengths that are used to monitor the NBD fluorescence intensity over time. The effect of the light scattering on NBD dequenching assay can be visualized by acquiring the complete fluorescence emission spectrum of NBD just before and after each time course experiment, which involves single wavelength acquisition (Figure 2.1 E). The increased tail on the left side of the spectrum before the NBD peak in Figure 2.1 E shows a perfect example of interference of light scattering on the NBD signal. Trypsin may also be used to assess the clustering effect as we used in this study.

Importantly, this study should not be interpreted as all the articles that used primarily NBD dequenching assays to study membrane fusion are misguided. On the other hand, this study strongly demonstrates that NBD dequenching assays may not be used without other proper controls and other techniques to study membrane fusion, actually not even lipid mixing. Fortunately, there are other well developed assays to complement NBD dequenching assays.

Monitoring lipid mixing by increase in FRET during lipid mixing of two fluorophores reconstituted into separate v-liposomes and t-liposomes, instead of decrease as in NBD dequenching assays is a replacement assay for NBD dequenching which provides numerous advantageous over NBD dequenching assays. (For example, loss of membrane integrity may be interpreted as lipid mixing in NBD dequenching assays but not in alternative method). Most importantly, a number of content mixing assays have been developed to validate complete membrane fusion lacking membrane leakiness [178, 180, 198]. At the end, cryo-EM should be used as the most powerful and accurate technique to understand the structure and integrity of the membranes during fusion reactions as the cryo-EM images of the membranes provided vital information in this study. Although many components of the fusion machinery have been reconstituted to study membrane fusion, it is still unclear how the membranes are perturbed to initiate membrane merging. Our results demonstrate that denaturation of amphipathic molecules should be considered as a potential actor in the membrane fusion mechanism.

## ***2.4 Materials and Methods***

### **2.4.1 Recombinant Proteins and Protein Purification**

Purification of rat Munc18-1, squid Munc18-1, rat synaptobrevin, rat syntaxin-1 and rat SNAP-25 is explained in the methods section of the fourth chapter of this manuscript.

#### **2.4.2 Preparation of Liposomes and Reconstitution of the SNAREs**

The 1-palmitoyl-2-oleoyl-sn-glycero-3-phosphatidylcholine (POPC), palmitoyl-2-oleoyl-sn-glycero-3-phosphoethanolamine (POPE), 1,2-dioleoyl-sn-glycero-3-phospho-L-serine (DOPS), phosphatidylinositol (PI) and cholesterol (Avanti Polar Lipids) in chloroform were mixed in a glass test tube in a POPC: POPE: DOPS:PI:cholesterol; 50:20:10:10:10 molar ratio and POPC:DOPS; 85:15 molar ratio. Chloroform was evaporated using dry nitrogen stream and the lipids were placed in a vacuum chamber overnight for complete removal of the organic solvent. Fluorescent donor liposomes included 1.5% N-(lissamine rhodamine B sulfonyl)-1,2-dipalmitoyl-sn-glycero-3-phosphatidylethanolamine (Rho-PE) and 1.5% N-NBD-1,2-dipalmitoyl-sn-glycero-3-phosphatidylethanolamine (NBD-PE) by replacing 3% POPC.

Lipid films were hydrated with reconstitution buffer (25 mM HEPES pH 7.4, 100 mM KCl, 2 mM MgCl<sub>2</sub>, 2 mM DTT) in an appropriate volume yielding 15 mM lipids. Lipids were vortexed for 5 minutes then frozen and thawed five times. Large unilamellar vesicles were prepared by extruding the hydrated lipid solution through 0.08- $\mu$ m polycarbonate membranes 23 times using an Avanti Mini-Extruder.

For direct method, proteins were solubilized in reconstitution buffer containing 1%  $\beta$ -OG + 1 mM TCEP were incubated on room temperature for 20 minutes and then slowly titrated to the preformed liposomes, while vortexing the liposomes. Volume of the protein was adjusted to keep the final concentration of  $\beta$ -OG below the solubilization concentration of the proteoliposomes. Proteoliposomes were incubated at room temperature for 20 minutes and

dialyzed 3 times against 1 L reconstitution buffer containing 1 g Bio-Beads (Bio-Rad) through a 10 kDa dialysis cassette for 1 hour, 2 hours and 16 hours at 4°C.

For standard method, proteins were solubilized in reconstitution buffer containing 1%  $\beta$ -OG + 1mM TCEP and incubated on room temperature for 20 minutes. Proteins were mixed with detergent solubilized lipids yielding 5 mM lipids and 5  $\mu$ M SNARE proteins. Protein-lipid solutions were incubated at room temperature for 20 minutes and quickly diluted with reconstitution buffer. Protein-lipid solutions were dialyzed 3 times against 1 L reconstitution buffer containing 1 g BioBeads (BioRad) or Amberlite XAD-2 (Sigma-Aldrich) through a 10 kDa dialysis cassette for 1 hour, 2 hours and 16 hours to remove the detergent at 4°C.

### **2.4.3 Lipid Mixing Assays**

Lipid mixing experiments using NBD emission at 533 nm were performed on a Photon Technology International spectrofluorometer with a 4 nm slit width and 460 nm excitation at 37 °C. The samples were prepared by mixing individual proteoliposomes and proteins in reconstitution buffer at the concentrations stated in the figure legends. Entire NBD emission was also acquired for selected samples before and after 1 hour reaction. The same spectrofluorometer was used to monitor the apparent fluorescence signal intensity at 375 nm as a function of time in the scattering assay of Figure 2.3 C (350 nm excitation).

### **2.4.4 Dynamic Light Scattering**

Samples were analyzed with a Protein Solutions DynaPro instrument from Wyatt Technology equipped with a temperature-controlled micro-sampler. Data were acquired for

each sample with 10 % laser power and 10 seconds acquisition time for 30 times. The samples were prepared in reconstitution buffer and diluted to a final lipid concentration of 30  $\mu$ M or 100  $\mu$ M lipids and centrifuged at 14,000 x g for 10 minutes before each acquisition. The results were analyzed with the Dynamics V6 software to calculate the size distribution of the macromolecules in the samples.

#### **2.4.5 NMR Spectroscopy**

NMR spectra were acquired on Varian INOVA600 spectrometer equipped with a cold probe. 1D  $^{13}\text{C}$ -edited  $^1\text{H}$  NMR spectra were acquired for 2  $\mu\text{M}$   $^{13}\text{C}$ -labeled sMunc18-1 dissolved in 20 mM HEPES (pH 7.4), 120 mM KCl, 1 mM TCEP in the presence and absence of 1 mM plain liposomes containing POPC and DOPS in a 85:15 molar ratio using  $\text{H}_2\text{O} / \text{D}_2\text{O}$  95:5 (volume / volume) as the solvent. Total acquisition times were 18 minutes and 1,000 scans were averaged for each spectrum. NMR data were processed with NMRPipe [210] and analyzed with NMRView [211].

#### **2.4.6 Circular Dichroism**

CD spectra were acquired with an Aviv model 62DS spectropolarimeter using a cuvette with 1 mm path length for both rMunc18-1 and sMunc18-1 samples. The samples were prepared in PBS buffer (pH 7.4). CD spectra for thermal denaturation curves were acquired at 220 nm. The fraction of unfolded protein for the thermal denaturation curves was calculated using the formula  $100 \times (I_{\text{obs}} - I_{\text{f}}) / (I_{\text{u}} - I_{\text{f}})$ , where  $I_{\text{obs}}$  is the observed signal intensity, and  $I_{\text{u}}$  and  $I_{\text{f}}$  are the signal intensities of the unfolded and folded states, respectively.

### 2.4.7 Cryo-Electron Microscopy

Both sides of Quantifoil 200 mesh copper, R2/2 hole shape, 2  $\mu$ m hole size and 4  $\mu$ m period grids were glow discharged in Denton Vacuum DV-502A instrument with 40 mA current for 45 seconds. 0.5 ml amylamine dropped Whatman paper was immediately used during glow discharging to prevent extensive sticking of liposomes onto carbon. 2.5 mM liposomes were incubated with 30  $\mu$ M sMunc18-1 in reconstitution buffer with 1 mM  $MgCl_2$  at 37°C for 5 minutes. 3  $\mu$ l of the sample is loaded onto the carbon side of a Quantifoil grid, incubated for 10 seconds and blotted with a piece of Whatman #4 paper from the edge of the grid for 5 seconds. Another 3  $\mu$ l of the sample was loaded onto the same side of the grid and rapidly frozen using Vitrobot FP 5350/60 type automated vitrification robot. Blotting time was 2.5 seconds and the humidity in the blotting chamber was above 90%. Standard Vitrobot Filter paper, Ø55/20mm, Grade 595 was used for blotting. Images were taken with an energy filter included JEOL 2200FS FEG transmission electron microscope at cryo temperatures keeping samples on an Oxford Instruments cryo holder. Images were taken at 61.95K calibrated magnification and recorded on a 2Kx2K Tietz slow scan CCD camera and Kodak SO-163 type films. Electron density was kept at 20-30 electrons/ $\text{Å}^2$  during each exposure by a minimum dosage system. Films were scanned with PhotoScan Instrument from Z/I Imaging at 14  $\mu$ m resolution. An extensive examination of whole area on grids was necessary due to massive vesicle fusion.

## CHAPTER 3

### 3 PREVALENT MECHANISM OF MEMBRANE BRIDGING BY SYNAPTOTAGMIN-1

#### 3.1 Introduction

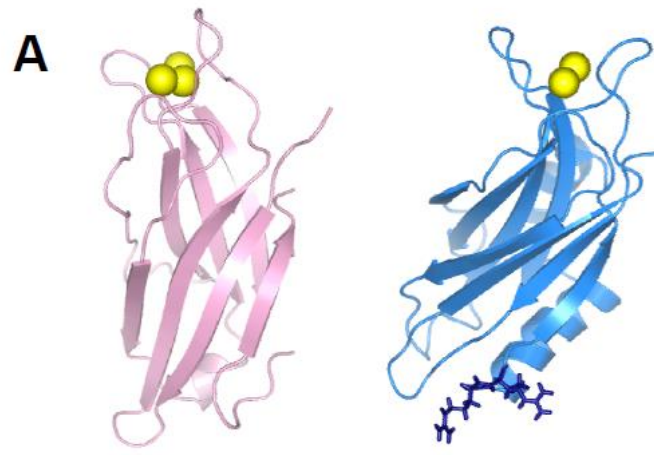
Synaptotagmin-1 is a conserved protein and vital for synchronous neurotransmitter release, which is a tightly regulated  $\text{Ca}^{2+}$  dependent process [212]. The synaptic vesicle protein synaptotagmin-1 acts as a  $\text{Ca}^{2+}$  sensor in fast release through the two  $\text{C}_2$  domains that form most of its cytoplasmic region (the  $\text{C}_2\text{A}$  and  $\text{C}_2\text{B}$  domains) [130, 135, 213-217] (Figure 3.1 A). This function is coupled to membrane fusion through the neuronal soluble N-ethylmaleimide sensitive factor adaptor protein receptor (SNARE) proteins [218, 219], which bring the synaptic vesicle and plasma membranes together by forming SNARE complexes [213, 215]. These SNARE proteins are highly conserved through different organisms and intracellular membrane fusion machineries, suggesting a common mechanism of membrane fusion which is carried out by SNAREs. The synaptotagmin-1  $\text{C}_2$  domains bind three or two  $\text{Ca}^{2+}$  ions through loops at the top of  $\beta$ -sandwich structures and these top loops also mediate  $\text{Ca}^{2+}$ -dependent phospholipid binding [135, 220].

The function of synaptotagmin-1 in neurotransmitter release is also tightly regulated by the interaction of the SNARE complex with complexins [221-223] as well as many other regulatory proteins in the process [66, 224]. *In vitro* experiments showed that the cytoplasmic

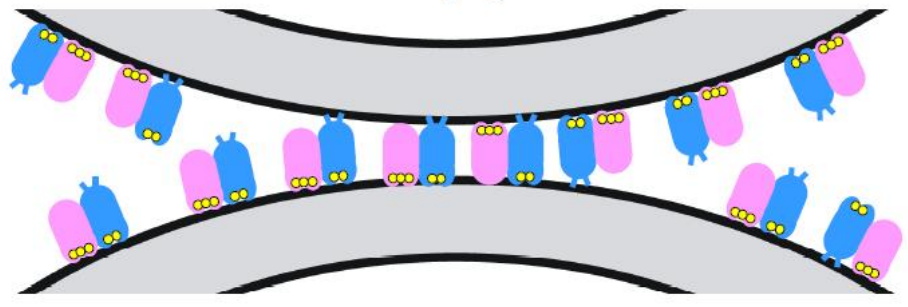
region of synaptotagmin-1 which is composed of mostly the two C<sub>2</sub> domains was able to aggregate liposomes and chromaffin granules [225]. A later cryo-EM study showed that a fragment of synaptotagmin-1 containing only the two C<sub>2</sub> domains can cluster vesicles by interacting with two membranes and bringing them into close proximity (~4 nm) [202].

In the same study it was discovered that C<sub>2</sub>B alone is sufficient for the vesicle clustering activity of synaptotagmin-1, which can explain the important role of Ca<sup>2+</sup> binding to the C<sub>2</sub>B domain in neurotransmitter release [202].

Mutation of two arginine residues at the bottom of the C<sub>2</sub>B domain (R398 and R399) strongly impairs neurotransmitter release, the liposome-clustering activity, and the ability to stimulate SNARE-dependent lipid mixing between liposomes indicating that these residues are important for the interaction between synaptotagmin-1 and the negatively charged phospholipid membranes [218]. Taken together these results suggest that synaptotagmin-1 facilitates membrane fusion by directly bridging the two membranes cooperatively with the SNARE complex in response to Ca<sup>2+</sup> influx through its arginine residues located at the bottom of the C<sub>2</sub>B domain and the Ca<sup>2+</sup> binding loops located at the top [131, 202, 218].



**B** direct bridging model



**C** oligomerization model

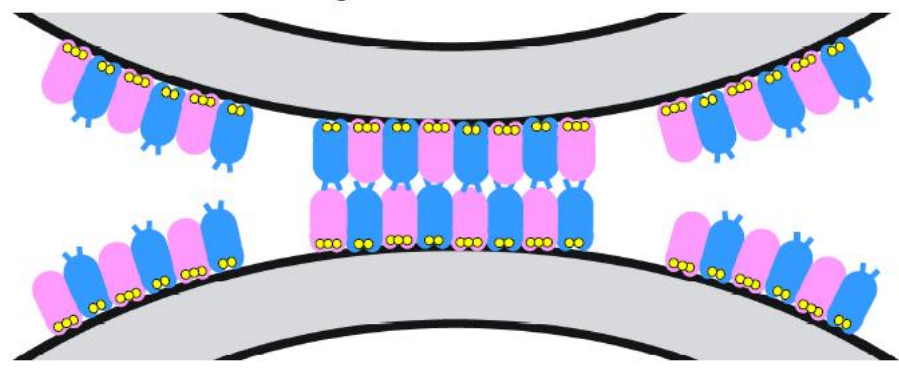


**Figure 3.1: Two models of membrane bridging by synaptotagmin-1.**

(A) Ribbon diagrams of the synaptotagmin-1 C<sub>2</sub>A domain (40) (left) and C<sub>2</sub>B domain (15) (right). Ca<sup>2+</sup> ions are shown as yellow spheres. The two arginines at the bottom of the C<sub>2</sub>B domain (R398 and 399) are shown as blue stick models.

(B) Direct bridging model whereby the C<sub>2</sub> domains bind simultaneously to the two apposed membranes, resulting in an inter-membrane distance of ca. 4 nm. The C<sub>2</sub>A and C<sub>2</sub>B domains are shown in pink and blue, respectively, with the Ca<sup>2+</sup> ions bound to the top loops in yellow; the R398 and R399 side chains at the bottom of the C<sub>2</sub>B domain are represented by blue lines. The diagram is meant to illustrate that the two C<sub>2</sub> domains can have parallel or antiparallel orientations, with the Ca<sup>2+</sup>-binding loops binding to the same membrane or to opposite membranes. R398 and R399 can cooperate in bridging in both orientations, but are more critical for bridging in the parallel orientation. Bridging requires multiple C<sub>2</sub>AB molecules but does not involve interactions between them (20). Oligomerization model whereby bridging is mediated by *trans* interactions between oligomers bound to separate membranes, resulting in an inter-membrane distance of ca. 8-9 nm. The model postulates that only the Ca<sup>2+</sup>-binding loops contact the membranes while R398 and R399 do not, instead mediating protein-protein interactions (29). The putative binding mode between oligomers is unknown and hence the model of interactions between the bottom sides of the C<sub>2</sub> domains shown is arbitrary.

The membrane bridging activity of synaptotagmin-1 is further supported by an EPR study, as well as many others, providing a vast amount of evidence suggesting that this membrane bridging by synaptotagmin-1 is physiologically relevant [218, 226-233]. However, a recent study proposed a different model of membrane bridging by synaptotagmin-1 in which oligomerized synaptotagmin-1 bridges the two membranes [230]. In this model, only the  $\text{Ca}^{2+}$  binding loops interact with membranes, while the arginines located at the bottom of the  $\text{C}_2\text{B}$  domain are involved in the oligomerization. This model is called the oligomerization model and is depicted in Figure 3.1 B along with our direct bridging model in Figure 3.1 C. The oligomerization model was supported by showing that the arginines at the bottom of the  $\text{C}_2\text{B}$  domain do not interact with phospholipid membranes using 7-nitrobenz-2-oxa-1,3-diazole (NBD) dequenching assays in the same study [230] but this data directly contradicts previous NBD dequenching assays which suggested the interaction of those arginines with phospholipid membranes [202]. Another study reported  $\sim 9$  nm intermembrane distances between vesicles bridged by the cytoplasmic region of synaptotagmin-1 [229] which is consistent with the oligomerization model. It is important to note that a longer fragment of synaptotagmin-1 was used in both of these studies. This longer fragment contains two  $\text{C}_2$  domains and almost the entire linker between  $\text{C}_2\text{A}$  and the N-terminal transmembrane region (Synaptotagmin-1 95-421) [229, 230]. On the other hand, the study that led to the direct bridging model used a fragment of synaptotagmin-1 containing only two  $\text{C}_2$  domains without the preceding N-terminal linker (Synaptotagmin-1 140-421) [202]. Throughout this chapter the longer fragment will be referred as  $\text{InC}_2\text{AB}$  and the shorter fragment will be referred as  $\text{C}_2\text{AB}$ .

It is important to investigate these contradictory results to further understand the synaptotagmin-1 membrane bridging activity and elucidate the molecular mechanism of neurotransmitter release and membrane fusion. I have performed a series of experiments focusing on the conflicting results that these studies provided to understand whether two slightly different synaptotagmin-1 fragments, lnC<sub>2</sub>AB and C<sub>2</sub>AB, behave differently and bridge membranes with different mechanisms. Our study showed, along with previous results, that both lnC<sub>2</sub>AB and C<sub>2</sub>AB behave similarly in solution and have no detectable aggregation. Both of these fragments exhibit the same mechanism of membrane bridging. NBD dequenching assays and NMR experiments on nanodiscs provide evidence that synaptotagmin-1 fragments bridge membranes where the C<sub>2</sub>A and C<sub>2</sub>B domains binds to membranes with antiparallel orientations, while the positively charged face of C<sub>2</sub>B directly interacts with the phospholipid membranes.

## **3.2 Results**

### **3.2.1 Do synaptotagmin-1 fragments behave differently?**

The inconsistent behavior of synaptotagmin-1 in different studies may result from the use of different fragments of the protein. In particular, the solubility of the proteins may vary extensively even by slightly changing the fragment that is used in *in vitro* studies. A longer fragment (Synaptotagmin-1 95-421-lnC<sub>2</sub>AB) was used in the study that proposes oligomerization of synaptotagmin-1 causing the clustering of the liposomes [230]. In this study lnC<sub>2</sub>AB was reported to aggregate above 10  $\mu$ M concentrations in the presence of 1 mM Ca<sup>2+</sup>, even in the absence of liposomes which indeed can be the actual reason of

oligomerization of InC<sub>2</sub>AB on membranes. The behavior of this fragment is very different from that of the highly soluble fragment of synaptotagmin-1 (Synaptotagmin-1 141-421 - C<sub>2</sub>AB) that we have used extensively over the years in many different studies in various conditions in high protein and calcium concentrations. Previously obtained high quality <sup>1</sup>H-<sup>15</sup>N transverse relaxation-optimized spectroscopy (TROSY)-heteronuclear single quantum coherence (HSQC) spectra of <sup>15</sup>N- or <sup>2</sup>H,<sup>15</sup>N-labeled C<sub>2</sub>AB clearly shows that C<sub>2</sub>AB is highly soluble and behaves as a non-oligomeric protein [131, 202]. The <sup>1</sup>H NMR spectrum of Figure 3.2 also shows the same behavior for 800 μM <sup>15</sup>N-labeled C<sub>2</sub>AB in the presence of up to 100 mM Ca<sup>2+</sup>. The line widths at this spectrum are those expected for a highly soluble and monomeric protein of this molecular weight.

To investigate whether the behavior of longer fragment of synaptotagmin-1 is responsible for its oligomerization in solution or/and on membranes, I prepared <sup>15</sup>N-labeled InC<sub>2</sub>AB sample for NMR analysis using <sup>1</sup>H-<sup>15</sup>N TROSY-HSQC spectra. I purified the InC<sub>2</sub>AB fragment with the same rigorous purification protocol that we use for the shorter C<sub>2</sub>AB fragment. This protocol consists of GST-tag affinity purification; many wash steps with detergent, high salt, and Ca<sup>2+</sup>, treatment with nuclease, cation exchange chromatography, and size exclusion chromatography (Please check methods section for complete purification protocol). The nuclease treatment used in this protocol is vital for the purification of synaptotagmin-1 fragments due to its tendency to bind poly acidic contaminants. These contaminants are potential reasons for synaptotagmin-1 aggregation. The <sup>1</sup>H-<sup>15</sup>N TROSY-HSQC spectrum that was obtained to assess the aggregation behavior of InC<sub>2</sub>AB at 100 μM in 20 mM Ca<sup>2+</sup> revealed a high quality spectrum showing that InC<sub>2</sub>AB does not aggregate under these

conditions (Figure 3.3). Any kind of oligomerization, even dimerization of  $\ln C_2AB$  whether in the fast or slow kinetic regime, should affect the  $^1H$ - $^{15}N$  TROSY-HSQC spectrum by broadening the peaks or shifting the peaks.

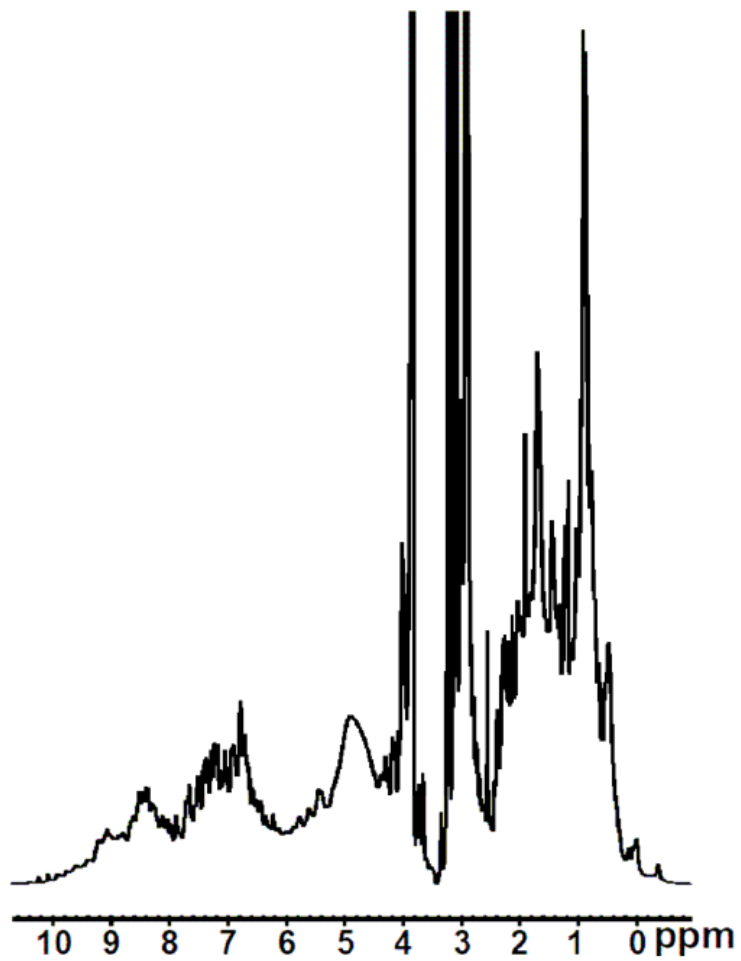


**Figure 3.2:  $^1\text{H}$  NMR spectrum of C2AB.**

$^1\text{H}$  NMR spectrum of  $800\ \mu\text{M}$   $^{15}\text{N}$ -C<sub>2</sub>AB in 50 mM MES (pH 6.3) containing 150 mM NaCl and 100 mM Ca<sup>2+</sup>.

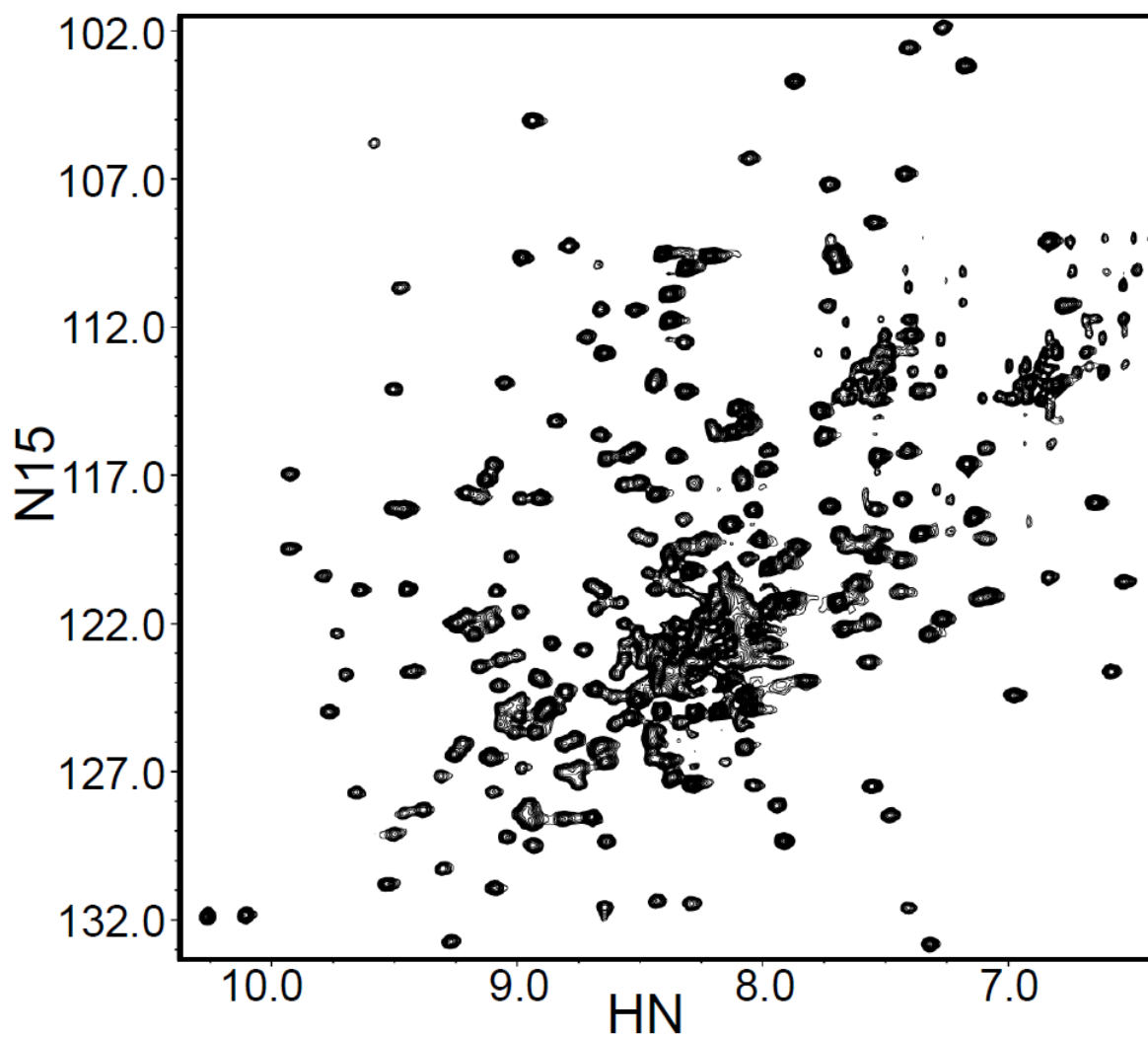


**Figure 3.3: Ca<sup>2+</sup>-bound InC<sub>2</sub>AB yields high-quality NMR data.**

The contour plot shows a  $^1\text{H}$ - $^{15}\text{N}$  TROSY-HSQC spectra of 100  $\mu\text{M}$   $^{15}\text{N}$ -InC<sub>2</sub>AB in 25 mM Tris (pH 7.4) containing 125 mM NaCl and 20 mM Ca<sup>2+</sup>.

Since the quality of the spectrum of  $\text{lnC}_2\text{AB}$  and the peak locations are very similar to the spectrum of  $\text{C}_2\text{AB}$ , these data show that there is no aggregation of  $\text{lnC}_2\text{AB}$  even at  $100\ \mu\text{M}$  in  $20\ \text{mM}\ \text{Ca}^{2+}$  concentrations. The only difference in the  $\text{lnC}_2\text{AB}$  spectrum is that there are more cross-peaks in the  $\text{lnC}_2\text{AB}$  spectrum all of which are located in the middle of the  $\text{lnC}_2\text{AB}$  spectrum (Figure 3.3). These peaks should belong to the residues in the linker region (Synaptotagmin-1 96-140), which does not exist in the  $\text{C}_2\text{AB}$  fragment. Since the extra peaks are in the middle of the  $^1\text{H}$ - $^{15}\text{N}$  TROSY-HSQC spectrum we expect that that this entire region is unstructured. N-H cross-peaks of the residues located in an unstructured region of a protein show average peptide chemical shifts. These results contradict the results reported in the previous study, which showed aggregation of  $\text{lnC}_2\text{AB}$  at even  $10\ \mu\text{M}$  protein concentrations [230]. In our hands, well purified fragments of both synaptotagmin-1  $\text{lnC}_2\text{AB}$  and  $\text{C}_2\text{AB}$  do not aggregate even at very high protein and calcium concentrations. However, we observed possible signs of aggregation of synaptotagmin-1 fragments that were not rigorously purified following the protocol outlined above. I also used the same turbidity assay that was used in the earlier study [230] that showed the tendency of  $\text{lnC}_2\text{AB}$  to aggregate above  $10\ \mu\text{M}$  protein concentrations in the presence of  $\text{Ca}^{2+}$  to understand the effect of the purification procedure on the aggregation behavior of  $\text{lnC}_2\text{AB}$ . It is important to note that below this concentration the turbidity assay may not be sensitive enough to report possible  $\text{lnC}_2\text{AB}$  aggregation because small aggregates of dilute  $\text{lnC}_2\text{AB}$  may not significantly change absorbance at  $400\ \text{nm}$ . In the purification of synaptotagmin-1 fragments there are three very important purification steps to remove contaminants that may be bound to highly positively charged regions of the  $\text{C}_2\text{A}$  and  $\text{C}_2\text{B}$  domains. These steps are washing

with a high concentration of  $\text{Ca}^{2+}$ , nuclease treatment, and cation-exchange chromatography. Here I further examined the effect of the cation-exchange chromatography purification step on the aggregation behavior of  $\text{InC}_2\text{AB}$ . I prepared  $\text{InC}_2\text{AB}$  sample using the same rigorous purification protocol, but excluded the cation-exchange chromatography step. After the  $\text{InC}_2\text{AB}$  was subjected to size-exclusion chromatography there were two major peaks detected on the chromatogram, while the fully purified protein only has one. One peak is eluted at a volume very similar to the pure  $\text{InC}_2\text{AB}$  (Figure 3.4 A – peak 2) and another peak is eluted at a much earlier volume (Figure 3.4 – peak 1). Reinjection of the corresponding eluted  $\text{InC}_2\text{AB}$  fragments into an analytical size-exclusion column showed that protein from both peaks are eluted at the same corresponding volumes, showing that both peaks contain stable  $\text{InC}_2\text{AB}$  species (Figure 3.5). The aggregation behavior of the  $\text{InC}_2\text{AB}$  fragment obtained from both peaks was examined by the turbidity assay at 400 nm and both peaks showed only background levels of turbidity in the absence of  $\text{Ca}^{2+}$ .  $\text{InC}_2\text{AB}$  from peak 2, which corresponds to the pure  $\text{InC}_2\text{AB}$  elution volume, showed background levels of turbidity in the presence of 1 mM  $\text{Ca}^{2+}$  even at 100  $\mu\text{M}$  of  $\text{InC}_2\text{AB}$  concentration (Figure 3.4 B – red triangles). We observed the same levels of turbidity for the pure  $\text{InC}_2\text{AB}$  samples that were purified using the full purification protocol including cation exchange chromatography (Figure 3.4 B – black circles). However,  $\text{InC}_2\text{AB}$  obtained from peak 1 consistently showed increasing levels of turbidity with increasing concentrations of  $\text{InC}_2\text{AB}$  in the presence of 1 mM  $\text{Ca}^{2+}$  (Figure 3.4 B – blue squares). The concentration dependent turbidity profile of the  $\text{InC}_2\text{AB}$  from peak 1 is indeed very similar to the turbidity profile of  $\text{InC}_2\text{AB}$  that was reported in the previous study suggesting the oligomerization model for  $\text{InC}_2\text{AB}$  [230]. It

seems that we are only able to reproduce the aggregation behavior of  $\text{lnC}_2\text{AB}$  with partially purified  $\text{lnC}_2\text{AB}$ . Fully purified  $\text{lnC}_2\text{AB}$  does not aggregate even at very high concentrations regardless of  $\text{Ca}^{2+}$  presence.

The purity of the  $\text{lnC}_2\text{AB}$  from both peaks was also assessed from their UV spectra.  $\text{lnC}_2\text{AB}$  from peak 2 showed a very common protein UV spectrum profile with a peak maximum at 280 nm, while the UV spectra profile of  $\text{lnC}_2\text{AB}$  from peak 1 showed a peak maximum at ~265 nm. When the UV maximum is close to 260 nm, it suggests that there are nucleic acid contaminants. This is expected since synaptotagmin-1 fragments, especially with the  $\text{C}_2\text{B}$  domain, tend to bind polyacidic compounds and partial purification is not sufficient to remove those contaminants [234].

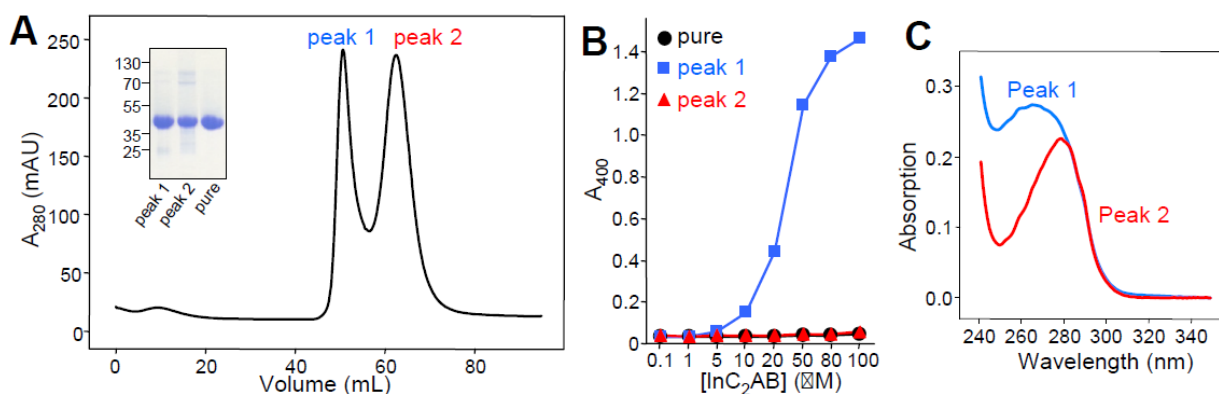


**Figure 3.4: Impurities promote aggregation of lnC<sub>2</sub>AB in solution.**

(A) Gel filtration profile on a Superdex 75 16/60 column of an lnC<sub>2</sub>AB sample that was purified by our usual procedure, including the benzonase treatment, but without ion exchange chromatography step. Inset: Peaks 1 and 2, as well as a control sample of fully purified lnC<sub>2</sub>AB (pure), were analyzed by SDS-PAGE and Coomassie blue staining.

(B) Analysis of lnC<sub>2</sub>AB aggregation using a turbidity assay. The turbidity as monitored from the absorption at 400 nm was measured as a function of protein concentration for the same control sample of purified lnC<sub>2</sub>AB (black circles), and for the samples from peaks 1 (blue squares) and 2 (red triangles) of the gel filtration experiment shown in panel A. The experiments were performed in 25 mM Tris (pH 7.4) containing 125 mM NaCl and 1 mM Ca<sup>2+</sup>.

(C) UV spectra of samples corresponding to peaks 1 and 2 in the gel filtration chromatogram shown in panel A.

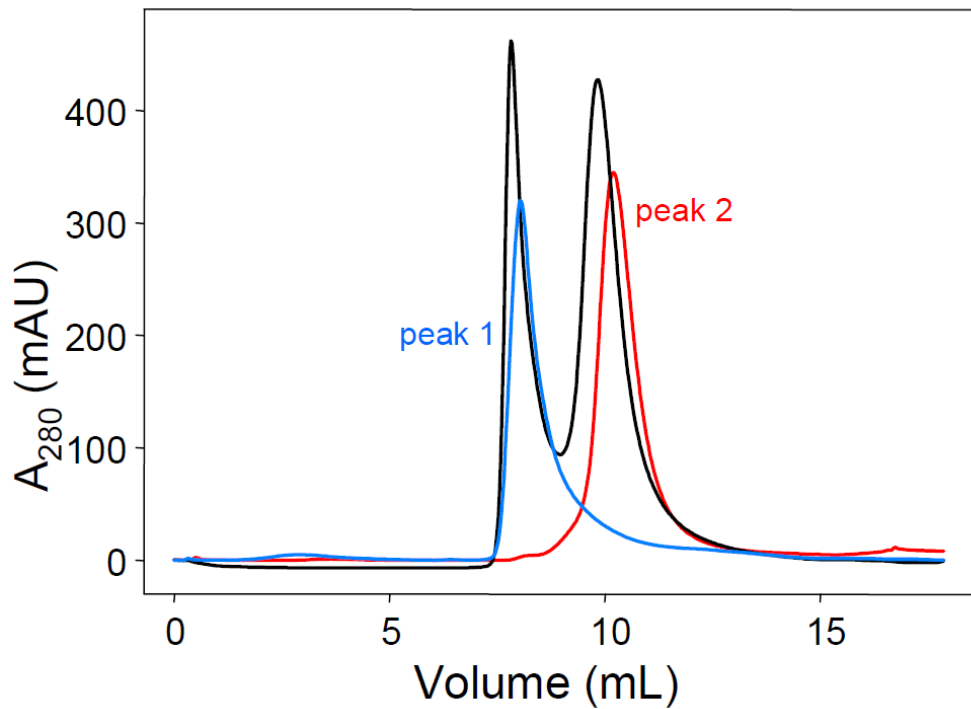


**Figure 3.5: Peaks 1 and 2 in the gel filtration profile of Fig. 3A correspond to table species.**

The black curve shows the gel filtration profile on an analytical Superdex 75 10/300 column of an InC2AB sample that was purified by our usual procedure, including the benzonase treatment, but without ion exchange chromatography step. A portion of the same sample was injected into a preparative Superdex 75 16/60 column; the fractions corresponding to peaks 1 and 2 were collected and then injected into the analytical Superdex 75 10/300 column (blue and red curves, respectively).

Additionally, the far UV region (below 245 nm) of the UV-spectrum for lnC<sub>2</sub>AB from peak 1 is dominated by scattering, potentially due to aggregation of lnC<sub>2</sub>AB.

In synaptotagmin-1 fragments containing only the C<sub>2</sub>B domain it is very difficult to get rid of the polyacidic contaminants [130, 234]. It is easier to remove those contaminants from synaptotagmin-1 fragments containing both C<sub>2</sub>A and C<sub>2</sub>B domains, but some of the steps are vital in their purification. (Please check methods section for complete purification protocol). Strikingly, when nuclease treatment is skipped from lnC<sub>2</sub>AB purification the protein behaves very differently during size-exclusion chromatography. Almost all of the protein elutes at a peak earlier than the corresponding pure lnC<sub>2</sub>AB peak suggesting that high salt and Ca<sup>2+</sup> wash on the GST affinity column is not sufficient to remove polyacidic contaminants from lnC<sub>2</sub>AB, which also suggests that high salt washes performed on an affinity column are not sufficient for removal of those contaminants. However high salt washes were claimed to be sufficient to get rid of those contaminants on the study proposing the oligomerization model of lnC<sub>2</sub>AB for vesicle clustering. Please note that in some occasions well purified C<sub>2</sub>AB that has the usual UV-spectrum profile at high concentrations gave very poor <sup>1</sup>H-<sup>15</sup>N HSQC spectra, showing the presence of contaminants [235]. Therefore, examining only the UV-spectra is not sufficient to assess the purity of synaptotagmin-1 fragments. Accordingly, we use HSQC experiments to assess purity of synaptotagmin-1 fragments on <sup>15</sup>N labeled synaptotagmin-1 fragments (Figure 3.3). <sup>1</sup>H-<sup>15</sup>N TROSY-HSQC experiment shows that more than 95% of our lnC<sub>2</sub>AB sample is free of contaminants based on the signal to noise ratio.

### **3.2.2 Direct membrane bridging by $\text{InC}_2\text{AB}$ is the prevalent model for liposome clustering**

Cryo-EM images provided the most direct evidence for the oligomerization model in which oligomerized  $\text{InC}_2\text{AB}$  molecules are responsible for membrane bridging [229]. These images reported that membranes are bridged and form extended flat surfaces with a continual separation of  $\sim 9$  nm. Between those extended flat membranes, electron density was observed and attributed to oligomerized  $\text{InC}_2\text{AB}$  molecules [229]. Intermediate structures of membranes with  $\text{InC}_2\text{AB}$  that were obtained from these images contradict with the results obtained from cryo-tomography images of membranes clustered by  $\text{C}_2\text{AB}$ . These clustered membranes were reported to be predominantly 4 nm apart from each other, which is the size of a single  $\text{C}_2$  domain [202]. 4 nm separation between membranes strongly supports that membranes are bridged directly with a single layer of  $\text{C}_2\text{AB}$  protein(s). Some larger separation between membranes is also reported in this study, but these membranes were not flattened as opposed to the ones clustered with  $\text{InC}_2\text{AB}$  in the oligomerization model study. Moreover, there is no clear protein density that would represent an oligomeric form of  $\text{C}_2\text{AB}$  between those apposed membranes. The dynamic nature of protein and liposomes interactions could lead to large distances between membranes during association and dissociation of these clustering liposomes.

To assess which mechanism of membrane bridging is accurate and whether the difference between these electron microscopy results arose from different synaptotagmin-1 fragments, I used cryo-electron microscopy experiments to understand prevalent mechanism of membrane clustering by  $\text{InC}_2\text{AB}$ . I used the same lipid composition that was used in the study that

proposed the membrane bridging model by  $\text{InC}_2\text{AB}$  oligomerization. I imaged clustering liposomes in two different protein concentrations, one sample with 1:120  $\text{InC}_2\text{AB}$  to lipid ratio, which is just sufficient to cluster vesicles, and another with 1:36  $\text{InC}_2\text{AB}$  to lipid ratio, which should further favor the association of membranes in the presence of  $\text{Ca}^{2+}$ . Extensive imaging and systematic analysis of both of these samples showed no evidence for the extended parallel flat membrane surfaces between apposed liposomes that was reported previously [229]. It is actually unclear how representative those flat surfaces are for the whole sample since there is no quantitative information reported. Extensive analysis of cryo-EM images of liposomes clustered by  $\text{InC}_2\text{AB}$  in our hands revealed only rare cases of membranes separated by 8-10 nm with clear electron density (potentially protein) between those membranes. This observation is far from supporting the model of membrane bridging by  $\text{InC}_2\text{AB}$  oligomers (Figure 3.6 E) reported previously [230]. It was very rare to see distant membranes with protein density in between and in no cases did we see flattening of membranes. Most of the distant membrane interfaces did not have clear protein density and in most cases the measured distance between apposed membranes was predominantly 3-4 nm.

I measured 697 apparent distances between clustered membranes to get representative data of the membrane bridging activity of  $\text{InC}_2\text{AB}$ . The vesicles with an apparent distance of longer than 15 nm were not accounted for the distance measurements for the  $\text{InC}_2\text{AB}$  clustered liposomes. Therefore vesicles that are apart beyond 15 nm are unlikely to be bridged by  $\text{InC}_2\text{AB}$ . It is important to note that these distances may arise after dissociation of clustered vesicles due to the dynamic nature of membrane bridging by  $\text{InC}_2\text{AB}$  (Figure 3.6 F). 697

measured apparent distances between clustered membranes are predominantly between 3 and 4 nm and decaying smoothly in larger distances (Figure 3.6 B).

Electron microscopy provides images of samples that are projected on 2 dimensions along the dimension of the incoming electron beam. Therefore, distances between membranes measured on EM images tend to underestimate the real distances between those membranes. This notion is especially pronounced for small distances and when there is a major size difference between apposed liposomes. To tackle this limitation, I optimized the freezing and blotting conditions of the EM grid to have consistent vitrified ice on EM grids that is close to 100 nm in thickness or less. The approximate thickness of the vitrified ice on EM grid is measured by a commonly used technique which involves burning a hole on vitrified ice at 45 degree tilt of the sample [236]. When the vitrified ice is less than 100 nm, it gave rise to visualization of vesicles that are approximately on the same plane (Figure 3.6). I only imaged vesicles in the regions where the ice thickness is around 100 nm or less and I avoided the other regions where the ice is thicker because it can give rise to staggering of vesicles and therefore underestimation of measured distances between  $\text{InC}_2\text{AB}$  bridged membranes.

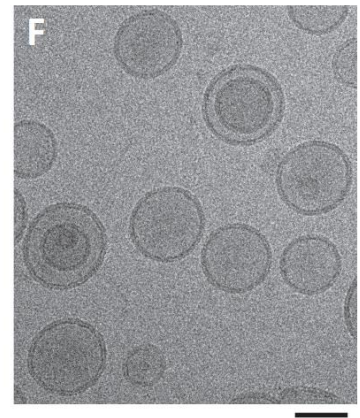
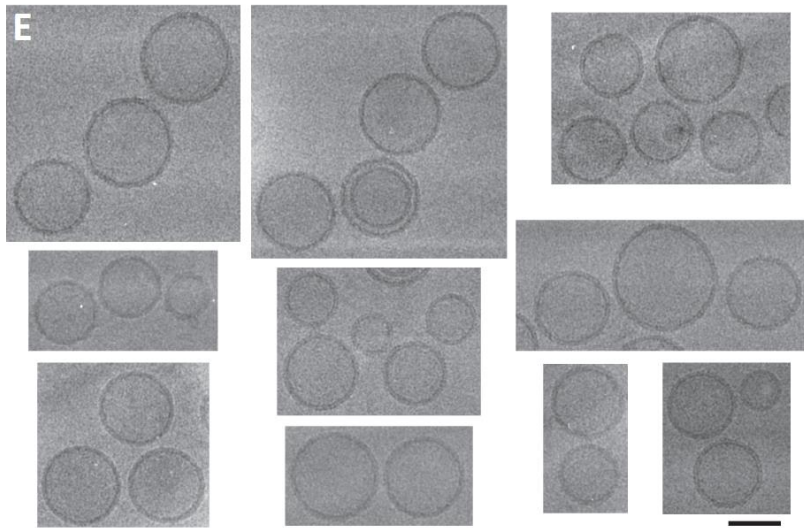
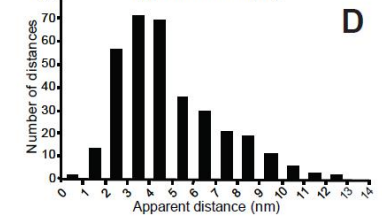
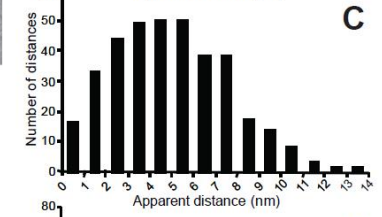
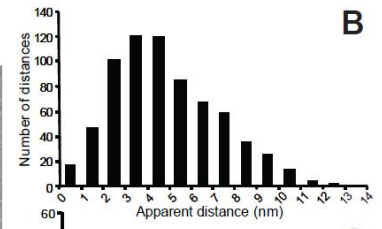
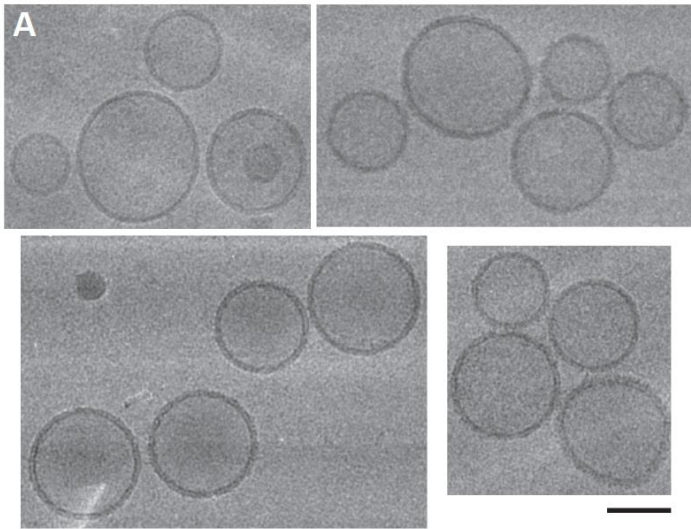


**Figure 3.6: Cryo-EM analysis of liposome clustering by InC<sub>2</sub>AB.**

Samples containing 3  $\mu\text{M}$  or 10  $\mu\text{M}$  InC<sub>2</sub>AB, 1 mM Ca<sup>2+</sup> and phospholipid vesicles (0.3 mg/mL lipids) were incubated and fast-frozen on EM grids (5 min after mixing the reagents).

**(A)** Examples of the cryo-EM images obtained. Arrows indicate liposome pairs with apparent intermembrane distances of 4 nm or less. Scale bar = 100 nm.

**(B)** Overall distribution of apparent distances measured between 697 selected liposome pairs bridged by InC<sub>2</sub>AB.

**(C) and (D)** Distribution of apparent distances measured between liposome pairs in samples containing 3  $\mu\text{M}$  InC<sub>2</sub>AB, yielding an InC<sub>2</sub>AB-to-lipid ratio of 1:120 **(C)**, or 10  $\mu\text{M}$  InC<sub>2</sub>AB, yielding an InC<sub>2</sub>AB-to-lipid ratio of 1:36

**(D)** The distribution of panel **B** includes all the distances included in panels **C** and **D**. Note that protein-free liposomes do not cluster under the conditions of our experiments (20).

**(E)** Additional images of the same experiments described in panel **A** and **B**. The arrows point to interfaces with inter-membrane distances of 8-10 nm and what appears to be electron density between them that could correspond to InC<sub>2</sub>AB oligomers. The image in **F** shows an example of loosely clustered vesicles. Scale bars = 100 nm.

To check whether there is any significant underestimation of the measured distances between membranes, I re-plotted the measured distances for larger pairs of liposomes (diameter > 70nm), which should be much less prone to underestimation (Figure 3.7 A). This plot resembles the overall distribution for all vesicles on Figure 3.6 B, but the distribution of distances on the histogram is less smooth as expected for the less number of measured intermembrane due to having fewer distance measurements. This plot still represents predominantly 3-4 nm intermembrane distances. The estimated error for intermembrane distances for EM projection is <30% for small distances and <10% for large distances (Figure 3.7 B and C).

Intermembrane distances measured on cryo-EM images reasonably resemble the actual distances between  $\text{InC}_2\text{AB}$  bridged membranes with slight underestimation for the shorter distances. Thus, we conclude that the predominant intermembrane distances of 3-4 nm plotted on histogram of Figure 3.6 B reflect actual intermembrane distance of 4-5 nm, which is the approximate size of a  $\text{C}_2$  domain from its bottom to  $\text{Ca}^{2+}$  binding loops. Therefore, this size corresponds to a single  $\text{C}_2$  domain between two membranes oriented perpendicularly, which allows simultaneous interaction of the  $\text{Ca}^{2+}$  binding loops and the bottom of  $\text{C}_2\text{B}$  domain with two apposed membranes (Figure 3.1 B). Our cryo-EM image analysis of  $\text{InC}_2\text{AB}$  bridged membranes is consistent with the results obtained from previous cryo-EM tomography results [202]. Both of these studies reported intermembrane distances which can only be explained by a model in which only a single layer of  $\text{C}_2\text{AB}$  or  $\text{InC}_2\text{AB}$  molecule(s) directly bridge two apposed membranes.

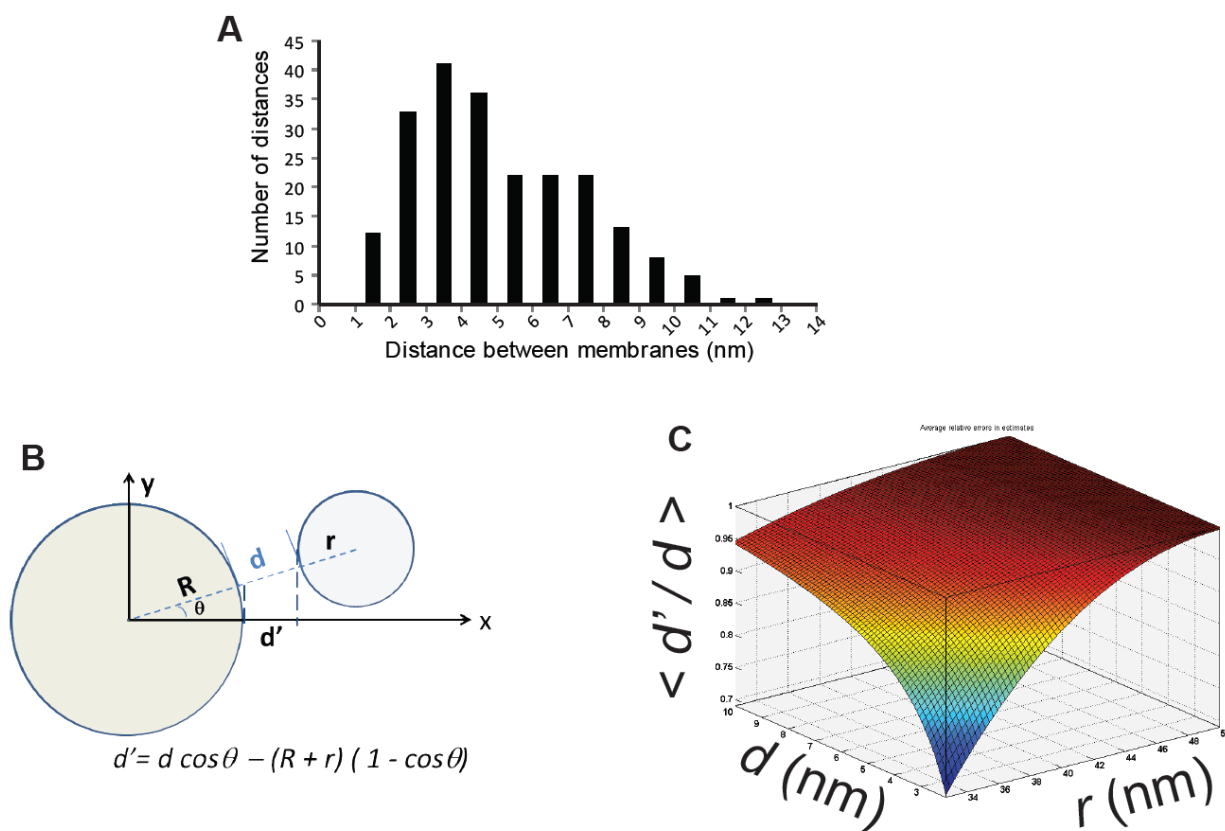


**Figure 3.7: Slight underestimation of intermembrane distance due to cryoEM projection.**

(A) Histogram of inter-membrane distances between vesicle pairs where both vesicles have diameters larger than 70 nm. The data correspond to a subpopulation of the whole set showed in Fig. 4b.

(B.) Geometrical considerations for two vesicles with inter-membrane distance  $d$  positioned in different vertical planes. The two vesicles have different diameters,  $R$  and  $r$ . The projection (along the y-axis) gives an underestimated distance  $d'$ .

(C) Average underestimation for the intermembrane distances between two vesicles. Without losing generality, here we assume that the diameter of the large vesicle is 100nm, and the

small vesicles vary from 65 to 100 nm in diameter. The thickness of the vitrified ice confined the possible displacement between these two vesicles. Since the big vesicles are close to the thickness of ice ( $\leq 100$  nm), they are positioned with the origin in the center of the ice. The small vesicles are assumed to take a random vertical position ( $y$ ) with an even probability,  $p(y) = 1/(2R - 2r)$ . The angle  $\theta$  is the (defined in panel **B**) is estimated by:

$$\sin \theta = \frac{y}{(R + r + d)}$$

The average of  $d'$  is then calculated by estimating the average of  $\cos \theta$ .

$$\langle \cos \theta \rangle = \int_y \text{SQRT}(1 - \sin^2 \theta) * p(y) dy$$

And the estimated average of  $d'/d$  becomes

$$\langle \frac{d'}{d} \rangle = \langle \cos \theta \rangle - \frac{R + r}{d} (1 - \langle \cos \theta \rangle)$$

We did numerical calculations of the average  $d'/d$ , plotted them as a function of the inter-membrane distance  $d$  (from 2-10 nm) and the radius of the small vesicles  $r$  (from 32 to 50 nm), and presented the results in a 3D surface plot. All the simulations were done in MATLAB11a (licensed through UT Southwestern).

The intermembrane distances larger than 5 nm plotted on the histogram in Figure 3.6 B show smooth decay as distance increases. We argue that these small fractions of intermembrane distances arose from the dynamic nature of vesicle clustering by  $\text{InC}_2\text{AB}$ . Vesicles before association and after dissociation should naturally lead to distances larger than the actual intermembrane distance during bridging of two membranes by  $\text{InC}_2\text{AB}$ .

To provide evidence for this argument about larger intermediate distances, I imaged two separate samples with 1:120 and 1:36  $\text{InC}_2\text{AB}$  molecules to lipid molecules ratio. The vesicle clustering activity of  $\text{InC}_2\text{AB}$  depends critically on the protein to lipid ratio and phosphatidylserine content in vesicles. 1:120 protein to lipid ratio is just sufficient to cluster vesicles with liposomes containing 15% phosphatidylserine. The distribution of distances between membranes for the 1:120 protein to lipid ratio is broader than the overall distribution of distances between membranes but still predominantly centered around 3-5 nm (Figure 3.6 B and C). On the other hand, the sample with 1:36 protein to lipid ratio showed a narrower distribution of intermembrane distances with the vast majority of distances centered at 3-4 nm. Much higher fractions of apposed vesicle pairs exhibited intermembrane distances at 3-4 nm than the sample with 1:120 protein to lipid ratio (less  $\text{InC}_2\text{AB}$ ). This analysis shows that addition of more  $\text{InC}_2\text{AB}$  shifts the equilibrium at association and dissociation towards the state where membranes are bridged by  $\text{InC}_2\text{AB}$ . Therefore, additional  $\text{InC}_2\text{AB}$  further stabilizes bridging of apposed membranes and we observed a higher population of apposed vesicles in which membranes are 3-4 nm apart. This observation resembles direct bridging of membranes by a single  $\text{C}_2$  domain. Lower concentration of  $\text{InC}_2\text{AB}$  leads to more dynamic

dissociation and association of vesicles, which give rise to broader distribution of intermembrane distances.

This analysis very strongly suggests that membrane bridging is carried out primarily following the direct bridging mechanism. If the oligomerization model would significantly account for membrane bridging by  $\ln C_2AB$ , higher protein to lipid ratio should have enhanced the population of larger intermembrane distances or shift the center of the distribution of intermembrane distances to larger values, which is opposite to what we observed in the analysis of these two EM samples with two different protein to lipid ratios. Therefore, these results showed that membranes are bridged directly by a single layer of  $\ln C_2AB$  molecule(s). It also suggests that the oligomerization of synaptotagmin-1 does not significantly contribute for membrane bridging by  $\ln C_2AB$ .

### **3.2.3 The bottom of the $C_2B$ domain contacts the phospholipid membranes**

NBD fluorescence is a commonly used environment sensitive probe whose emission fluorescence increases after its transition from an aqueous to hydrophobic environment [237]. Previously, the bottom of the synaptotagmin-1  $C_2B$  domain was shown to bind to phospholipid membranes with phosphatidylserine using a cysteine mutant of  $C_2AB$  labeled with NBD on residue 396. Addition of  $Ca^{2+}$  into a sample containing  $C_2AB$  396-NBD and phosphatidylserine containing liposomes leads to an increase in the emission intensity of NBD, which suggests that the region of the  $C_2B$  domain close to residue 396 is indeed interacting with membranes in a calcium-dependent manner [202]. However, similar experiments using  $\ln C_2AB$  labeled at residue 396 exhibited no increase in the intensity of

NBD [230] which directly contradicts the previously reported data with the C<sub>2</sub>AB fragment. In order to understand the true nature of the interaction of synaptotagmin-1 with phospholipid membranes, I performed side by side NBD experiments for both of the InC<sub>2</sub>AB and C<sub>2</sub>AB fragments. They were labeled with NBD at cysteine mutated residue 396 and the same lipid composition was used in the study that claimed C<sub>2</sub>B does not interact with membranes. It is important to note that this lipid composition contains 15% phosphatidylserine, which is lower than the other study. The study that suggested interaction between C<sub>2</sub>B and the membrane used 30% phosphatidylserine. This difference may also account for the discrepancy between these two studies since phosphatidylserine (negatively charged lipids) is vitally important for the Ca<sup>2+</sup> dependent synaptotagmin-1 interaction with phospholipid membranes. These experiments showed that both Ca<sup>2+</sup> dependent phospholipid binding of both InC<sub>2</sub>AB and C<sub>2</sub>AB lead to similar increase in the intensity of NBD fluorescence (Figure 3.8 A, B and E), which is also comparable to the intensity change in NBD fluorescence performed previously with 30% PS containing liposomes [202]. These results are reproducible in different preparation of liposomes on different days. These results have been performed with a protein to lipid ratio in which liposomes are clustered.

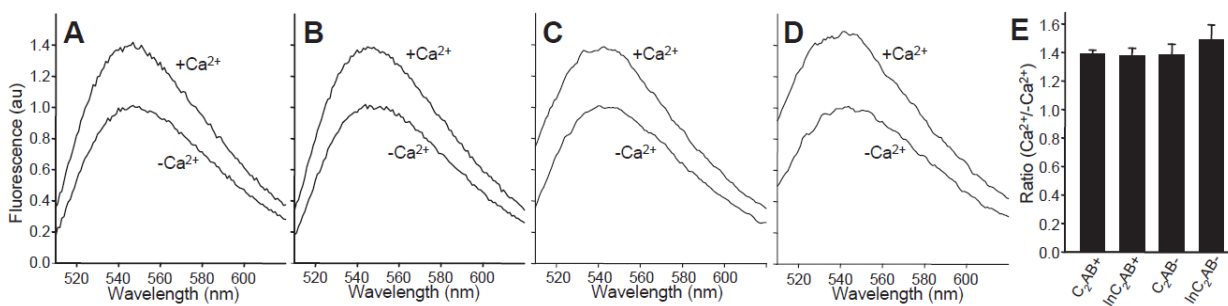


**Figure 3.8: Increased fluorescence of NBD probes placed at the bottom of the C<sub>2</sub>B domain upon membrane binding.**

(A) and (B) Representative fluorescence emission spectra of 0.3  $\mu$ M samples of NBD-labeled N396C mutant C<sub>2</sub>AB (A) or InC<sub>2</sub>AB (B) acquired side-by-side in the presence of phospholipid vesicles (100  $\mu$ M lipids) and 1 mM EGTA or 1 mM Ca<sup>2+</sup> (clustering conditions).

(C) and (D) Analogous spectra acquired under the same conditions but using 1 mM lipids (non-clustering conditions). For each set of experiments in (A-D), spectra acquired with identical samples containing unlabeled C<sub>2</sub>AB or InC<sub>2</sub>AB were subtracted to remove contributions from light scattering to the observed intensities. The data were then normalized to the maximum fluorescence intensity observed in the absence of Ca<sup>2+</sup>.

(E) Quantification of NBD fluorescence increases upon membrane binding. NBD fluorescence emission spectra analogous to those shown in (A-D) were acquired in triplicate under clustering conditions (C<sub>2</sub>AB+ and InC<sub>2</sub>AB+) or non-clustering conditions (C<sub>2</sub>AB- and InC<sub>2</sub>AB-). Bars represent averages of the ratios between the NBD fluorescence intensity maxima observed in 1 mM Ca<sup>2+</sup> and 1 mM EGTA in three separate pairs of experiments performed under identical conditions. Error bars represent standard deviations.

This ratio was determined for both  $\ln C_2AB$  and  $C_2AB$  using dynamic light scattering. Interestingly, similar experiments under non clustering conditions also exhibited similar NBD intensity changes, which show that the bottom of  $C_2B$  domain can interact with phospholipid membranes in non-clustering conditions (Figure 3.8 C and E). Additionally, a modest increase in NBD fluorescence intensity compared to the  $Ca^{2+}$  binding loops of the  $C_2$  domains [202] suggests that clustering is mediated by only a small portion of  $C_2AB$  or  $\ln C_2AB$  molecules, where  $Ca^{2+}$  binding loops and the bottom of the  $C_2B$  domain simultaneously interact with the apposing membranes. This observation is compatible with the direct mechanism of liposome clustering since only a small percentage of membrane surfaces come in close proximity during vesicle clustering.

The  $Ca^{2+}$  dependent modest increase in NBD fluorescence intensity upon phospholipid interaction of the bottom part of  $C_2B$  can be explained with two different scenarios. One scenario is synaptotagmin-1 interacts with phospholipid membranes giving a small increase in NBD fluorescence intensity due to the interfacial location of NBD probe. If this scenario is true, we would expect that most the bottom of the  $C_2B$  domain of the most of the synaptotagmin-1 fragments in the sample interacts with phospholipid membranes. The other scenario would be that the interaction of synaptotagmin-1 with phospholipid membranes gives rise to a large increase in NBD fluorescence intensity, in which case the bottom part of  $C_2B$  domain of only small percentage of the synaptotagmin-1 fragments in the sample interacts with phospholipid membranes. The second scenario is more probable since previous studies have provided evidence showing that interaction of  $C_2A$  and  $C_2B$  domains with phospholipid membranes are mediated primarily through  $Ca^{2+}$  binding loops located at the

top of C<sub>2</sub> domains [130, 238-240]. Analogous NBD experiments in which NBD probes are located near the Ca<sup>2+</sup> binding loops showed significantly larger increases in the NBD fluorescence intensity upon Ca<sup>2+</sup> dependent phospholipid membrane interaction [202]. It is important to note that this difference may also arise from the interfacial location of the NBD probe, which may lead to small changes in NBD fluorescence intensity due to environmental changes near NBD probe upon Ca<sup>2+</sup> dependent phospholipid membrane interaction. If the increase in the NBD fluorescence intensity is comparable for NBD probes located either at the bottom region or near the Ca<sup>2+</sup> binding loops of C<sub>2</sub>B domain per synaptotagmin-1 molecule, according to our results, at least 5-10 % of the synaptotagmin-1 fragments in each sample should interact with phospholipid membranes through the bottom of the C<sub>2</sub>B domain. This percentage would be much higher if the change in the NBD fluorescence intensity for synaptotagmin-1 fragments with the NBD probe at the bottom of C<sub>2</sub>B domain is lower upon Ca<sup>2+</sup> dependent phospholipid membrane interaction.

### **3.2.4 Substantial populations of antiparallel orientations of the two C<sub>2</sub> domains on nanodiscs**

The C<sub>2</sub>A domain of synaptotagmin-1 interacts with phospholipid membranes through its Ca<sup>2+</sup> binding loops, which are located at the top of the C<sub>2</sub>A domain. Our NBD dequenching experiments showed that a small but significant population of synaptotagmin-1 molecules interact with phospholipid membranes through the bottom of the C<sub>2</sub>B domain. These two observations require that sizable populations of synaptotagmin-1 molecules should interact with phospholipid membranes where C<sub>2</sub>A and C<sub>2</sub>B domains are oriented antiparallel to each

other. This model is compatible with the distances measured by EPR between both spin labeled C<sub>2</sub>A and C<sub>2</sub>B domains in InC<sub>2</sub>AB molecules [231]. However, this EPR study lacks a direct distance measurement between the top of C<sub>2</sub>A domain and the bottom of C<sub>2</sub>B domain. Therefore, Kyle Brewer performed NMR experiments to obtain distance information between opposite ends of C<sub>2</sub>A and C<sub>2</sub>B domains, which could provide direct evidence for the antiparallel orientation of the two C<sub>2</sub> domains. In these experiments Kyle used nanodiscs as a membrane partner for C<sub>2</sub>AB molecules instead of liposomes. Nanodiscs are discs of phospholipid bilayer in which the hydrophobic tails of phospholipids are stabilized with modified ApoA1, an amphipathic scaffold protein [241]. Their size is about 10 nm in diameter, which gives nanodiscs advantages in NMR experiments over liposomes as a membrane system since liposomes are much bigger than nanodiscs and broaden all of the NMR signals to undetectable levels. To test the antiparallel model, the methyl groups of isoleucines, leucines, and valines were specifically labeled with <sup>13</sup>C-<sup>1</sup>H<sub>3</sub> isotopes with specific aminoacid precursors in the C<sub>2</sub>AB fragment and the rest of C<sub>2</sub>AB fragment was deuterated (<sup>2</sup>H-ILV-<sup>13</sup>C<sup>1</sup>H<sub>3</sub>-C<sub>2</sub>AB). This labeling technique allows us to obtain high sensitivity <sup>1</sup>H-<sup>13</sup>C heteronuclear multiple quantum coherence (HMQC) data from very large biomolecular complexes [242]. In this case we used this method to study C<sub>2</sub>AB-Nanodisc complexes.

The <sup>1</sup>H-<sup>13</sup>C HMQC spectrum of <sup>2</sup>H-ILV-<sup>13</sup>C<sup>1</sup>H<sub>3</sub>-C<sub>2</sub>AB gave rise to <sup>1</sup>H-<sup>13</sup>C correlation cross peaks from only ILV methyl groups. The <sup>1</sup>H-<sup>13</sup>C HMQC spectrum of the <sup>2</sup>H-ILV-<sup>13</sup>C<sup>1</sup>H<sub>3</sub>-C<sub>2</sub>AB exhibits sharp cross-peaks in the presence of 15% phosphatidylserine containing nanodiscs without Ca<sup>2+</sup>. Addition of Ca<sup>2+</sup> to the sample significantly broadens the cross-

peaks due to size increase upon binding of C<sub>2</sub>AB to nanodiscs. However, cross-peaks are easily observable with high signal to noise in the presence of Ca<sup>2+</sup> (Figure 3.9 A and B). Comparison of <sup>1</sup>H-<sup>13</sup>C HMQC spectra of isolated <sup>2</sup>H-ILV-<sup>13</sup>CH<sub>3</sub>-C<sub>2</sub>AB in the presence of 0, 1, and 20 mM Ca<sup>2+</sup> revealed progressive changes in cross-peaks from methyl groups in the Ca<sup>2+</sup>-binding loops (Figure 3.9). This notion is consistent with the previous observation for the amide groups of amino acids on the Ca<sup>2+</sup> binding loops of C<sub>2</sub>AB [217]. There are additional movements of some of the methyl cross-peaks in the <sup>1</sup>H-<sup>13</sup>C HMQC spectrum of the <sup>2</sup>H-ILV-<sup>13</sup>C<sup>1</sup>H<sub>3</sub>-C<sub>2</sub>AB in the presence of both 1 mM Ca<sup>2+</sup> and nanodiscs. These observations showed that in the presence of Ca<sup>2+</sup> and nanodiscs all of the C<sub>2</sub>AB molecules are bound to nanodiscs and DLS experiments showed that there are no higher order protein-nanodisc complexes. This means that only one C<sub>2</sub>AB molecule binds to only one nanodisc molecule.

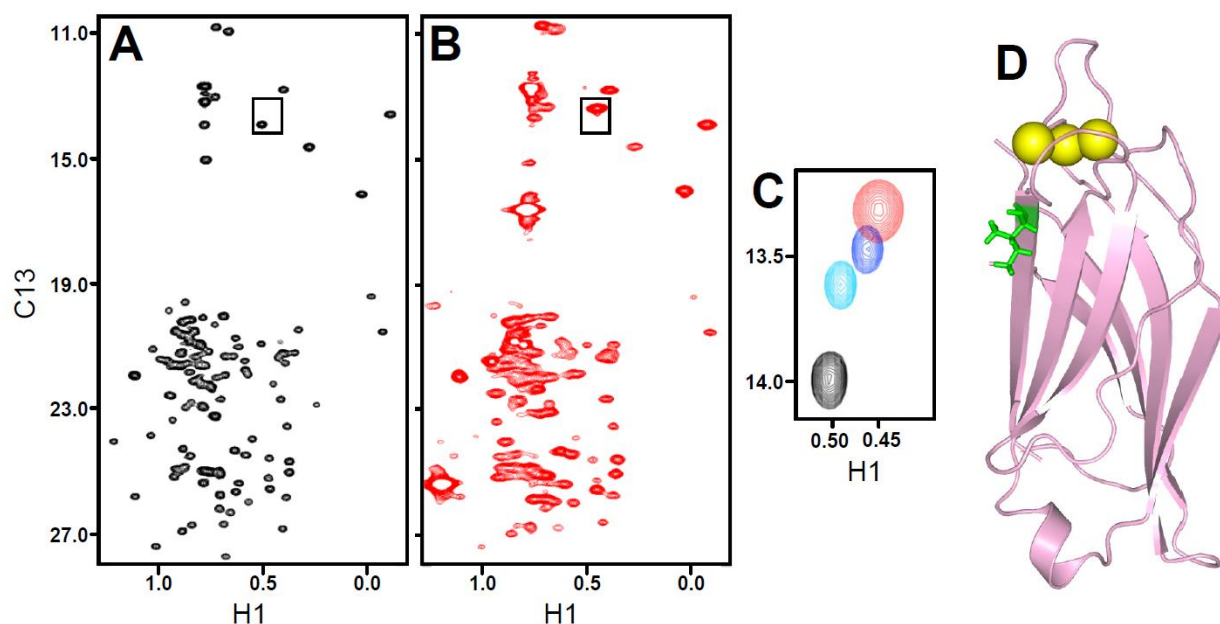


**Figure 3.9: NMR analysis of C2AB on nanodiscs.**

(A) and (B)  $^1\text{H}$ - $^{13}\text{C}$  HMQC spectrum of  $50\ \mu\text{M}$   $^2\text{H}$ -ILV- $^{13}\text{CH}_3$ -C<sub>2</sub>AB in 1 mM EDTA (A) or in 1 mM  $\text{Ca}^{2+}$  in the presence of  $60\ \mu\text{M}$  nanodiscs (B).

(C) Superposition of expansions showing the cross-peak from Ile239 (rectangle shown in panels A,B) of  $^1\text{H}$ - $^{13}\text{C}$  HMQC spectra of  $50\ \mu\text{M}$   $^2\text{H}$ -ILV- $^{13}\text{CH}_3$ -C<sub>2</sub>AB in 1 mM EDTA (black), 1 mM  $\text{Ca}^{2+}$  (cyan), 20 mM  $\text{Ca}^{2+}$  (blue) or 1 mM  $\text{Ca}^{2+}$  plus  $60\ \mu\text{M}$  nanodiscs (red).

(D) Ribbon diagram of the synaptotagmin-1 C<sub>2</sub>A domain showing the location of I239 as a green stick model.  $\text{Ca}^{2+}$  ions are shown as yellow spheres.

To obtain information about the relative orientations of the two C<sub>2</sub> domains, <sup>2</sup>H-ILV-<sup>13</sup>C<sup>1</sup>H<sub>3</sub>-C<sub>2</sub>AB was labeled with a paramagnetic probe called (1-oxyl-2,2,5,5-tetramethyl-3-pyrroline-3-methyl) methanethiosulfonate (MTSL) at the bottom of the C<sub>2</sub>A domain (N248) or at the top of the C<sub>2</sub>A domain (V304) through single cysteine mutations. MTSL allows us to extract distance information for nearby residues through paramagnetic broadening effects (PBE). MTSL is expected to broaden the cross-peaks of nearby residues in <sup>1</sup>H-<sup>13</sup>C HMQC spectra that are within 25 Å [243]. Reduction of the MTSL probe removes its magnetic property, which allows the recovery of the broadened cross-peaks to their original levels [244]. PBEs, measured as the ratios of the cross-peak intensities before and after reduction of MTSL, allowed us to understand which residues are close and which residues are far from the MTSL probe in C<sub>2</sub>AB. Therefore, comparison of <sup>1</sup>H-<sup>13</sup>C HMQC spectra of either nanodisc bound <sup>2</sup>H-ILV-<sup>13</sup>CH<sub>3</sub>-C<sub>2</sub>AB 248-MTSL or <sup>2</sup>H-ILV-<sup>13</sup>CH<sub>3</sub>-C<sub>2</sub>AB 304-MTSL provide information to assess the relative orientation of the two C<sub>2</sub> domains. The measured PBEs were examined to determine intra-domain distances such as distances from an MTSL probe on the C<sub>2</sub>A domain to residues in the C<sub>2</sub>A domain. These intra-domain distances were compared with the real distances reported by the crystal structures of individual C<sub>2</sub> domains as a control to test whether this experimental setup provides accurate measurements. The sample with MTSL labeled on the C<sub>2</sub>A domain gave rise to broadening of cross peaks from residues of the C<sub>2</sub>A domain within the typical r<sup>-6</sup> distance dependence (distance between an MTSL probe on the C<sub>2</sub>A domain to residues in the C<sub>2</sub>A domain) and the measured distances are similar to the actual distances. Very similar results were observed for the sample with MTSL labeled on

the C<sub>2</sub>B domain along with its corresponding PBE measurements and distance dependence of the PBE measurements [129, 130, 216].

Previous single-molecule fluorescence studies [245, 246] and EPR studies [231] reported that the two C<sub>2</sub> domains exhibit dynamic orientations relative to each other. The measured inter-domain PBEs from both MTSL labeled on C<sub>2</sub>A domain and MTSL labeled on C<sub>2</sub>B domain are consistent with this notion of dynamic relative orientation of two C<sub>2</sub> domains.

For the MTSL labeled sample on the bottom of the C<sub>2</sub>A domain, some strong (< 0.4) and medium (0.4 to 0.6) PBEs were observed from MTSL located at the bottom of the C<sub>2</sub>A domain to several methyl cross-peaks that belong to residues located at bottom and middle of the C<sub>2</sub>B domain (Figure 3.10 A and B). This suggests that the majority of the C<sub>2</sub>A and C<sub>2</sub>B domains in C<sub>2</sub>AB molecules are oriented parallel to each other on nanodiscs. It is important to note that this mode of orientation is compatible with simultaneous interaction of both C<sub>2</sub>A and C<sub>2</sub>B Ca<sup>2+</sup> binding loops with phospholipid membranes on nanodiscs. Therefore, the results observed for strong and medium PBEs are consistent with binding of C<sub>2</sub>AB molecules to phospholipid membranes predominantly through the Ca<sup>2+</sup> binding loops. However, for this sample (MTSL located on the C<sub>2</sub>A domain), some medium (0.4 to 0.6) PBEs were also observed from MTSL located at bottom of C<sub>2</sub>A domain to several methyl cross-peaks that belong to residues located at the top of the C<sub>2</sub>B domain (Figure 3.10 A and B). Since the distance between MTSL at the bottom of C<sub>2</sub>A and methyl groups located at the top of C<sub>2</sub>B domain are not close enough in a parallel orientation of C<sub>2</sub> domains to observe medium PBEs, these PBEs should arise from the antiparallel orientation of two C<sub>2</sub> domains in which

the top of the C<sub>2</sub>B domain comes into close proximity to the bottom of the C<sub>2</sub>A domain where MTSL is located.

The measured inter-domain PBEs from MTSL labeled on C<sub>2</sub>B domain at residue 304 are generally smaller than the ones measured from MTSL labeled on the C<sub>2</sub>A domain. It is likely that the smaller PBEs probably originated from residue 304 being at the edge of the most outside loop on C<sub>2</sub>B. This puts this residue significantly farther from the methyl groups on the C<sub>2</sub>A domain. However, one strong PBE was observed from a methyl group on the top of the C<sub>2</sub>A domain. This is the closest isotopically labeled methyl to the MTSL located on top of C<sub>2</sub>B domain, suggesting a parallel orientation of the two C<sub>2</sub> domains. Additionally, multiple medium PBEs were observed from MTSL labeled on C<sub>2</sub>B domain to methyl cross-peaks that are located at the top, middle and bottom of the C<sub>2</sub>A domain (Figure 3.10 C and D). Hence, the PBEs observed from MTSL labeled on the C<sub>2</sub>B domain also show that there are at least two conformations of C<sub>2</sub>AB bound to the nanodisc.

In the predominant conformation, the two C<sub>2</sub> domains are oriented parallel to each other, allowing both the Ca<sup>2+</sup>-binding loops of the two C<sub>2</sub> domains to simultaneously bind to the same phospholipid membranes. In the other conformation, the two C<sub>2</sub> domains are oriented antiparallel to each other and the Ca<sup>2+</sup>-binding loops of the two C<sub>2</sub> domains bind to opposite membranes. Due to the dynamic nature of the interaction of C<sub>2</sub>AB molecules with nanodiscs, it is not possible to do quantification on our PBE experiments. Nevertheless, all the data support the conclusions obtained from the NBD dequencing experiments, which shows that the bottom of the C<sub>2</sub>B domain interacts with phospholipid membranes.

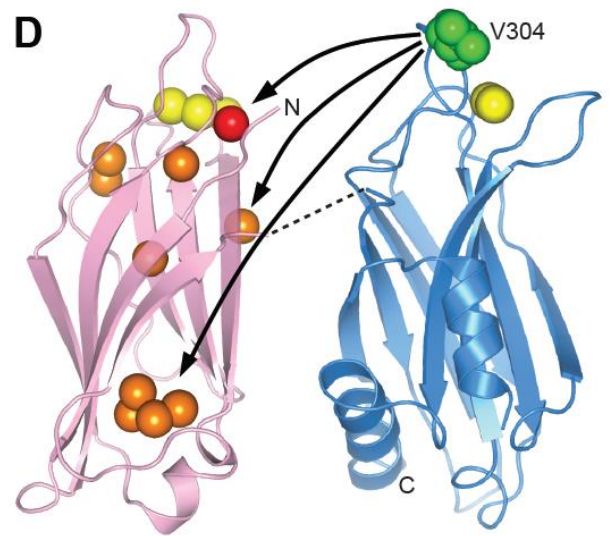
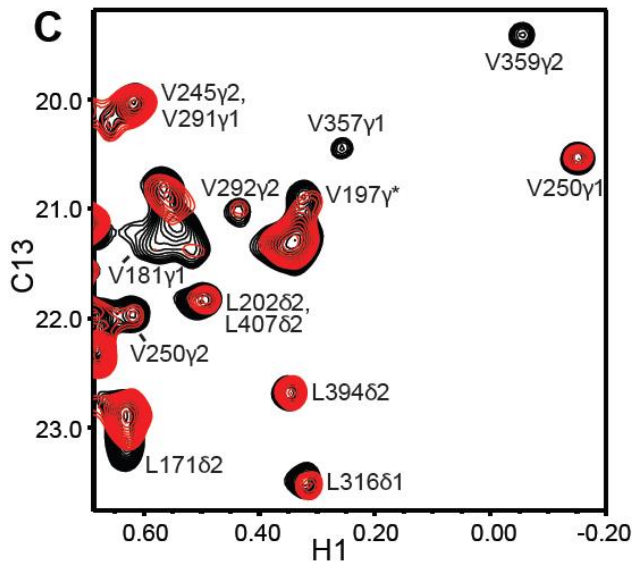
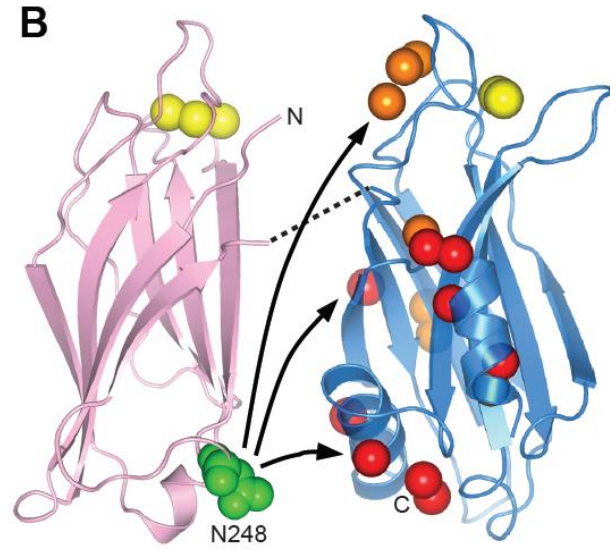
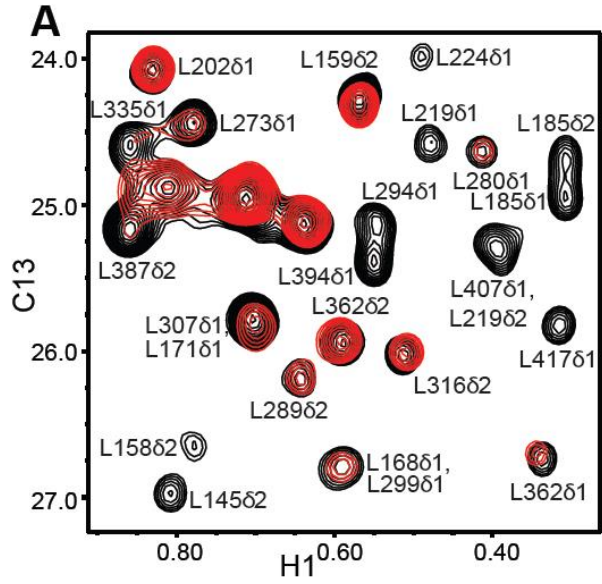


**Figure 3.10: Analysis of PBEs within C2AB bound to nanodiscs.**

(A) and (C)  $^1\text{H}$ - $^{13}\text{C}$  HMQC spectra of 50  $\mu\text{M}$  MTSL-labeled  $^2\text{H}$ -ILV- $^{13}\text{CH}_3$ -C<sub>2</sub>AB N248C (A) or V304C (C) mutant in the presence of 1 mM  $\text{Ca}^{2+}$  and 60  $\mu\text{M}$  nanodiscs before (red) or after (black) reduction with 1 mM dithionite and 1 mM ascorbic acid. Assignments based on our previous NMR studies of the isolated C<sub>2</sub>A and C<sub>2</sub>B domains (15, 40) are indicated for well-resolved cross-peaks. Cross-peaks from methyl groups that exhibit PBEs indicative of antiparallel orientations of the C<sub>2</sub> domains (at the top of the C<sub>2</sub>B domain in A and to the bottom of the C<sub>2</sub>A domain in C) are labeled in blue. **B,D.** Summary of the interdomain PBEs measured for the N248C (B) or V304C (D) mutant. Ribbon diagrams of the C<sub>2</sub>A and C<sub>2</sub>B domains are shown on the left and the right, respectively, with the  $\text{Ca}^{2+}$  ions shown as yellow spheres and the atoms of the residues that were mutated to place the MTSL labels shown as green spheres. The methyl carbons that exhibited strong (between 0 and 0.4) or medium (0.4-0.6) interdomain PBEs are shown as red or orange spheres, respectively. The residues bearing these methyl groups are: 294, 387, 394, 401, 409, 413 and 417 (red) and 273, 291, 292, 307 and 335 (orange) in (B); 171 (red), and 149, 158, 181, 197, 239, 240 and 250 (orange) in (D) The curved arrows are meant to illustrate that the MTSL label placed at the bottom of the C<sub>2</sub>A domain (N248C) induces substantial PBEs in the bottom, middle and top of the C<sub>2</sub>B domain, while the MTSL label placed at the top of the C<sub>2</sub>B domain (V304C) induces substantial PBEs at the top, middle and bottom of the C<sub>2</sub>A domain. The dashed lines represent the linker between the C<sub>2</sub>A and C<sub>2</sub>B domains.

### ***3.3 Discussion***

Previous studies showed that synaptotagmin-1 can cluster liposomes and chromaffin granules in vivo [225] and C<sub>2</sub>AB can cluster liposomes and bring membranes close together (~4 nm) in the presence of Ca<sup>2+</sup>. These observations provided a working model in which synaptotagmin-1 can bring plasma membranes and synaptic vesicles very close to each other with the help of the SNARE complex in a Ca<sup>2+</sup> dependent manner [202]. The following mutational studies support this model. Mutation of the two arginines at the bottom of the C<sub>2</sub>B domain of synaptotamin-1 led to complete abrogation of Ca<sup>2+</sup> dependent evoked neurotransmitter release. The same pair of mutations also impaired the liposome clustering activity of C<sub>2</sub>AB and its ability to stimulate SNARE-dependent lipid mixing between liposomes [218]. On the other hand, other studies about synaptotagmin-1-phospholipid membrane interactions provided contradictory results and led to another model of membrane bridging by synaptotagmin-1 where oligomerized lnC<sub>2</sub>AB molecules in opposite membranes interact with each other. This interaction of lnC<sub>2</sub>AB molecules on separate membranes brings those opposite membranes in close proximity. In this model the bottom of the C<sub>2</sub>B domain does not directly interact with phospholipid membranes [230]. Another study provided cryo-EM pictures that supported this model of membrane bridging by oligomerized lnC<sub>2</sub>AB [229]. Understanding the validity of these contradictory results from different studies and clarifying which model is physiologically relevant is important to assess how synaptotagmin-1 brings synaptic vesicles and the plasma membrane together, triggering vesicle fusion and neurotransmitter release. Our study showed strongly that both C<sub>2</sub>AB and lnC<sub>2</sub>AB bridge the two membranes by direct interaction of these molecules with apposing membranes. This

bridging activity involves direct interaction of the bottom of C<sub>2</sub>B domain with phospholipid membranes. It is important to note that the bottom of C<sub>2</sub>B domain in a significant population of C<sub>2</sub>AB or lnC<sub>2</sub>AB molecules interact with phospholipid membranes. This interaction exists even in the protein to lipid ratios that is not sufficient cluster liposomes.

It is also important to note that there has been no study reporting membrane bridging by oligomerization of the shorter synaptotagmin-1 fragment (C<sub>2</sub>AB). On the other hand 1D NMR experiments established that even high concentrations of C<sub>2</sub>AB do not aggregate or self-associate in solution in the presence or absence of Ca<sup>2+</sup> (Figure 3.2) [131, 202]. Additionally, in a previous study, no crosslinking had been observed between highly localized C<sub>2</sub>AB molecules bound to membranes with a very efficient cross-linker (Tris-(bipyridine) ruthenium (II)) [202]. Additionally, the same study showed with a FRET assay that C<sub>2</sub>AB does not oligomerize on vesicles even at very high local protein concentrations [202]. Intermembrane distances between C<sub>2</sub>AB bridged liposomes are primarily ~4 nm [202], which shows that membranes are bridged directly by a single C<sub>2</sub> domain and these results are inconsistent with the oligomerization model. Previous studies also reported similar stimulating activity of C<sub>2</sub>AB [218] and lnC<sub>2</sub>AB [247] in SNARE dependent lipid mixing assays. Therefore, all these studies showed that oligomerization of lnC<sub>2</sub>AB or C<sub>2</sub>AB is not required for stimulation of lipid mixing by C<sub>2</sub>AB or C<sub>2</sub>AB.

Direct bridging model was also supported by two separate studies using lnC<sub>2</sub>AB. An EPR study [231] and a fluorescence study [248] reported that lnC<sub>2</sub>AB bridge two membranes without oligomerization. The oligomerization model in the previous study [230] was proposed by disregarding EPR and fluorescence studies for lnC<sub>2</sub>AB and previously available

results for C<sub>2</sub>AB [202]. The proposal of the oligomerization model relied on indirect experiments and cryo-EM images of a separate study [229] where flat membrane surfaces were observed. On the other hand, this study [230] did not support oligomerization of lnC<sub>2</sub>AB with any direct evidence for protein-protein interactions that facilitate bridging of two apposing membranes. Previous cryo-EM images [229] provided the only direct evidence that supports oligomerization model [230] where membranes formed extended parallel surfaces separated at a constant 9 nm distance, and there was an ordered protein density between apposed membranes. However these structures were not observed in our extensive cryo-EM analysis (Figure 3.6). It is not clear how representative those parallel flat surfaces were for the entire sample [229] and whether the observations contradict with our results due to lack of statistical analysis of previous cryo-EM pictures [229]. The apparent distances between lnC<sub>2</sub>AB bridged membranes are predominantly between 3-4 nm according to the analysis of 697 bridged vesicle interfaces in our cryo-EM images. We estimate the real distance between membranes as 4-5 nm. Our cryo-EM analysis shows that lnC<sub>2</sub>AB bridges membranes prevalently by the direct method. We observed very rare cases of membrane separation of 8-10 nm and protein density between those 8-10 nm separated membranes. However, these cases were less than 1% of the membrane interfaces we have analyzed and there were no membrane flattening and well defined accumulation of lnC<sub>2</sub>AB. These rare interfaces may arise from small aggregates of lnC<sub>2</sub>AB due to residual polyacidic contamination. Our well purified lnC<sub>2</sub>AB did not aggregate in solution even at very high protein concentrations regardless of presence of Ca<sup>2+</sup>. However, lnC<sub>2</sub>AB that is not well purified (without ion-exchange chromatography) was observed to aggregate at above 10 μM

of  $\text{InC}_2\text{AB}$  concentration in the presence of  $\text{Ca}^{2+}$  (Figure 3.4) by a turbidity assay which is very similar to the results previously reported in the study that proposed oligomerization model [230].

It is important to note that the study that proposed the oligomerization model reported that the  $\text{InC}_2\text{AB}$  samples used in their study aggregate above 10  $\mu\text{M}$  concentration [230]. Moreover, the primary evidence provided to conclude that membrane bridging requires *trans* interactions between  $\text{InC}_2\text{AB}$  molecules bound to separate membranes relied on the finding that immobilized liposomes containing pre-bound  $\text{InC}_2\text{AB}$  pulled down target liposomes containing pre-bound  $\text{InC}_2\text{AB}$ , but not free liposomes [230]. The interpretation of this assay relied on the assumption of a slow dissociation constant for the interaction between  $\text{InC}_2\text{AB}$  and membranes described in reference [249]. The reference study [249] reported this rate in the order of  $10 \text{ s}^{-1}$ . Hence,  $\text{InC}_2\text{AB}$  should readily redistribute among liposome populations in the time scale of the pull-down assays, and the lack of binding of the target plain liposomes can be attributed merely to the overall decrease in  $\text{InC}_2\text{AB}$  concentration. Redistribution of  $\text{InC}_2\text{AB}$  molecules with plain liposomes resulted in protein to lipid ratios that are not sufficient to cluster liposomes (Figure 3.4 in Reference [230]). Additionally the direct bridging model was supposedly eliminated by NBD dequenching assays where NBD probes were placed at the bottom of the  $\text{C}_2\text{B}$  domain. Furthermore, direct membrane bridging by  $\text{InC}_2\text{AB}$  was presumably ruled out by the lack of an increase in fluorescence for NBD probes placed at the bottom of the  $\text{C}_2\text{B}$  domain (including residue 396) upon membrane binding, and by the absence of FRET between these probes and rhodamine-labeled lipids [230]. However, we observed a modest increase in NBD fluorescence signal from both

lnC<sub>2</sub>AB and C<sub>2</sub>AB samples (Figure 3.8) that were labeled with NBD at residue 396 (the bottom of C<sub>2</sub>B). A modest increase in the NBD fluorescence is expected since only a small fraction of C<sub>2</sub>B domain is expected to contribute to bridging membranes. These contradictory NBD dequenching results may arise from inadequate purification of lnC<sub>2</sub>AB considering the fact that lnC<sub>2</sub>AB reportedly aggregate in solution in the study where NBD fluorescence increase was not observed [230].

The NBD data shows a modest increase in fluorescence intensity for C<sub>2</sub>AB and lnC<sub>2</sub>AB labeled with NBD at the bottom of C<sub>2</sub>B domain upon binding to membranes in a Ca<sup>2+</sup> dependent manner (Figure 3.8). On the other hand, the NBD data shows a large increase for C<sub>2</sub>AB and lnC<sub>2</sub>AB labeled with NBD at the Ca<sup>2+</sup>-binding loops [202]. PBE experiments with nanodiscs suggest that the predominant population of C<sub>2</sub>AB binds to a single membrane through both of the Ca<sup>2+</sup>-binding loops (Figure 3.10) and also suggests that a sizeable population of C<sub>2</sub>AB molecules interact with the membrane in an orientation where the Ca<sup>2+</sup>-binding loops of two C<sub>2</sub> domains are oriented antiparallel. The predominant interaction of Ca<sup>2+</sup>-binding loops of C<sub>2</sub> domains with the membranes is not unexpected due to their high affinity for phospholipid bilayer and this observation is not incompatible with the direct bridging model. Interaction of the bottom of the C<sub>2</sub>B domain of a small fraction of C<sub>2</sub>AB or lnC<sub>2</sub>AB with an apposed membrane is sufficient to bridge two membranes and this bridging can occur when C<sub>2</sub> domains align in either parallel or antiparallel orientation (Figure 3.1 B). Binding of the bottom of the C<sub>2</sub>B domain to membrane was also observed for a sizable population of both C<sub>2</sub>AB and lnC<sub>2</sub>AB molecules in NBD experiments. According to changes in NBD signal, this population is estimated to be 5-10%. However, it could be larger if the

NBD labeled on the bottom of the C<sub>2</sub>B domain interacts with the membrane at the interface between hydrophobic tails and the polar layer of phospholipids, whereas NBD labeled on the Ca<sup>2+</sup>-binding loops interacts directly with hydrophobic tails. PBE measurements of C<sub>2</sub>AB on nanodiscs and previously obtained EPR data for lnC<sub>2</sub>AB also agree with the NBD data where the bottom of the C<sub>2</sub>B domain was shown to interact with membrane surface and the predominant population of lnC<sub>2</sub>AB molecules exists in antiparallel orientations [231].

Due to uncertainties in the estimation of the populations of the antiparallel orientation of C<sub>2</sub>AB and lnC<sub>2</sub>AB molecules by both NBD and EPR experiments, the analysis of EPR and NBD data is not incompatible. Overwhelming evidence provided from NBD, EPR, and PBE experiments clearly show that substantial populations of C<sub>2</sub>AB and lnC<sub>2</sub>AB molecules bridge membranes where C<sub>2</sub> domains are oriented antiparallel.

We observed very rare formation of aggregates of lnC<sub>2</sub>AB between apposed membranes. Therefore, we cannot completely eliminate the possibility of formation of lnC<sub>2</sub>AB oligomers between apposed membranes. However, there is no evidence that lnC<sub>2</sub>AB forms well defined oligomers and extensive analysis of cryo-EM images of membranes bridged by lnC<sub>2</sub>AB showed no indication of extended flat membrane interfaces. It is possible that residual polyacidic contaminants may be responsible for the rare occurrence of lnC<sub>2</sub>AB aggregates since they cause aggregation of synaptotagmin fragments in solution.

Additionally, there is an overwhelming amount of data presented here and previously [202], which shows that synaptotagmin-1 brings membranes into close proximity by the direct bridging mechanism. These data also provide evidence against oligomerization of synaptotagmin molecules both in solutions and on membranes [202].

Local concentration of synaptotagmin-1 in synaptic vesicles may be argued to be critical for formation of oligomers of synaptotagmin fragments. It is reported in a very thorough quantitative study that synaptic vesicles contain 15 molecules of synaptotagmin-1 on average [207]. However, membrane bound C<sub>2</sub>AB molecules were shown not to oligomerize even at 3 fold higher concentrations [202].

Additionally, synaptotagmin is located right at the interface between two membranes when it bridges them. The oligomerization model does not seem compatible with promoting membrane fusion since it requires the relocation of synaptotagmin oligomers from the fusion interface on the microsecond time scale. On the other hand, individual synaptotagmin molecules can diffuse away from inter-membrane space and interact with other members of the release machinery to bridge synaptic vesicles to plasma membranes and promote fusion in the direct bridging mechanism [131] (Figure 3.11).

The direct bridging mechanism should be further validated by better characterization of synaptotagmin-1 mutants and the clustering abilities of these mutants should be better correlated with *in vivo* results in functional studies [218]. Furthermore, understanding the interaction between SNARE complexes and synaptotagmin is crucial to elucidate the mechanistic contribution of clustering activity of synaptotagmin on membrane fusion.

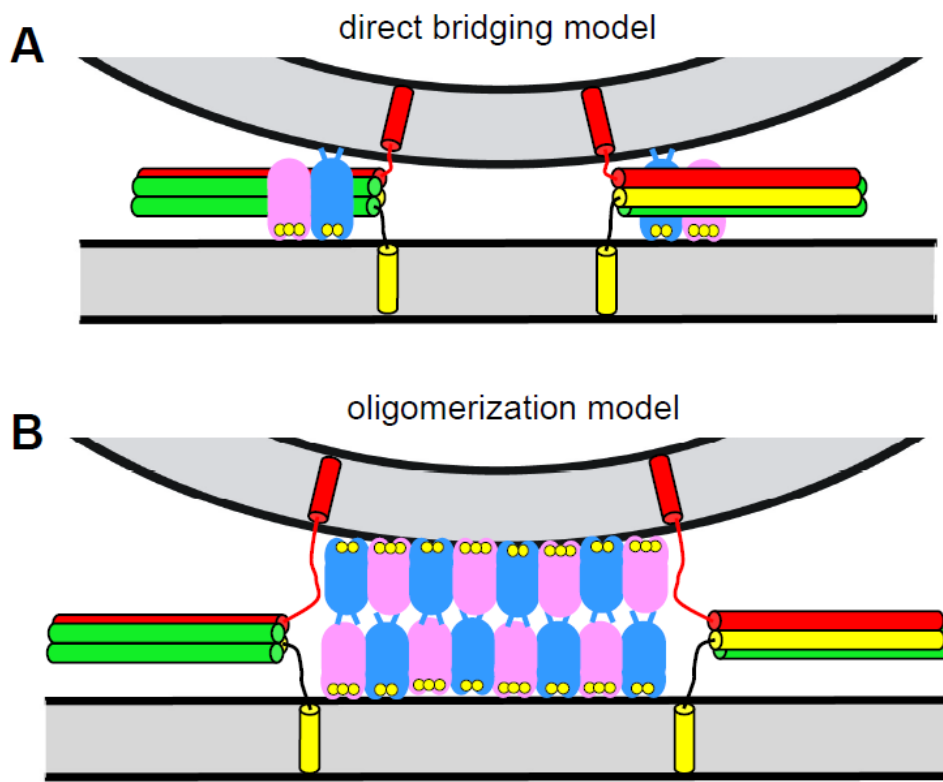


**Figure 3.11: Mechanistic implications of the direct bridging and oligomerization models.**

Both diagrams show the SNARE complex (syntaxin-1 in yellow, SNAP-25 in green and synaptobrevin in red) bridging the synaptic vesicle and plasma membranes (shown in gray), and are intended to illustrate potential relative orientations of the synaptotagmin-1 C<sub>2</sub> domains (C<sub>2</sub>A domain in pink, C<sub>2</sub>B domain in blue, Ca<sup>2+</sup> ions in yellow) with respect to the membranes and the SNARE complex. **(A)** In the direct bridging model, synaptotagmin-1 could bind simultaneously to the SNARE complex and the two membranes, which would allow a natural cooperation between synaptotagmin-1 and the SNAREs in bringing the membranes together to induce membrane fusion (1, 2). **(B)** In the oligomerization model, formation of a single synaptotagmin-1 oligomer between the membranes would hinder membrane fusion. It could be envisaged that multiple synaptotagmin-1 oligomers could form around the fusion pore area and each oligomer could bind to a SNARE complex, but neurotransmitter release is believed to normally involve a minimum of three SNARE complexes (3) and hence this model would require an unrealistic number of synaptotagmin-1 molecules.

### **3.4 Materials and Methods**

#### **3.4.1 Recombinant Proteins**

##### **3.4.1.1 Purification of the synaptotagmin-1 fragments:**

N-terminal glutathione S-transferase (GST) fusion proteins of synaptotagmin-1 fragments 95–421 (InC<sub>2</sub>AB)<sup>1</sup> and 140–421 (C<sub>2</sub>AB) were expressed in *Escherichia coli* BL21 (DE3-T1<sup>R</sup>) cells using PGEX-KG expression vector. PGEX-KG expression vectors containing synaptotagmin-1 fragments were inserted in chemically competent *Escherichia coli* BL21 (DE3-T1<sup>R</sup>) cells by the commonly used heat-shock transformation method and plated onto Lennox L Broth (LB) - Agar plates using ampicillin as the antibiotic selection. After overnight 37 °C incubation, minimal amount of bacteria from the edge of a bacterial colony containing synaptotagmin-1 fragments was inoculated into 2 ml LB media and sequentially transferred to 100 ml and 1 L LB media when the optical density (OD) of the cultures reached 0.8 and incubated at 37 °C by rotating at 250 RPM. The incubation temperature was dropped to 25 °C when the OD of the desired number of 1 L cultures (final yield is ~15 mg per 1 L of LB culture) reached 0.8. Isopropyl β-D-1-thiogalactopyranoside (IPTG) at 0.4 mM concentration was added to the 1 L cultures when the cultures reached the desired expression temperature condition. Synaptotagmin-1 fragments were expressed for 18 hours by rotating at 250 RPM and at 25 °C. Cells were incubated 10 minutes on ice and harvested at 4500 × g by centrifuging them at H600A swinging bucket rotor in a Sorvall RC 3C Plus centrifuge for 30 minutes. Cells were resuspended in buffer A [40 mM Tris·HCl (pH 8.2), 200 mM NaCl, 2

---

<sup>1</sup> We thank Bazbek Davletov for providing a sample of InC<sub>2</sub>AB protein and a vector to express InC<sub>2</sub>AB in bacteria.

mM DTT] with 1% Triton X-100 and protease inhibitor mixture (25 ml buffer A per 1 L bacterial culture) and lysed using an Avestin EmulsiFlex-C5 homogenizer at 10000 psi for 3 times. The soluble fraction of the cell lysate was collected after centrifugation at 48,000  $\times g$  for 30 min and incubated with Glutathione Sepharose 4B resin (1 ml resin per 1 L bacterial culture) (GE Healthcare) at 4 °C for 12 hours. The resin was washed with buffer A, buffer A + 50 mM CaCl<sub>2</sub>, buffer A + 50 mM CaCl<sub>2</sub> + 1 M NaCl (20 ml each buffer per 1 ml resin). Synaptotagmin-1 fragments were then treated with benzonase to clean nucleic acid contaminants (40 units per milliliter of solution, corresponding to ~1,000 units per liter of cell culture) in benzonase buffer [50 mM Tris (pH 8.0), 2 mM MgCl<sub>2</sub>] for 2 hours at room temperature with gentle rotation of the beads. The GST tag was cleaved with thrombin on the resin at room temperature for 3 hours in thrombin cleavage buffer [50 mM Tris (pH 8.0), 150 mM NaCl, 2 mM CaCl<sub>2</sub>]. Synaptotagmin-1 fragments were further purified with an ion exchange Source S column (GE Healthcare) [buffers: 50 mM NaAc (pH 6.2), 5 mM CaCl<sub>2</sub>; and 50 mM NaAc (pH 6.2), 5 mM CaCl<sub>2</sub>, 1 M NaCl] and size-exclusion chromatography on a Superdex 75 16/60 column (GE Healthcare) using 25 mM Tris (pH 7.4) containing 125 mM NaCl as the buffers.

Synaptotagmin C277S and N396C double mutations for both C<sub>2</sub>AB and InC<sub>2</sub>AB were generated by the QuikChange site-directed mutagenesis kit (Stratagene).

The proteins were labeled with *N,N'*-dimethyl-*N*-(iodoacetyl)-*N'*-(7-nitrobenz-2-oxa-1,3-diazol-4-yl)ethylenediamine (IANBD amide) (Invitrogen) according to manufacturer's protocol using 50–60  $\mu$ M of synaptotagmin-1 fragments and 400  $\mu$ M IANBD amide in the presence of 100  $\mu$ M Tris(2-carboxyethyl)phosphine at room temperature with 2-h incubation

time. All of the experiments were performed in 25 mM Hepes (pH 7.4), 150 mM KCl, and 1 mM MgCl<sub>2</sub> reconstitution buffer unless otherwise indicated.

#### ***3.4.1.2 Purification of the Apo-A1 fragment***

N-terminal hexa-histidine fusion protein of human ApoA1 fragment 68–267 was expressed in *Escherichia coli* BL21 (DE3-T1<sup>R</sup>) cells using pET-28a (Novagen) expression vector. pET-28a ApoA1 68-267 expression vector was inserted in chemically competent *Escherichia coli* BL21 (DE3-T1<sup>R</sup>) cells by the commonly used heat-shock transformation method and plated onto Lennox L Broth (LB) - Agar plates using kanamycin as the antibiotic selection. After overnight 37 °C incubation, minimal amount of bacteria from the edge of a bacterial colony containing ApoA1 68-267 was inoculated into 2 ml Terrific Broth (TB) media and sequentially transferred to 100 ml and 1 L TB media when the optical density (OD) of the cultures reached 1.5 and incubated at 37 °C by rotating at 250 RPM. Isopropyl β-D-1-thiogalactopyranoside (IPTG) at 1 mM concentration was added to the 1 L cultures when the OD of the desired number of 1 L cultures (final yield is >50 mg per 1 L of TB culture) reached 1.5. ApoA1 68-267 was expressed for 3 hours by rotating at 250 RPM and at 37 °C. Cells were incubated 10 minutes on ice and harvested at 4500 × *g* by centrifuging them at H600A swinging bucket rotor in a Sorvall RC 3C Plus centrifuge for 30 minutes. Cells were resuspended in buffer B [40 mM Tris·HCl (pH 8.0), 300 mM NaCl] with 1% Triton X-100, DNase and protease inhibitor mixture (40 ml buffer B per 1 L bacterial culture) and lysed using an Avestin EmulsiFlex-C5 homogenizer at 10000 psi for 3 times. The soluble fraction of the cell lysate was collected after centrifugation at 48,000 × *g* for 30 min and incubated

with Ni-NTA resin (2 ml resin per 1 L bacterial culture) (Qiagen) at 4 °C for 10 minutes. The resin was washed with buffer B + 1% Triton X-100, buffer B + 50 mM cholate + 20 mM imidazole, buffer B + 50 mM imidazole (40 ml each buffer per 1 ml resin). ApoA1 68-267 was eluted from Ni-NTA resin with Buffer B + 0.5 M imidazole and fractionated. Fractions containing ApoA1 68-267 was cleaved with TEV to remove hexa-histidine tag and dialyzed against 25 mM Tris·HCl (pH 7.4) + 125 mM NaCl + 0.5 mM EDTA.

### **3.4.2 Preparation of Phospholipid Vesicles**

The 1,2-dioleoyl-*sn*-glycero-3-[phospho-L-serine] (DOPS), 1-palmitoyl-2-oleoyl-*sn*-glycero-3-phosphocholine (POPC), and 1-palmitoyl-2-oleoyl-*sn*-glycero-3-phosphoethanolamine (POPE) (Avanti Polar Lipids) in chloroform were mixed in a glass test tube in a desired ratio, and chloroform was evaporated using dry nitrogen stream. The lipids were placed in a vacuum chamber overnight for complete removal of the organic solvent. Lipid films were hydrated with reconstitution buffer in an appropriate volume yielding 10 mM lipids. Lipids were vortexed for 5 minutes then frozen and thawed five times. Large unilamellar vesicles were prepared by extruding the hydrated lipid solution through 0.08- $\mu$ m polycarbonate membranes 23 times using an Avanti Mini-Extruder. The homogeneity of the vesicle size distribution was confirmed by dynamic light scattering and cryo-EM, and was centered around a diameter of 80 nm.

### **3.4.3 Fluorescence Experiments**

NBD fluorescence emission (500 - 620 nm) experiments were performed on a Photon Technology International spectrophotometer with a 4 nm slit width and 485 nm excitation at room temperature using 0.3  $\mu\text{M}$  synaptotagmin-1 fragments and 0.1 or 1 mM lipid vesicles (DOPS:POPC:POPE 15:55:30) in reconstitution buffer including 1 mM EGTA or 1 mM  $\text{CaCl}_2$ . Experiments under all of the conditions were repeated at least three times, and standard deviations were calculated. All of the experiments were repeated with unlabeled synaptotagmin-1 fragments, and the data were subtracted from actual data as background. Microsquare cuvettes with 5 mm interior width and 400  $\mu\text{L}$  volume capacity were used to obtain reliable data. Cuvettes with lower volume capacity (e.g., submicrocuvettes) gave considerably more variability in the data.

### **3.4.4 Turbidity**

Aggregation of differentially purified synaptotagmin-1 InC<sub>2</sub>AB fragments was monitored from the absorbance at 400 nm using a Varioskan Flash Plate Reader on a clear-bottom black 96-well plate. Experiments were performed in 25 mM Tris (pH 7.4) containing 125 mM NaCl, 1 mM  $\text{Ca}^{2+}$ , and the indicated protein concentrations.

### **3.4.5 Cryo-EM**

Both sides of Quantifoil 200 mesh copper, R2/2 hole shape, 2  $\mu\text{m}$  hole size and 4  $\mu\text{m}$  period grids were glow-discharged in a Denton Vacuum DV-502A instrument with 40-mA current for 45 s. Whatman paper with a 0.2-mL drop of amylamine was prepared immediately before

use and included during the glow discharge to prevent extensive binding of liposomes onto the carbon surface of the grid. Samples for cryo-EM were prepared by incubating 0.3 mg/mL lipid vesicles (DOPS:POPC 20:80) with 3  $\mu$ M or 10  $\mu$ M InC<sub>2</sub>AB fragment (resulting in protein to lipid ratios of 1:120 or 1:36, respectively) in reconstitution buffer at room temperature for 2 minutes; 3  $\mu$ L of the sample were loaded onto the carbon side of a Quantifoil grid, incubated for 10 seconds, and blotted with a piece of Whatman no. 4 paper from the edge of the grid for 5 s. Another 3  $\mu$ L of the sample were loaded onto the same side of the grid and rapidly frozen using Vitrobot FP 5350/60-type automated vitrification robot. The total incubation time up to the blotting step was  $\sim$ 5 min. The blotting time was 2 seconds and the humidity in the blotting chamber was above 95%. Standard Vitrobot Filter paper,  $\varnothing$ 55/20 mm, grade 595, was used for blotting. Images were taken with a JEOL 2200FS transmission electron microscope equipped with an energy filter at liquid nitrogen temperatures, keeping samples in an Oxford Instruments cryo-holder. Images were taken at 52.95 K calibrated magnification and were recorded on a 2K  $\times$  2K Tietz slow scan CCD camera or Kodak SO-163-type films. The electron density was kept at 20–30 electrons per square angstrom during each exposure by a minimum dosage system. Films were scanned with a PhotoScan Instrument from Z/I Imaging at 14  $\mu$ m resolution. Measurements of distances between membranes were performed using ImageJ.

### **3.4.6 Nanodisc Preparation**

The 1,2-dioleoyl-*sn*-glycero-3-[phospho-L-serine] (DOPS), 1-palmitoyl-2-oleoyl-*sn*-glycero-3-phosphocholine (POPC), and 1-palmitoyl-2-oleoyl-*sn*-glycero-3-phosphoethanolamine

(Avanti Polar Lipids) in chloroform were mixed in a glass test tube in the ratio of DOPS:POPC 15:85, and chloroform was evaporated using dry nitrogen stream. The lipids were placed in a vacuum chamber overnight for complete removal of organic solvent. Lipid films were hydrated with reconstitution buffer in an appropriate volume yielding 13 mM lipids. Nanodiscs were prepared as previously described [250] with small modifications [251]. Briefly, ApoA1 and lipids at an ApoA1:lipid ratio of 2:130 were mixed and supplied with 1% n-octyl- $\beta$ -D-glucopyranoside and 1% sodium cholate. The mixture was briefly vortexed and then incubated at room temperature for 30 minutes. The nanodiscs were formed by passing the mixture over a 4-cm-high column of Extracti-Gel D resin (Pierce) to remove the detergent. The nanodiscs were then purified on a Superdex-200 HiLoad 16/60 column (GE Healthcare) in 25 mM Tris·HCl (pH 7.4), 125 mM NaCl, 1 mM CaCl<sub>2</sub>, concentrated using a 30-kDa molecular weight cutoff filter, and exchanged to the same buffer in 100% D<sub>2</sub>O.

### **3.4.7 Spin Labeling of Synaptotagmin-1**

Synaptotagmin-1 C277S, N248C and C277S, V304C double mutations for C<sub>2</sub>AB were generated by the QuikChange site-directed mutagenesis kit (Stratagene). To prepare the <sup>2</sup>H-ILV-<sup>13</sup>CH<sub>3</sub>-C<sub>2</sub>AB N248C or V304C mutants for spin labeling, they were first treated with 10 mM DTT, and the DTT was then removed by cation exchange chromatography on Source S. The final buffer composition after cation exchange was ~50 mM sodium acetate (NaOAc), pH 6.2, 400 mM NaCl, 5 mM CaCl<sub>2</sub>. The protein was concentrated to 40–60  $\mu$ M and a 10-fold excess of MTSL was added from a 40-mM stock in dimethyl sulfoxide. The mixture was

rotated overnight at 4 °C to allow complete cysteine labeling; the excess MTSL was removed by buffer exchange in 25 mM Tris·HCl (pH 7.4), 125 mM NaCl, 1 mM CaCl<sub>2</sub> using a 10-kDa molecular weight cutoff filter; and the sample was exchanged to the same buffer in 100% D<sub>2</sub>O. The paramagnetic activity of MTSL was removed by reduction with 1 mM sodium dithionite and 1 mM ascorbic acid from 100-mM stocks. The dithionite stocks were prepared immediately before addition (< 30 minutes) due to its high instability.

### **3.4.8 NMR Spectroscopy**

NMR spectra were acquired at 25 °C on Varian INOVA800 or INOVA600 spectrometers. <sup>1</sup>H-<sup>15</sup>N HSQC and <sup>1</sup>H-<sup>13</sup>C HMQC spectra were acquired under the conditions indicated in the figure legends using H<sub>2</sub>O / D<sub>2</sub>O 95:5 (volume / volume) or 100% D<sub>2</sub>O, respectively, as the solvent. Total acquisition times were 2 - 12 hours. NMR data were processed with NMRPipe [210] and analyzed with NMRView [211].

## CHAPTER 4

# 4 MUNC13-1 DOCKS THE VESICLES AND SYNAPTOTAGMIN-1 OPENS THE FUSION PORE

### *4.1 Introduction*

Munc13s are multi-domain proteins that play important roles in neurotransmitter release in synapses. Neurotransmitter release is abrogated in the absence of Munc13s in animal studies [88, 90, 91, 252]. Synaptic vesicle priming was severely affected in the absence of Munc13s, which has been hypothesized to be the main reason for the strong phenotype in neurotransmitter release. Additionally, a synaptic vesicle docking activity was reported for Munc13 in some electron microscopy studies with distinct conclusions [93-95, 252].

MUN is the critical domain for Munc13 function and is responsible for opening of syntaxin-1 [66, 115]. Other domains of Munc13s are hypothesized to regulate the function of the MUN domain by coordinating membrane and protein interactions to perform its function (Figure 1.6). The C<sub>1</sub> domain interacts with diacylglycerol (DAG) and the C<sub>2</sub>B domain can bind to phospholipids in a Ca<sup>2+</sup> dependent manner. On the other hand, other C<sub>2</sub> domains in Munc13-1 do not bind Ca<sup>2+</sup> [110, 112]. The C<sub>2</sub>A domain interacts with the  $\alpha$ RIM zinc-finger domain [112] and a calmodulin binding motif interacts with calmodulin [253]. Biophysical studies and knock out studies in *C. elegans* clearly showed that the MUN domain leads to opening of the closed conformation of syntaxin-1, which is believed to be a key part of the priming step

of the neurotransmitter release. [58, 101, 102, 104]. However, interactions of C<sub>1</sub> and C<sub>2</sub>B domains with membranes are potentially important for the vesicle docking and priming functions of Munc13s. Additionally, overexpression of the open LE mutant of syntaxin-1 could only partially rescue release in *C. elegans* [105] and could not rescue release in Munc13-1/2 double knockout mouse [106]. These observations showed that Munc13-1 has another vital role in neurotransmitter release apart from facilitating the conformational transition of syntaxin-1. In this study, we elucidated the docking activity of Munc13-1, which can potentially account for this vital role. We also show that Munc13-1, in concert with Munc18-1, causes Ca<sup>2+</sup>-dependent, efficient lipid mixing and slow content mixing, which suggests the direct involvement of Munc13-1 in the membrane fusion process. We also found that Synaptotagmin-1 makes fusion pore formation more efficient, which correlates with its vital importance in fast synchronous release.

## **4.2 Results**

### **4.2.1 Munc13-1 clusters liposomes and facilitates lipid mixing between liposomes.**

We reconstituted syntaxin-1/SNAP-25 complex into plain liposomes and synaptobrevin into the liposomes that include 1,2-dipalmitoyl-sn-glycero-3-phosphoethanolamine-N-(7-nitro-2-1,3-benzoxadiazol-4-yl) (NBD-PE) and 1,2-dipalmitoyl-sn-glycero-3-phosphoethanolamine-N-(lissamine rhodamine B sulfonyl) (Rhod-PE). Merging of these two separate liposomes causes lipid mixing (Figure 4.1 A). Lipid mixing was analyzed in the presence of various proteins by dequenching of NBD fluorescence which arises from the dilution of NBD-PE and

Rhod-PE FRET pairs [33, 66]. Lipid mixing between these liposomes was quantified after 1000 seconds, which reflects the efficiency and the extent of fusion for each reaction. Each experiment was repeated three times and error bars are included in the lipid quantification results. To test the effect of Munc13-1 on SNARE-dependent lipid mixing, we used a Munc13-1 fragment ( $C_1C_2BMUN$ ) including its  $C_1$  domain, which is important for diacylglycerol (DAG) binding,  $C_2B$  domain, which is important for phosphatidylinositol-4,5-bisphosphate ( $PIP_2$ ) binding, and the catalytically active MUN domains, which facilitate the transition of syntaxin-1 from its closed conformation to open conformation (Figure 1.2 A and B).

Almost no lipid mixing was observed when we mixed synaptobrevin and syntaxin-1/SNAP-25 containing liposomes (Figure 4.1 B). Addition of a synaptotagmin-1 fragment containing both  $C_2A$  and  $C_2B$  domains ( $C_2AB$ ) efficiently increased lipid mixing between these liposomes in the presence of  $Ca^{2+}$  (Figure 4.1 B), which was observed previously in various studies [254]. Addition of  $C_1C_2BMUN$  to the liposomes containing SNAREs also efficiently increased lipid mixing in the absence of  $Ca^{2+}$  and addition of  $Ca^{2+}$  did not further enhance the lipid mixing (Figure 4.1 B). A lipid mixing enhancement effect of Munc13-4 in the presence of the  $Ca^{2+}$  was reported previously [255]; however, the effect was moderate, involved only SNAREs and required addition of  $Ca^{2+}$ . We have observed for the first time that the  $C_1C_2BMUN$  fragment of Munc13 can facilitate lipid mixing between liposomes containing only the SNARE proteins without  $Ca^{2+}$ . This is a very important observation because Munc13-1 has been hypothesized to have important roles in vesicle docking and priming, which takes places before  $Ca^{2+}$  influx in the active zone, and this observation can be

associated with the priming or docking functions of Munc13-1. Our observation can be explained by several scenarios. C<sub>1</sub>C<sub>2</sub>BMUN can cluster the vesicles without Ca<sup>2+</sup>, which facilitates the formation of the SNARE complex and cause more efficient lipid mixing between liposomes. Another explanation would be that C<sub>1</sub>C<sub>2</sub>BMUN may be directly involved in merging of the two membranes.

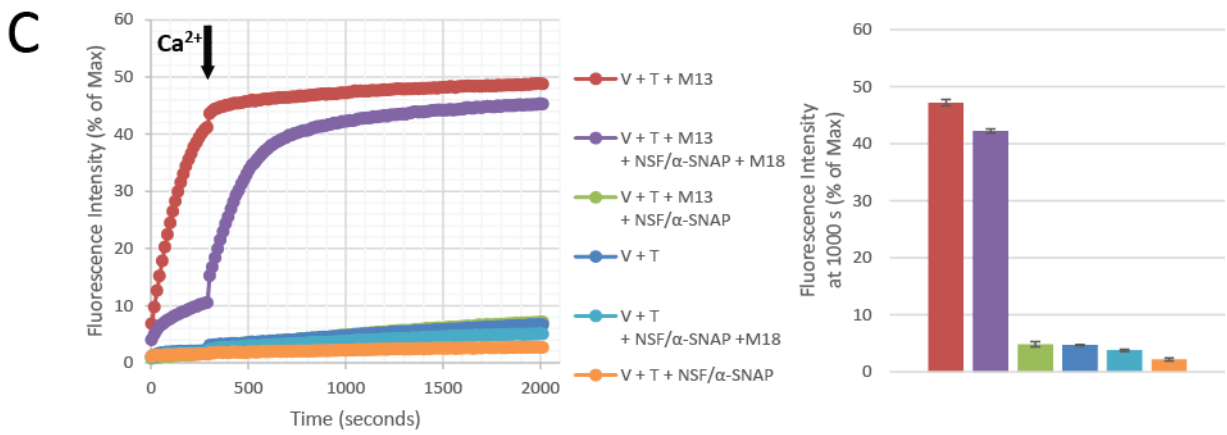
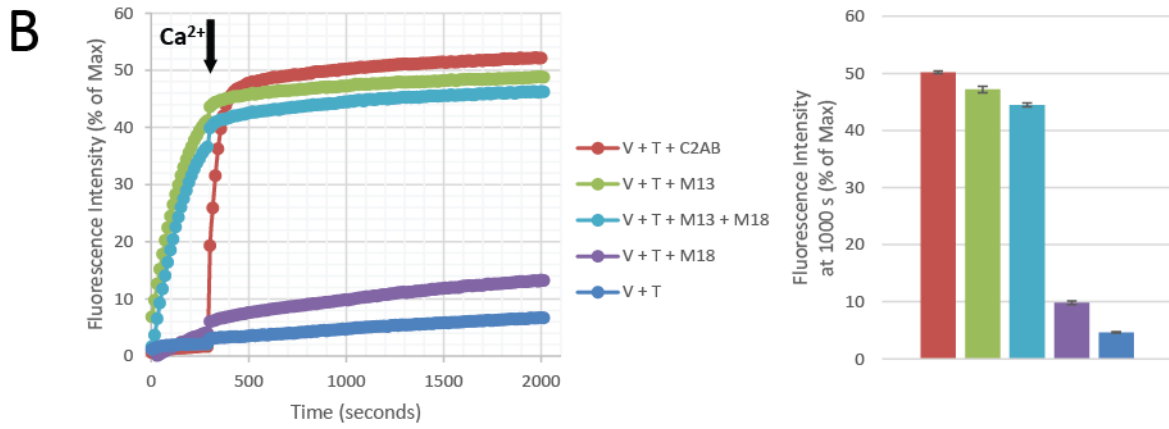
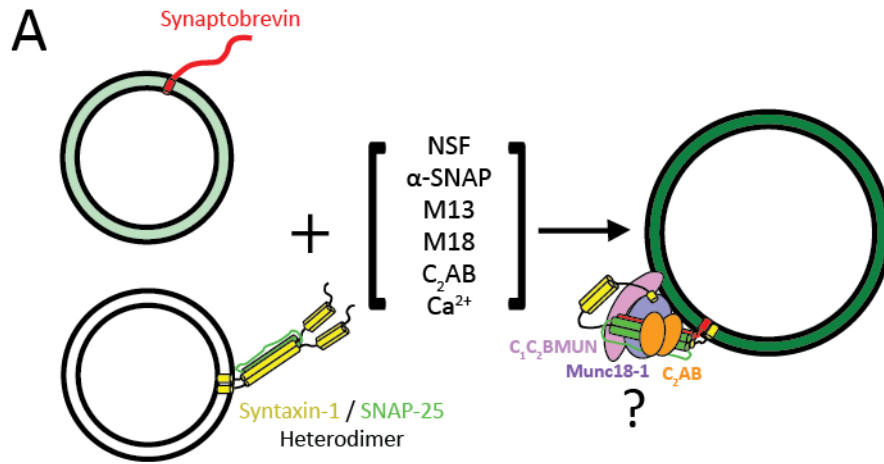


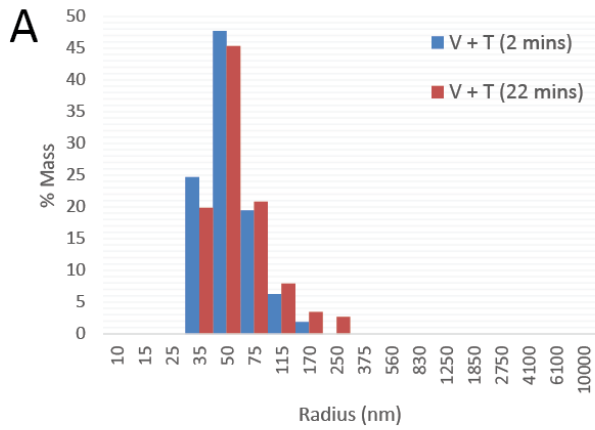
**Figure 4.1: Munc13-1 enhances lipid mixing**

(A) Summary of the lipid mixing experiments, which were performed with the synaptobrevin reconstituted liposomes (V) and syntaxin-1/SNAP-25 reconstituted liposomes (T). NBD-PE is quenched by Rhod-PE in the liposomes that contain synaptobrevin. Mixing of these liposomes with various protein combinations leads to merging of the liposomes containing fluorescent lipids with plain liposomes, and lipid mixing is monitored by dequenching of the NBD-PE due to loss of FRET upon dilution of fluorescent lipids. All the experiments in this study was performed by Alpay B. Seven and Xiaoxia Liu.

(B and C) Graphs showing the lipid mixing observed upon mixing of the SNARE reconstituted liposomes in the presence of various combinations of NSF,  $\alpha$ -SNAP, Munc13-1 C<sub>1</sub>C<sub>2</sub>BMUN fragment (M13), Munc18-1 (M18) and synaptotagmin-1 C<sub>2</sub>AB fragment (C<sub>2</sub>AB). Data acquisition were started without Ca<sup>2+</sup> and Ca<sup>2+</sup> was added at 5 minutes. The Y axis represents the percent of maximum NBD fluorescence intensity upon complete solubilization of the lipid molecules by detergent addition (Right panel). Quantification of the observed lipid mixing at 1000 seconds. Each experiment was repeated three times and error bars are included on the bar diagram as standard deviation (Right panel). Colors for the traces on the left panels match with the bar diagrams on the right panels.

To understand the mechanism of lipid mixing enhancement effect of C<sub>1</sub>C<sub>2</sub>BMUN, we analyzed the lipid mixing samples using dynamic light scattering (DLS) to show whether C<sub>1</sub>C<sub>2</sub>BMUN can cluster the vesicles and we performed lipid mixing experiments in the presence of NSF and  $\alpha$ -SNAP. NSF and  $\alpha$ -SNAP was previously shown in our lab to disassemble the syntaxin-1/SNAP-25 heterodimers. Enhancement of lipid mixing between the SNARE-containing liposomes by C<sub>2</sub>AB without Munc18-1 and Munc13-1 requires the syntaxin-1/SNAP-25 heterodimers [66]. Therefore, addition of NSF and  $\alpha$ -SNAP to the SNARE-containing liposomes abrogated the lipid mixing enhancement effect of C<sub>2</sub>AB [66]. Similarly, if Munc13-1 enhances lipid mixing by just clustering liposomes and facilitating the formation of the SNARE complex, addition of NSF and  $\alpha$ -SNAP should abrogate this effect. Addition of the NSF and  $\alpha$ -SNAP indeed abrogated the lipid mixing to the level of lipid mixing observed only in the presence of the SNAREs, and addition of Ca<sup>2+</sup> did not enhance lipid mixing (Figure 4.1 C). DLS results showed clustering of the SNARE-containing liposomes upon addition of C<sub>1</sub>C<sub>2</sub>BMUN regardless of the presence of Ca<sup>2+</sup> (Figure 4.2 A and C). These results strongly suggest that C<sub>1</sub>C<sub>2</sub>BMUN clusters the SNARE-containing liposomes. Clustering of the liposomes facilitates the formation of the SNARE complex, which gives rise to enhanced lipid mixing between liposomes. To further test whether the effect of C<sub>1</sub>C<sub>2</sub>BMUN is dependent on SNARE complex formation, we repeated these experiments in the presence of a soluble fragment of synaptobrevin containing only its SNARE motif. This synaptobrevin fragment is expected to compete with the full length synaptobrevin that is attached to liposomes to form the SNARE complex with the syntaxin-1/SNAP-25 heterodimers located on separate liposomes. Addition of the SNARE motif of

synaptobrevin severely impaired lipid mixing between liposomes (Figure 4.3). We also repeated these experiments in the absence of each individual SNARE protein. Absence of any of the SNAREs also severely impaired the lipid mixing between the SNARE-containing liposomes in the presence of C<sub>1</sub>C<sub>2</sub>BMUN and addition of Ca<sup>2+</sup> did not significantly affect lipid mixing (Figure 4.3). Additionally, C<sub>1</sub>C<sub>2</sub>BMUN clustered the liposomes of all these samples regardless of the presence of any SNAREs and Ca<sup>2+</sup> (Figure 4.2 B). These results clearly show that lipid mixing enhancement by C<sub>1</sub>C<sub>2</sub>BMUN is carried out through clustering of liposomes and thus causing acceleration of SNARE complex formation. It is important to note that clustering of the liposomes increase scattering; therefore there might be contribution of scattering to the observed fluorescence signal for any sample with C<sub>1</sub>C<sub>2</sub>BMUN.



**B**

Sample Components	Before Ca <sup>2+</sup>	After Ca <sup>2+</sup>
V + T	-	-
V + T + C2AB	-	+
V + T + M13	+	+
V + T + NSF/ $\alpha$ -SNAP	-	-
V + T + NSF/ $\alpha$ -SNAP + C2AB	-	+
V + T + NSF/ $\alpha$ -SNAP + M13	+	+
T (PIP2-) + M13	+	+
T (DAG-) + M13	+	+
T (PIP2-, DAG-) + M13	+	+
T (Syx-) + M13	+	+
T (SN25-) + M13	+	+
V + M13	+	+
V (Syb-) + M13	+	+

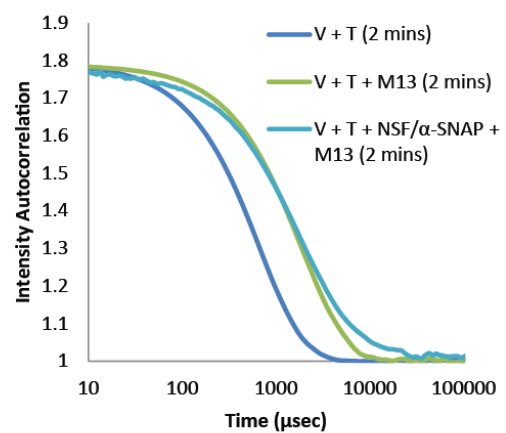
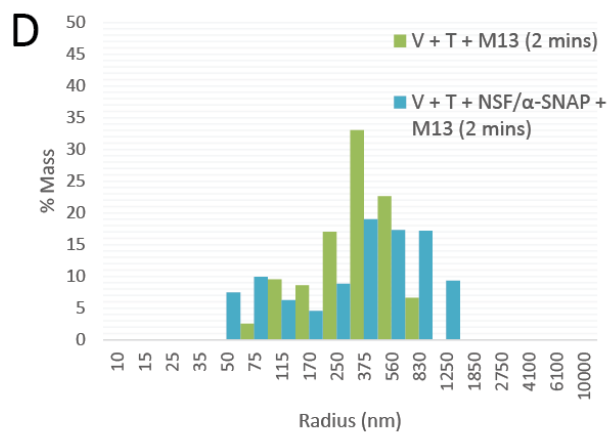
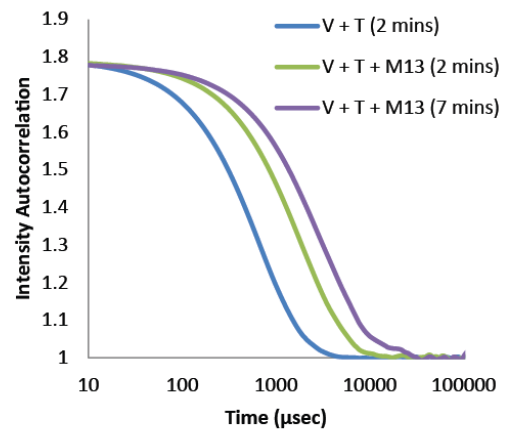
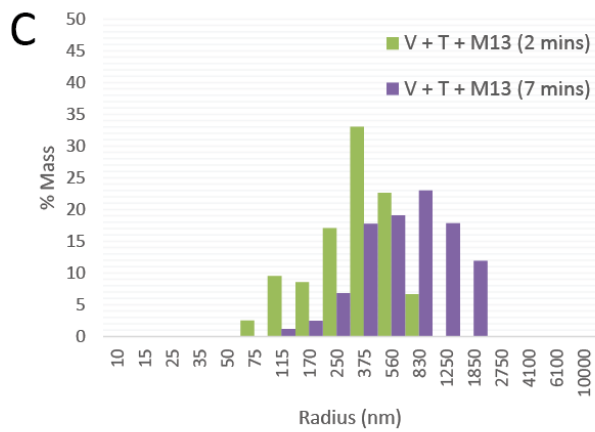


**Figure 4.2: Munc13-1 clusters of liposomes**

(A) Dynamic light scattering (DLS) results of samples where SNARE-containing liposomes (V and T) were mixed without any other protein at different time points.  $\text{Ca}^{2+}$  was added after 5 minutes to each sample.

(B) Summary of the clustering results for some of the key samples. All lipid mixing experiments were analyzed with DLS and all the samples that contain  $\text{C}_1\text{C}_2\text{BMUN}$  showed liposomes clustering regardless of  $\text{Ca}^{2+}$  presence.

(C) DLS results of the SNAREs containing liposomes with  $\text{C}_1\text{C}_2\text{BMUN}$  at different time points;  $\text{Ca}^{2+}$  was added after 5 minutes. Size distribution are shown in each sample (left panel) and autocorrelation curve of each sample (right panel)

(D) DLS results in the presence of NSF and  $\alpha$ -SNAP with  $\text{C}_1\text{C}_2\text{BMUN}$ .

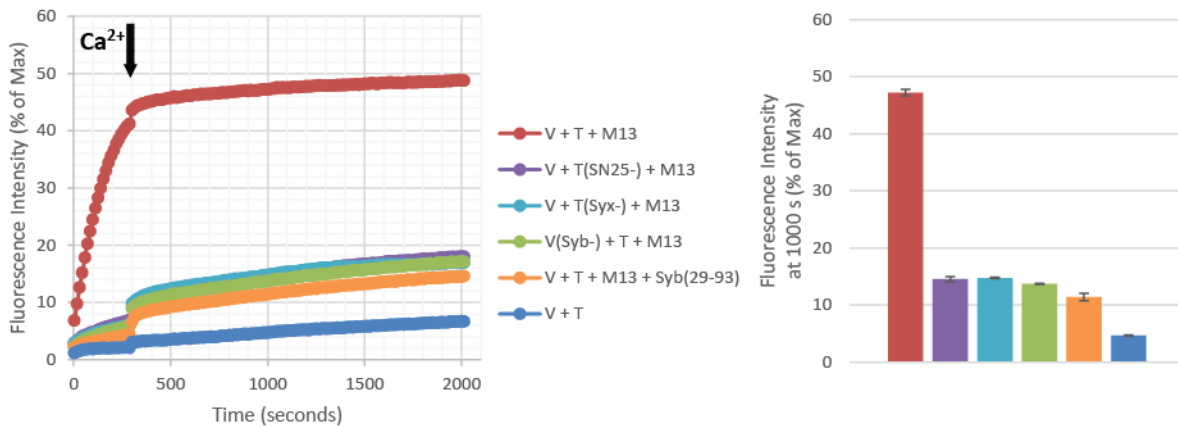


**Figure 4.3: Munc13-1 lipid mixing enhancement depends on the SNARE complex formation**

Time dependent lipid mixing observed after mixing the SNARE-containing liposomes (V and T) with  $C_1C_2BMUN$ . One SNARE protein is removed from each sample (Syntaxin-1 - Syx, SNAP-25 - SN25 and synaptobrevin - syb) or the SNARE motif of synaptobrevin is included (left panel). Quantification of the lipid mixing at 1000 seconds (right panel).  $Ca^{2+}$  was added after 5 minutes.

#### **4.2.2 $\text{Ca}^{2+}$ -dependent lipid mixing enhancement by $\text{C}_1\text{C}_2\text{BMUN}$ and Munc18-1**

To test whether Munc18-1 can affect the lipid mixing enhancement activity of  $\text{C}_1\text{C}_2\text{BMUN}$ , we also included Munc18 in the lipid mixing experiments. NSF and  $\alpha$ -SNAP inhibited the  $\text{C}_1\text{C}_2\text{BMUN}$  enhanced lipid mixing (Figure 4.1 C).

Surprisingly, addition of Munc18-1 together with  $\text{C}_1\text{C}_2\text{BMUN}$ , NSF and  $\alpha$ -SNAP to the SNARE-containing liposomes slightly increased the lipid mixing before addition of  $\text{Ca}^{2+}$  (Figure 4.1 C). This was not expected since Munc18-1 keeps syntaxin-1 in its closed conformation and inhibits formation of the SNARE complex. Addition of  $\text{Ca}^{2+}$  to this sample yielded very efficient lipid mixing (Figure 4.1 C). Here, we observed  $\text{Ca}^{2+}$ -dependent efficient lipid mixing in the presence of  $\text{C}_1\text{C}_2\text{BMUN}$ , NSF and  $\alpha$ -SNAP together with Munc18-1. It is important to note that liposomes were also clustered in this sample before and after addition of  $\text{Ca}^{2+}$  (Figure 4.2 D). Therefore this lipid mixing enhancement should arise from a different mechanism than just clustering and facilitating the SNARE complex formation from the syntaxin-1/SNAP-25 heterodimers and synaptobrevin. Liposomes in this sample were still clustered in the absence of  $\text{Ca}^{2+}$  and the syntaxin-1/SNAP-25 heterodimers were disassembled by NSF and  $\alpha$ -SNAP; but no efficient lipid mixing was observed before addition of  $\text{Ca}^{2+}$ . Efficient lipid mixing could only be observed after addition of  $\text{Ca}^{2+}$  and in the presence of Munc18-1. This can be explained either by direct involvement of  $\text{C}_1\text{C}_2\text{BMUN}$  in the membrane merging process or regulation of the trans-SNARE complex formation by  $\text{C}_1\text{C}_2\text{BMUN}$  and Munc18-1. Both scenarios require the involvement of Munc18-1 to cause efficient  $\text{Ca}^{2+}$ -dependent lipid mixing, likely because Munc18-1 is critical to protect against SNARE complex disassembly by NSF and  $\alpha$ -SNAP.

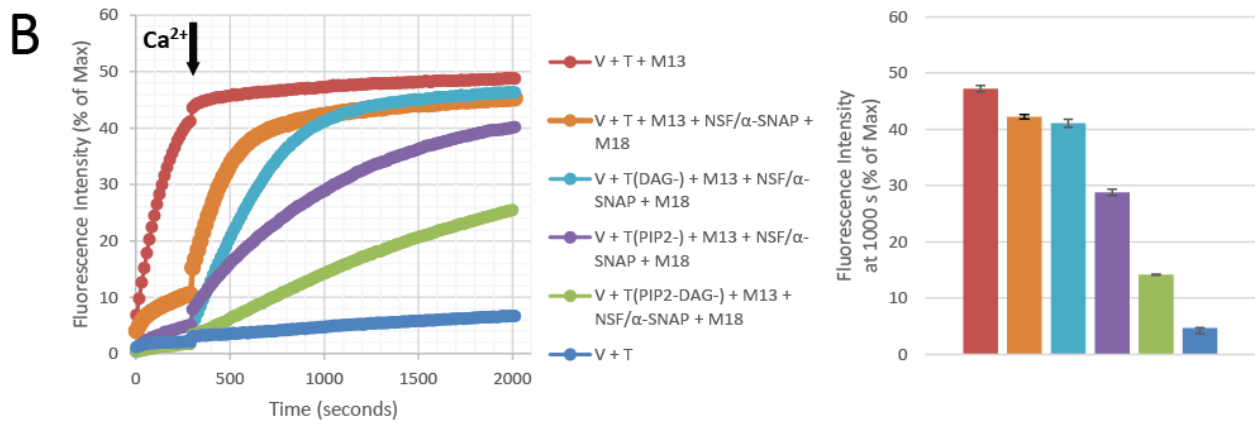
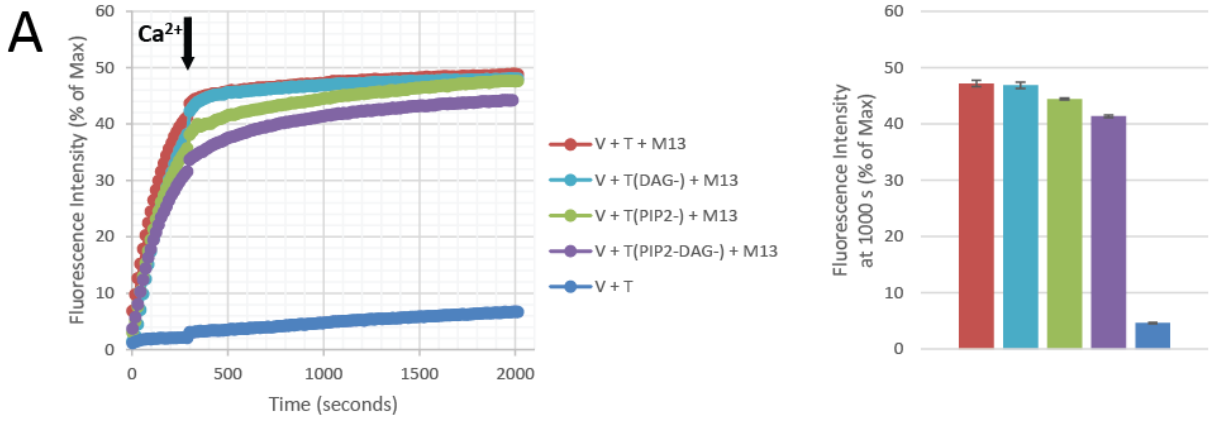
DAG and PIP<sub>2</sub> are lipid molecules present in the presynaptic plasma membrane. DAG and PIP<sub>2</sub> were shown to enhance Munc13-1 binding to phospholipid membranes through the C<sub>1</sub> and C<sub>2</sub>B domains, respectively [110, 256]. Synaptic vesicles were shown not to contain DAG and PIP<sub>2</sub> in a comprehensive analysis of synaptic vesicles [207]. The liposomes that contain the syntaxin-1/SNAP-25 heterodimers used in this study contain both DAG and PIP<sub>2</sub>. We repeated the lipid mixing experiments by removing DAG, PIP<sub>2</sub> or both from the liposomes that contains syntaxin-1/SNAP-25. We tested the effect of absence of these lipid molecules on enhancement of lipid mixing using both C<sub>1</sub>C<sub>2</sub>BMUN alone and C<sub>1</sub>C<sub>2</sub>BMUN with Munc18-1, NSF and  $\alpha$ -SNAP. Lipid mixing in the presence of only the SNARE proteins and C<sub>1</sub>C<sub>2</sub>BMUN was slightly diminished by removal of either DAG or PIP<sub>2</sub> from liposomes and removal of both had a modest but an additive effect (Figure 4.4 A). On the other hand, DAG and PIP<sub>2</sub> severely affected the Ca<sup>2+</sup>-dependent lipid mixing enhancement activity of Munc13-1 in the presence of NSF,  $\alpha$ -SNAP and Munc18-1 (Figure 4.4 B). Removal of DAG abrogated the residual lipid mixing completely before Ca<sup>2+</sup> addition and slightly decreased the Ca<sup>2+</sup>-dependent lipid mixing in the presence of the SNARE proteins, C<sub>1</sub>C<sub>2</sub>BMUN, NSF,  $\alpha$ -SNAP and Munc18-1 (Figure 4.4 B). Removal of PIP<sub>2</sub> had less effect on the residual lipid mixing before Ca<sup>2+</sup> addition; however it significantly decreased the efficiency of the Ca<sup>2+</sup>-dependent component of the lipid mixing (Figure 4.4 B). Removal of both DAG and PIP<sub>2</sub> abrogated the lipid mixing before Ca<sup>2+</sup> addition and severely diminished the Ca<sup>2+</sup>-dependent component of the lipid mixing (Figure 4.4 B). The accentuated effect of removal of both DAG and PIP<sub>2</sub> suggests that these lipid molecules have a synergistic role in the lipid mixing enhancement activity of C<sub>1</sub>C<sub>2</sub>BMUN. Liposomes can still be clustered without DAG and

PIP<sub>2</sub> (Figure 4.2 B). These results also show that the C<sub>1</sub>C<sub>2</sub>BMUN effect on lipid mixing in the presence and absence of Munc18-1, NSF and  $\alpha$ -SNAP is achieved through two distinct mechanisms. C<sub>2</sub>B is the only domain in Munc13-1 that has been shown to bind to Ca<sup>2+</sup> [110] and Ca<sup>2+</sup>-dependent localization of Munc13-1 to the PIP<sub>2</sub> rich plasma membrane was shown to be required for Munc13-1 activity [257].

DAG and PIP<sub>2</sub> binding to the C<sub>1</sub> and C<sub>2</sub>B domains of Munc13-1 does not seem to be required for the clustering of the liposomes and enhancement of lipid mixing between the SNARE-containing liposomes. This notion was supported by co-floatation assays, where binding of C<sub>1</sub>C<sub>2</sub>BMUN to liposomes lacking both DAG and PIP<sub>2</sub> lipid molecules is significantly diminished in co-floatation assays (Figure 4.4 C). The extent of decrease varies for liposomes prepared with two different methods, the so called direct and standard methods but some of the C<sub>1</sub>C<sub>2</sub>BMUN remained bound which was sufficient to cluster these liposomes and enhance the lipid mixing.

As previously stated, C<sub>1</sub>C<sub>2</sub>BMUN clusters liposomes, and thus facilitates the formation of the SNARE complex from synaptobrevin and the syntaxin-1/SNAP-25 heterodimers, which enhances lipid mixing NSF and  $\alpha$ -SNAP disassemble the syntaxin-1/SNAP-25 heterodimers. Therefore, they abrogate C<sub>1</sub>C<sub>2</sub>BMUN enhanced lipid mixing. Addition of Munc18-1 together with NSF,  $\alpha$ -SNAP and C<sub>1</sub>C<sub>2</sub>BMUN could not efficiently enhance lipid mixing without Ca<sup>2+</sup> even though liposomes were clustered; however addition of Ca<sup>2+</sup> facilitated lipid mixing. Removal of DAG and PIP<sub>2</sub> in lipid mixing experiments shows that the C<sub>1</sub> and C<sub>2</sub>B domains plays an important role in the Ca<sup>2+</sup>-dependent component of the lipid mixing. In addition, C<sub>1</sub>

binding to DAG seems to have a significant effect on the  $\text{Ca}^{2+}$ -independent component of the lipid mixing in the presence of  $\text{C}_1\text{C}_2\text{BMUN}$ , Munc18-1, NSF and  $\alpha$ -SNAP (Figure 4.4 B).



**C**

	1	2	3	4	5	6	7
PIP <sub>2</sub>	+	-	-	+	-	-	Control
DAG	+	+	-	+	+	-	
Ca <sup>2+</sup>	-	-	-	-	-	-	
Method	Standard			Direct			

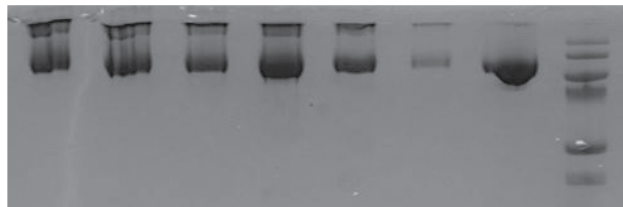


**Figure 4.4: Munc13 lipid mixing enhancement depends on DAG and PIP<sub>2</sub>**

Time dependent lipid mixing observed in the absence of PIP<sub>2</sub>, DAG or both from liposomes containing syntaxin-1/SNAP-25 (T) (left panel). Quantification of the lipid mixing at 1000 seconds (right panel). Ca<sup>2+</sup> was added after 5 minutes.

**(A)** Samples containing only the SNARE proteins and C<sub>1</sub>C<sub>2</sub>BMUN

**(B)** Samples containing the SNARE proteins, C<sub>1</sub>C<sub>2</sub>BMUN, Munc18-1, NSF and  $\alpha$ -SNAP.

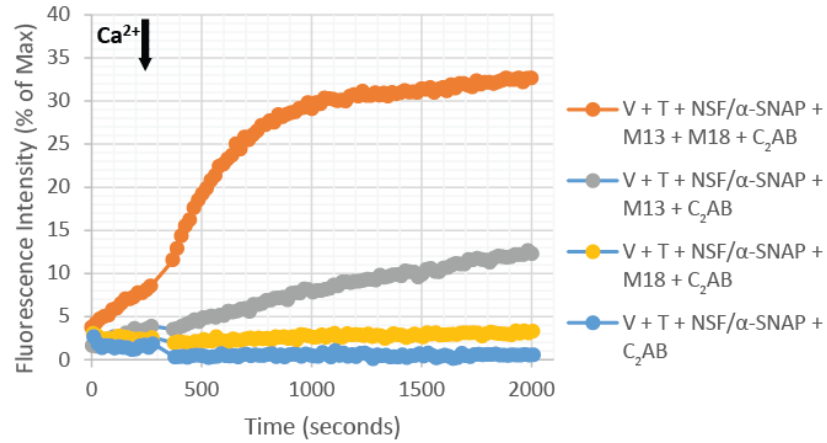
**(C)** Co-floatation of C<sub>1</sub>C<sub>2</sub>BMUN in histodenz with liposomes prepared with two different methods (standard and direct method) after 30 minutes of incubation were run on an SDS PAGE. Presence of DAG and PIP<sub>2</sub> in the liposomes containing syntaxin-1/SNAP-25 is denoted in the table. The last lane represents the total C<sub>1</sub>C<sub>2</sub>BMUN included in each co-floatation experiment.

### 4.2.3 Synaptotagmin-1 helps with the fusion pore opening

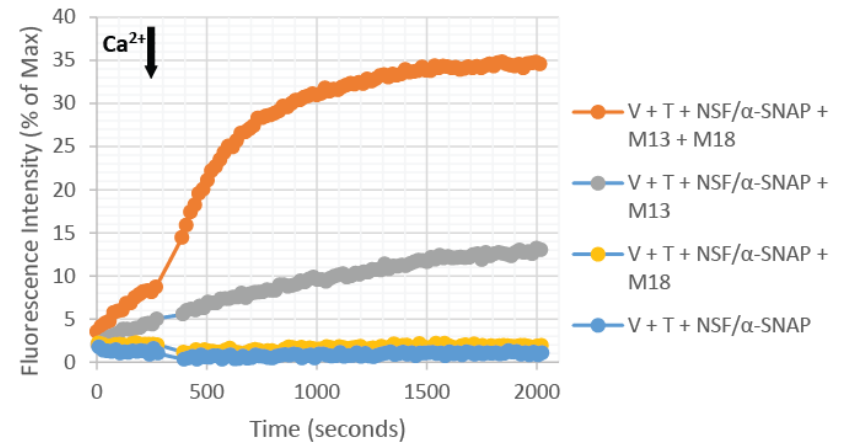
We have observed two separate lipid mixing enhancement activities of Munc13-1 which do not require synaptotagmin-1. One of these activities involves clustering of liposomes by  $C_1C_2$ BMUN in the absence of  $Ca^{2+}$  which is related to the docking or priming activities of Munc13-1. Surprisingly, we have also observed  $Ca^{2+}$ -dependent lipid mixing enhancement by  $C_1C_2$ BMUN. This type of activity was reported before for Munc13-4 [255] but, in this study, Munc13-4 enhanced lipid mixing in the presence of only the SNARE proteins. This effect of Munc13-4 can be through clustering of liposomes and facilitating the SNARE complex formation. On the other hand, the  $Ca^{2+}$ -dependent lipid mixing enhancement that was observed in our study involves a different mechanism. This activity surprisingly does not require synaptotagmin-1 which is vitally required for synchronous release. To understand the functional interplay between Munc13-1 and synaptotagmin-1, we performed content mixing experiments using a sulforhodamine and 1,1'-Dioctadecyl-3,3,3',3'-Tetramethylindodicarbocyanine Perchlorate (DiD) based dequenching assay. The synaptobrevin containing liposomes included DiD lipid molecules and encapsulated sulforhodamine, both of which are self-dequenched at their corresponding concentrations. Syntaxin-1/SNAP-25 containing liposomes do not include any fluorescent probes. Lipid mixing between these separate liposomes leads to dilution of the DiD and increases its fluorescence intensity due to dequenching of DiD. However sulforhodamine is only diluted upon full fusion and reports on content mixing between liposomes. No lipid or content mixing occurred between synaptobrevin and syntaxin-1/SNAP-25 containing liposomes, and addition of  $C_1C_2$ BMUN triggered efficient lipid mixing but not efficient content mixing

(Figure 4.6 A). These data show that only SNARE mediated merging of membranes cannot efficiently cause full fusion of the membranes on the time scale of these experiments (30 minutes). Addition of NSF and  $\alpha$ -SNAP together with C<sub>1</sub>C<sub>2</sub>BMUN abrogates the lipid mixing, which is similar to the results reported by NBD dequenching lipid mixing assays (Figure 4.1 and 4.6 A). Munc18-1 without C<sub>1</sub>C<sub>2</sub>BMUN did not cause either lipid or content mixing regardless of the presence of C<sub>2</sub>AB (Figure 4.5 B). Addition of C<sub>1</sub>C<sub>2</sub>BMUN with Munc18-1 triggered efficient lipid mixing in the presence of Ca<sup>2+</sup> similar to the levels reported in the NBD dequenching assays in this study and also caused slow content mixing between liposomes upon Ca<sup>2+</sup> addition (Figure 4.5 C and D). This result, together with the observation that no content mixing was observed in the presence of only the SNARE proteins and C<sub>1</sub>C<sub>2</sub>BMUN, also provides evidence that C<sub>1</sub>C<sub>2</sub>BMUN has a direct role in the membrane fusion process together with Munc18-1, which is Ca<sup>2+</sup>-dependent.

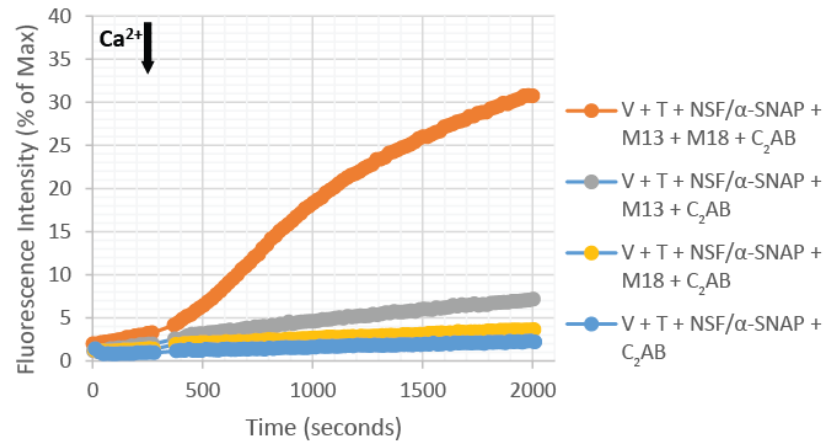
**A** Lipid Mixing with Synaptotagmin-1



**B** Lipid Mixing without Synaptotagmin -1



**C** Content Mixing with Synaptotagmin-1



**D** Content Mixing without Synaptotagmin-1

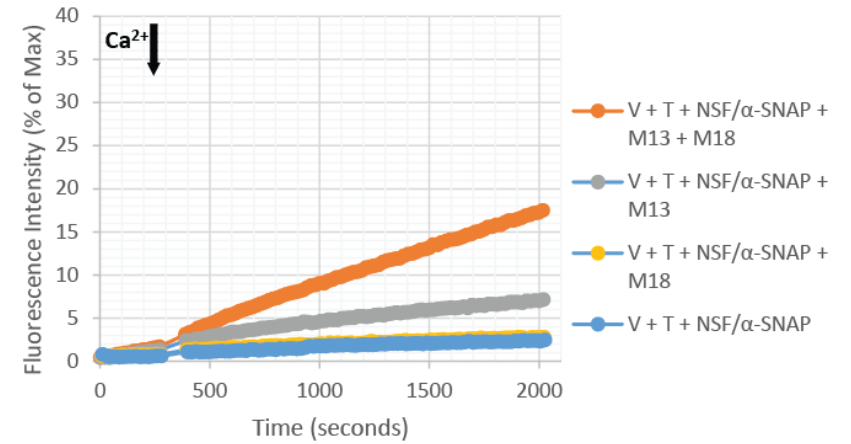


**Figure 4.5: Synaptotagmin-1 helps opening the fusion pore**

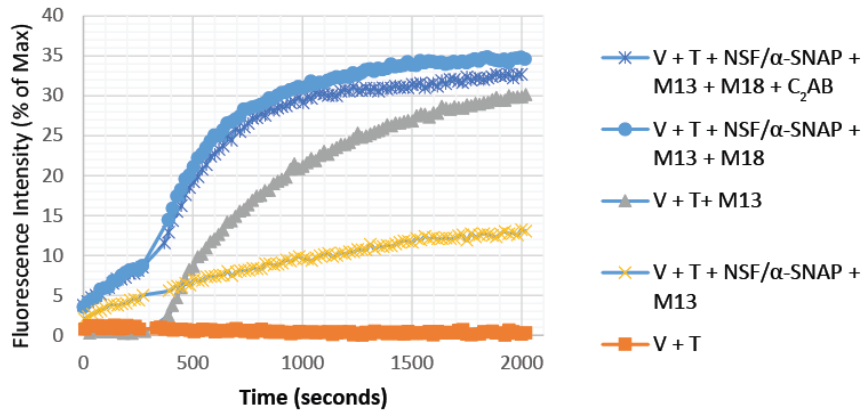
Graphs in the top panels showing the lipid mixing observed upon mixing of the SNARE reconstituted liposomes in the presence of various combinations of NSF,  $\alpha$ -SNAP, Munc13-1 C<sub>1</sub>C<sub>2</sub>BMUN fragment (M13), Munc18-1 (M18) and synaptotagmin-1 C<sub>2</sub>AB fragment (C<sub>2</sub>AB). Data acquisition were started without Ca<sup>2+</sup> presence and Ca<sup>2+</sup> was added at 5 minutes. The Y axis represents the percent of maximum DiD fluorescence intensity upon complete solubilization of the lipid molecules by detergent addition.

Graphs in the bottom panels show the content mixing observed in the same samples of the upper panels. The Y axis represents the percent of maximum sulforhodamine fluorescence intensity upon solubilization of the liposomes and following complete solubilization of sulforhodamine by detergent addition.

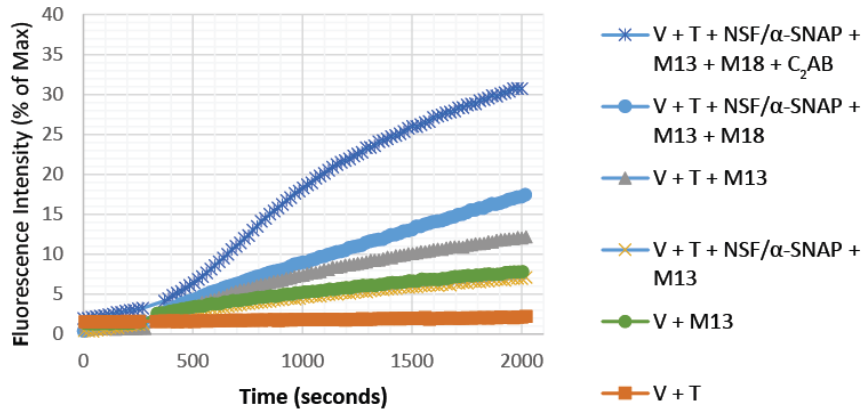
- (A) Lipid mixing observed from DiD lipid dequenching in the presence of C<sub>2</sub>AB.
- (B) Lipid mixing observed from DiD lipid dequenching in the absence of C<sub>2</sub>AB.
- (C) Content mixing observed from sulforhodamine dequenching in the presence of C<sub>2</sub>AB.
- (D) Content mixing observed from sulforhodamine dequenching in the absence of C<sub>2</sub>AB.

**A**

Lipid Mixing



Content Mixing



**B**

Extent of Leakiness by Munc13-1 in Content Mixing

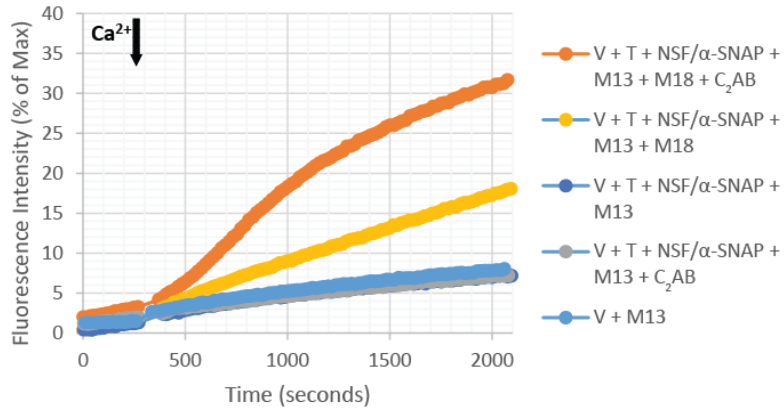


**Figure 4.6: Leakiness of the synaptobrevin liposomes with C1C2BMUN**

The graph in the bottom panels show the content mixing observed in the same samples of the upper panels. The Y axis represents the percent of maximum sulforhodamine fluorescence intensity upon solubilization of the liposomes and following complete solubilization of sulforhodamine by detergent addition.

(A) The graph in the top panels showing the lipid mixing observed upon mixing of the SNARE reconstituted liposomes in the presence of various combinations of NSF,  $\alpha$ -SNAP, Munc13-1 C<sub>1</sub>C<sub>2</sub>BMUN fragment (M13), Munc18-1 (M18) and synaptotagmin-1 C<sub>2</sub>AB fragment (C<sub>2</sub>AB). Data acquisitions were started without Ca<sup>2+</sup> presence and Ca<sup>2+</sup> was added at 5 minutes. M13 is added at 5 minutes only in grey dataset. The Y axis represents the percent of maximum DiD fluorescence intensity upon complete solubilization of the lipid molecules by detergent addition.

The graph in the bottom panels show the content mixing observed in the same samples of the upper panels. The Y axis represents the percent of maximum sulforhodamine fluorescence intensity upon solubilization of the liposomes and following complete solubilization of sulforhodamine by detergent addition.

(B) Comparison of the key content mixing experiments with the leakiness of the synaptobrevin liposomes (V) with C<sub>1</sub>C<sub>2</sub>BMUN, where only synaptobrevin liposomes are incubated with C<sub>1</sub>C<sub>2</sub>BMUN without syntaxin-1/SNAP-25 liposomes.

Addition of C<sub>2</sub>AB with Munc18-1 and C<sub>1</sub>C<sub>2</sub>BMUN showed similar levels of lipid mixing that was observed without C<sub>2</sub>AB (Figure 4.5 C). However, addition of C<sub>2</sub>AB with C<sub>1</sub>C<sub>2</sub>BMUN, Munc18-1, NSF and  $\alpha$ -SNAP caused very efficient content mixing between the SNARE-containing liposomes (Figure 4.5 D). This data shows that C<sub>2</sub>AB facilitates fusion pore opening at the membrane fusion process. It is important to note that slow but significant content mixing was observed with C<sub>1</sub>C<sub>2</sub>BMUN, Munc18-1, NSF,  $\alpha$ -SNAP and the SNARE proteins. This notion suggests that C<sub>1</sub>C<sub>2</sub>BMUN together with other proteins can cause complete fusion of the membranes; however C<sub>2</sub>AB makes the fusion pore opening more efficient.

### ***4.3 Discussion***

The results presented in this study suggest two novel functions for Munc13-1 in neurotransmitter release that enlighten the essential roles of Munc13-1 in synaptic vesicle docking, priming and actual merging of the two membranes. Our study showed that C<sub>1</sub>C<sub>2</sub>BMUN can cluster liposomes regardless of the presence of SNAREs, which facilitates the reconstituted synaptobrevin and syntaxin-1/SNAP-25 to form the SNARE complex. The SNARE complex formation in the presence of only C<sub>1</sub>C<sub>2</sub>BMUN is insufficient to efficiently cause full fusion of the membranes. However, efficient lipid mixing was achieved under these conditions. Lipid mixing mediated solely by SNAREs has been extensively studied and a recent cryo-EM study suggested that only SNAREs can trigger slow lipid mixing between liposomes and lead to hemifusion of the membranes [258]. The levels of lipid mixing in that

study are very low, in the order of 3-4% of normalized fluorescence intensity over a 10 minutes period which is comparable to the levels observed for the samples that contain only the SNARE proteins in our study. Our results show that addition of C<sub>1</sub>C<sub>2</sub>BMUN accelerates the SNARE complex formation and enhances the lipid mixing between membranes. We suggest that this lipid mixing arises from the close apposition and perhaps hemifusion of membranes. DAG and PIP<sub>2</sub> binding to the C<sub>1</sub> and C<sub>2</sub>B domains of Munc13-1 does not seem to be required for the clustering of the liposomes and enhancement of lipid mixing between the SNARE-containing liposomes. However, binding of C<sub>1</sub>C<sub>2</sub>BMUN to liposomes lacking both DAG and PIP<sub>2</sub> lipid molecules is significantly diminished in co-floatation assays (Figure 4.4 C). The effect of DAG and PIP<sub>2</sub> on C<sub>1</sub>C<sub>2</sub>BMUN binding varied for the liposomes prepared with different methods. Some of the C<sub>1</sub>C<sub>2</sub>BMUN remained bound, which was sufficient to cluster these liposomes and enhance the lipid mixing. It is important to note that lipid composition, preparation method of the liposomes and even the size of the dialysis cassettes that is used to remove detergent from detergent solubilized lipid/protein solutions can cause variation in lipid mixing results and interaction of proteins with the membranes. C<sub>1</sub>C<sub>2</sub>BMUN binding to liposomes is one example for this kind of variation. The kinetics of the detergent removal is one of the important parameters in the standard method of liposome preparation in which lipids and proteins are solubilized with detergent and removal of the detergent leads to formation of liposomes.

The effect of C<sub>1</sub>C<sub>2</sub>BMUN on the SNARE-mediated lipid mixing critically depends on the presence of the syntaxin-1/SNAP-25 heterodimers. NSF and  $\alpha$ -SNAP were previously shown to abrogate C<sub>2</sub>AB enhanced lipid mixing by disassembling these heterodimers [66]. Addition

of NSF and  $\alpha$ -SNAP also abrogated the C<sub>1</sub>C<sub>2</sub>BMUN enhanced lipid mixing but did not affect the clustering of the liposomes caused by C<sub>1</sub>C<sub>2</sub>BMUN in our study. C<sub>1</sub>C<sub>2</sub>BMUN enhanced lipid mixing is also abolished with the removal of any of the SNARE proteins or addition of a soluble fragment of synaptobrevin, which contains its SNARE motif. These results clearly show that C<sub>1</sub>C<sub>2</sub>BMUN enhances lipid mixing through clustering of liposomes and the ensuing facilitation of the SNARE complex formation.

Significant sequence homology between the MUN domain and various tethering complexes was observed in recent computational studies [259]. Tethering complexes are involved in various membrane fusion machineries and play important roles in bridging membranes, which allows the fusion machinery to assemble [212]. The sequence homology between the MUN domain and tethering complexes is low. However, comparison of the crystal structure of the C-terminal half of the MUN domain with structures of several subunits of these complexes revealed that they have similar characteristic elongated multi-helical structures (Figure 1.6 C) [260]. The results presented here show that the MUN domain can also bridge membranes to facilitate the formation of the fusion machinery and provides more evidence for the homology between the MUN domain and tethering complexes. This activity of C<sub>1</sub>C<sub>2</sub>BMUN is likely to underlie the docking function of Munc13-1.

Munc18-1 was also claimed to accelerate SNARE-mediated lipid mixing in the presence of the syntaxin-1/SNAP-25 heterodimers. However, syntaxin-1/Munc18 was shown to be the true starting point in neurotransmitter release instead of the syntaxin-1/SNAP-25 heterodimers [66]. After NSF and  $\alpha$ -SNAP disassemble the syntaxin-1/SNAP-25 heterodimers, Munc18-1 interacts with syntaxin-1 and keeps syntaxin-1 in its closed

conformation, which prevents formation of the SNARE complex. In our study Munc18-1 in the presence of NSF and  $\alpha$ -SNAP cannot enhance lipid mixing between the SNARE-containing liposomes. However, addition of Munc18-1 with C<sub>1</sub>C<sub>2</sub>BMUN shows Ca<sup>2+</sup>-dependent lipid mixing enhancement. Liposomes are clustered in this condition regardless of Ca<sup>2+</sup> presence and efficient lipid mixing can only occur in the presence of both Munc18-1 and Ca<sup>2+</sup> together with C<sub>1</sub>C<sub>2</sub>BMUN. Therefore, this enhancement is carried out using a different mechanism than facilitation of the SNARE complex formation from synaptobrevin and the syntaxin-1/SNAP-25 heterodimers. We hypothesize that C<sub>1</sub>C<sub>2</sub>BMUN and Munc18-1 either regulate the formation of the trans-SNARE complex formation or are directly involved in the merging of membranes. Another line of evidence for our hypothesis is the fact that lipid mixing enhancement by C<sub>1</sub>C<sub>2</sub>BMUN was not severely affected by removing DAG and PIP<sub>2</sub> lipid molecules since the liposomes could still be clustered in the presence of only the SNARE proteins and C<sub>1</sub>C<sub>2</sub>BMUN. However removal of DAG and PIP<sub>2</sub> significantly decreased both the Ca<sup>2+</sup>-dependent and independent components of the lipid mixing in the presence of NSF,  $\alpha$ -SNAP C<sub>1</sub>C<sub>2</sub>BMUN and Munc18-1. The Ca<sup>2+</sup>-independent component observed under these conditions depends on the concentrations of Munc18-1 and syntaxin-1/SNAP-25, and the efficiency of NSF and  $\alpha$ -SNAP. Addition of freshly purified NSF and  $\alpha$ -SNAP led to almost no lipid mixing without Ca<sup>2+</sup> in the presence of C<sub>1</sub>C<sub>2</sub>BMUN, Munc18-1 and the SNARE proteins (Figure 4.7). In addition, this residual Ca<sup>2+</sup>-independent lipid mixing allowed us to understand that the presence of DAG is also critically important for the Ca<sup>2+</sup>-independent component of the lipid mixing. It is important to note that apart from the importance of the interaction between DAG and the C<sub>1</sub> domain of Munc13-1, DAG is a cone-

shaped lipid molecule and important for the bending of the membranes and stalk formation [11].

Observation of the  $\text{Ca}^{2+}$ -dependent lipid mixing enhancement of  $\text{C}_1\text{C}_2\text{BMUN}$  with Munc18-1 in the absence of synaptotagmin-1 was an unexpected result since the  $\text{Ca}^{2+}$ -dependent neurotransmitter release machinery has been well characterized and synaptotagmins had been shown to be the  $\text{Ca}^{2+}$  sensors for this process [202, 261]. The vital importance of synaptotagmin-1 on  $\text{Ca}^{2+}$ -dependent synchronous release was previously shown [261]. Lipid mixing experiments are valuable tools to understand the functions of protein that are involved in membrane fusion processes. However, lipid mixing assays should be carefully interpreted since these assays cannot report actual full fusion of the membranes. Therefore, we hypothesized that synaptotagmin-1 may play an important role in the formation of the fusion pore and full fusion of the membranes. Content mixing experiments showed that neither  $\text{C}_1\text{C}_2\text{BMUN}$  nor Munc18-1 alone could accelerate the full fusion between the SNARE-containing liposomes regardless of the presence of NSF and  $\alpha$ -SNAP (Figure 4.5 D). Content mixing was slightly enhanced by the addition of  $\text{Ca}^{2+}$  when both Munc18-1 and  $\text{C}_1\text{C}_2\text{BMUN}$  were included together with NSF and  $\alpha$ -SNAP (Figure 4.5 D). However, very efficient content mixing was achieved only after addition of  $\text{C}_2\text{AB}$  (Figure 4.5 D). Removal of Munc18-1 or Munc13-1 abrogated content mixing even in the presence of the  $\text{C}_2\text{AB}$ , which is consistent with our previous studies [66]. These results show that  $\text{C}_2\text{AB}$  has an important role in the formation of the fusion pore and  $\text{C}_2\text{AB}$  can perform this function in the presence of Munc18-1 and  $\text{C}_1\text{C}_2\text{BMUN}$ , where the syntaxin-1/SNAP-25 heterodimers are disassembled by NSF and  $\alpha$ -SNAP.

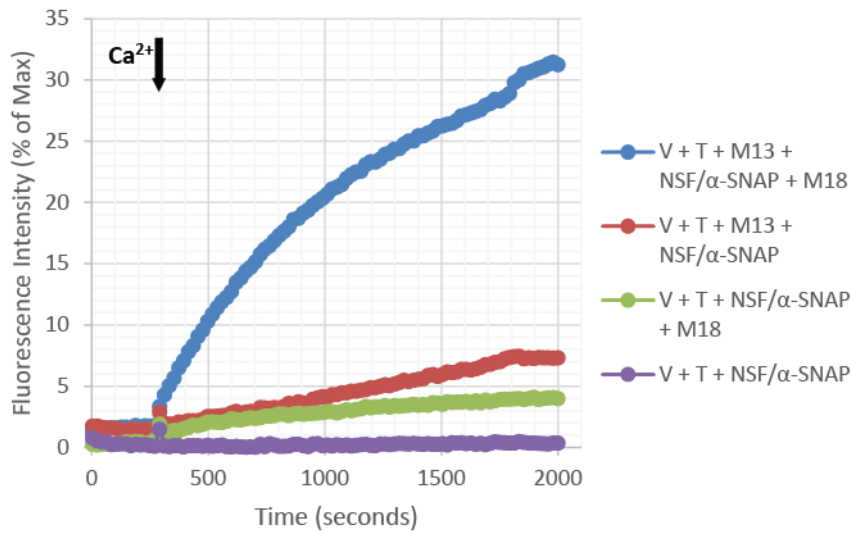


**Figure 4.7: Lipid mixing with freshly purified NSF and  $\alpha$ -SNAP**

Graphs showing the lipid mixing observed upon mixing of the SNARE reconstituted liposomes in the presence of freshly purified NSF,  $\alpha$ -SNAP and various combinations of Munc13-1 C<sub>1</sub>C<sub>2</sub>BMUN fragment (M13), Munc18-1 (M18) and synaptotagmin-1 C<sub>2</sub>AB fragment (C<sub>2</sub>AB). Data acquisition was started without Ca<sup>2+</sup> and Ca<sup>2+</sup> was added at 5 minutes. The Y axis represents the percent of maximum NBD fluorescence intensity upon complete solubilization of the lipid molecules by detergent addition (Right panel). This set of data is analogous to the data set in Figure 4.4 B. This data set is shown to illustrate that there is no lipid mixing without Ca<sup>2+</sup> with freshly purified NSF and  $\alpha$ -SNAP in the presence of C<sub>1</sub>C<sub>2</sub>BMUN and Munc18-1.

Content mixing was observed previously with the SNARE-containing liposomes, where the syntaxin-1/SNAP-25 heterodimers were not disassembled [262, 263]. It is important to remember that some content mixing was observed without C<sub>2</sub>AB (Figure 4.5 D). This observation suggests that full membrane fusion can be achieved with C<sub>1</sub>C<sub>2</sub>BMUN and Munc18-1 at a slower rate. All the SNARE mediated membrane fusion machineries involve homologs of Munc18-1 and Munc13-1. However, synaptotagmin-1 is specialized for neurotransmitter release. It is important to note that some of the membrane fusion processes occur without C<sub>2</sub>AB. Another explanation of Ca<sup>2+</sup>-dependent lipid mixing enhancement of C<sub>1</sub>C<sub>2</sub>BMUN with Munc18-1 would be that C<sub>1</sub>C<sub>2</sub>BMUN together with Munc18-1 may carry an intermediate step in fusion of membranes, which involves rearrangement of lipid molecules. The vesicles can then be ready for fusion upon the Ca<sup>2+</sup> response of C<sub>2</sub>AB after this potential priming step. Incorporation of other components of the release machinery, especially complexins, and investigation of fusion intermediates using cryo-EM microscopy are important next steps to clarify the mechanisms underlying docking and priming of the vesicles.

## ***4.4 Materials and Methods***

### **4.4.1 Recombinant Proteins and Protein Purification**

#### ***4.4.1.1 C<sub>1</sub>C<sub>2</sub>BMUN purification***

N-terminal hexa-histidine fusion protein of a Munc13-1 fragment including residues 529-1407, EF and 1453-1531 (C<sub>1</sub>C<sub>2</sub>BMUN) was expressed in Sf9 insect cells using pFastBacTMHT B vector with Bac-to-Bac system (Invitrogen). The pFastBacTMHT B

vector containing C<sub>1</sub>C<sub>2</sub>BMUN was used to generate baculo-viruses to infect Sf9 insect cells. Sf9 cells were harvested after 68-72 hours of infection at 4500 × g by centrifuging them at H600A swinging bucket rotor in a Sorvall RC 3C Plus centrifuge for 30 minutes, and re-suspended in Buffer A containing 50 mM Tris·HCl (pH 8.0), 250 mM NaCl, 10 mM imidazole and a protease inhibitors mixture (15 ml buffer per 1 liter of Sf9 cells). Sf9 cells were frozen in liquid nitrogen and thawed on ice to lyse the cells. The soluble fraction of the cell lysate was collected after centrifugation at 48,000 × g for 30 min and incubated with Ni-NTA resin (2 ml resin per 1 L Sf9 cell culture) (Qiagen) at 4 °C for 10 minutes. The resin was washed with buffer A, buffer A + 1 % Triton X-100, buffer A + 1 M NaCl + 5 % glycerol and buffer A (20 ml of each buffer per 1 ml resin). C<sub>1</sub>C<sub>2</sub>BMUN fragment on Ni-NTA resin was then treated with benzonase to clean nucleic acid contaminants (40 units per milliliter of solution, corresponding to ~1,000 units per liter of cell culture) in Buffer A + 2 mM MgCl<sub>2</sub> for 1 hour at room temperature with gentle rotation of the beads. C<sub>1</sub>C<sub>2</sub>BMUN was eluted from Ni-NTA resin with Buffer A + 0.2 M imidazole and fractionated. Fractions containing C<sub>1</sub>C<sub>2</sub>BMUN was cleaved with tobacco etch virus (TEV) to remove hexa-histidine tag during dialysis against a buffer containing 20 mM Tris·HCl (pH 8.0), 250 mM NaCl, 5 % glycerol and 1 mM TCEP for 16 hours at 4°C. C<sub>1</sub>C<sub>2</sub>BMUN fragment was further purified with an ion exchange Source Q column (GE Healthcare) [Buffers for Surce Q: 20 mM Tris·HCl (pH 8.0), 5 % glycerol, 1 mM TCEP and the same buffer with 1 M NaCl] and size-exclusion chromatography on a Superdex 200 16/60 column (GE HEalthcare) using 20 mM Tris·HCl (pH 8.0), containing 250 mM NaCl , 10 % glycerol and 1 mM TCEP as the buffers.

#### **4.4.1.2 NSF / $\alpha$ -SNAP purification**

N-terminal glutathione S-transferase (GST) fusion proteins of NSF and  $\alpha$ -SNAP were expressed, harvested and purified similar to synaptotagmin-1 fragments described in the third chapter with the following differences. NSF and  $\alpha$ -SNAP were expressed at 20 °C and 25 °C respectively and harvested in a buffer containing 50 mM Hepes (pH 7.6), 400 mM KCl, 10% glycerol, 2 mM DTT, and protease inhibitors mixture. Cells were lysed and incubated with GST resin. NSF and  $\alpha$ -SNAP bound to GST resin was washed with PBS+ 1 mM DTT, PBS + 1 mM DTT + 1 % Triton and PBS + 1 mM DTT + 0.5 M NaCl. NSF and  $\alpha$ -SNAP were treated with benzonase and then cleaved with trombin on GST resin. NSF and  $\alpha$ -SNAP were further purified with size-exclusion chromatography on a Superdex 200 16/60 column and Superdex 75 16/60 column respectively using a buffer containing 20 mM Hepes (pH 7.6), 150 mM KCl, 10% glycerol, 1 mM TCEP. All the NSF purification buffers included 0.5 mM ATP and 2 mM MgCl<sub>2</sub>.

#### **4.4.1.3 Syntaxin-1 purification**

N-terminal hexa-histidine fusion protein of rat syntaxin-1 was expressed in *Escherichia coli* BL21 (DE3-T1<sup>R</sup>) cells using pET-28a (Novagen) expression vector. pET-28a expression vector containing syntaxin-1 was inserted in chemically competent *Escherichia coli* BL21 (DE3-T1<sup>R</sup>) cells by the commonly used heat-shock transformation method and plated onto Lennox L Broth (LB) - Agar plates using kanamycin as the antibiotic selection. After overnight 37 °C incubation, minimal amount of bacteria from the edge of a bacterial colony containing syntaxin-1 was inoculated into 2 ml LB media and sequentially transferred to 100

ml and 1 L LB media when the optical density (OD) of the cultures reached 0.8 and incubated at 37 °C by rotating at 250 RPM. Isopropyl  $\beta$ -D-1-thiogalactopyranoside (IPTG) at 0.4 mM concentration was added to the 1 L cultures when the OD of the desired number of 1 L cultures reached 0.8. Syntaxin-1 was expressed for 18 hours by rotating at 250 RPM and at 23 °C. Cells were incubated 10 minutes on ice and harvested at  $4500 \times g$  by centrifuging them at H600A swinging bucket rotor in a Sorvall RC 3C Plus centrifuge for 30 minutes. Cells were resuspended in a buffer containing 50 mM Tris·HCl (pH 8.0), 500 mM NaCl, 5% Triton X-100, 8 mM imidazole, DNase and protease inhibitor mixture (20 ml buffer per 1 L bacterial culture) and lysed using an Avestin EmulsiFlex-C5 homogenizer at 10000 psi for 3 times. The soluble fraction of the cell lysate was collected after centrifugation at  $48,000 \times g$  for 30 min and incubated with Ni-NTA resin (1 ml resin per 1 L bacterial culture) (Qiagen) at 4 °C for 10 minutes. The resin was washed with a buffer containing 50 mM Tris·HCl (pH 8.0), 250 mM NaCl, 1.5% Triton X-100, 8 mM imidazole (50 ml buffer per 1 ml of resin). The Ni-NTA tag was cleaved with thrombin in thrombin cleavage buffer with 1 %  $\beta$ -OG on the resin at room temperature for 3 hours. Syntaxin-1 was further purified with an ion exchange Source Q column (GE Healthcare) [buffers: 20 mM Tris·HCl (pH 8.0), 1%  $\beta$ -OG, 1 mM TCEP and the same buffer with 1 M NaCl].

#### ***4.4.1.4 Synaptobrevin purification***

N-terminal glutathione S-transferase (GST) fusion protein of rat synaptobrevin (VAMP-2) was expressed, harvested and purified similar to synaptotagmin-1 fragments described in the third chapter with the following differences. Synaptobrevin was expressed at 23 °C and

harvested in PBS with 0.05 % Tween-20, 0.4 % Triton X-100, 0.5 % n-Lauroyl Sarcosine, 5 mM DTT and protease inhibitors mixture. Cells were lysed and incubated with GST resin. Synaptobrevin bound to GST resin was washed with PBS + 1 mM DTT + 1 % Triton X-100 (25 ml PBS per 1 ml of resin). Synaptobrevin was treated with benzonase in benzonase buffer with 1 % Triton X-100 and then cleaved with thrombin in thrombin cleavage buffer with 1 %  $\beta$ -OG on GST resin. Synaptobrevin was further purified with an ion exchange Source S column (GE Healthcare) [buffers: 25 mM NaAc (pH 5.5), 5 mM  $\text{CaCl}_2$ , 1 mM TCEP. and the same buffer with 1 M NaCl].

#### ***4.4.1.5 SNAP-25 purification***

N-terminal hexa-histidine fusion protein of rat SNAP-25 was expressed, harvested and purified similar to synaptotagmin-1 fragments described in the third chapter with the following differences. Synaptobrevin was expressed at 23 °C and harvested with a buffer containing 50 mM Tris·HCl (pH 8.0), 500 mM NaCl, 4 mM imidazole, 1 % Triton X-100, and protease inhibitors mixture. Cells were lysed and incubated with Ni-NTA resin (1 ml resin per 1 liter of cell culture). SNAP-25 bound to Ni-NTA resin was washed with with a buffer containing 50 mM Tris·HCl (pH 8.0), 500 mM NaCl, 20 mM imidazole, and 1 % Triton X-100 (25 ml buffer per 1 ml of resin). SNAP-25 was treated with benzonase in benzonase buffer and then cleaved with thrombin. SNAP-25 was further purified with size-exclusion chromatography on a Superdex 75 16/60 column (GE HEalthcare) using 50 mM Tris (pH 8.0) containing 125 mM NaCl as the buffers. One mg of SNAP-25 was used for size-exclusion chromatography.

#### ***4.4.1.6 Munc18-1 purification***

N-terminal glutathione S-transferase (GST) fusion proteins of Munc18-1 was expressed, harvested and purified similar to synaptotagmin-1 fragments described in the third chapter with the following differences. Munc18-1 was expressed at 20 °C and harvested in PBS with 1 mM DTT and protease inhibitors mixture. Cells were lysed and incubated with GST resin. Munc18-1 bound to GST resin was washed with PBS+ 1 mM DTT, PBS + 1 mM DTT + 1 % Triton and PBS + 1 mM DTT + 0.5 M NaCl. Munc18-1 was treated with benzonase and then cleaved with thrombin on GST resin. Munc18-1 was further purified with size-exclusion chromatography on a Superdex 200 16/60 column using a buffer containing 25 mM Hepes (pH 7.4), 150 mM KCl, 10% glycerol, 1 mM TCEP.

#### ***4.4.1.7 C<sub>2</sub>AB purification***

C<sub>2</sub>AB purification is explained in methods section of the third chapter of this manuscript.

### **4.4.2 Preparation of Phospholipid Vesicles**

The 1-palmitoyl-2-oleoyl-*sn*-glycero-3-phosphocholine (POPC), 1,2-dioleoyl-*sn*-glycero-3-[phospho-L-serine] (DOPS), 1-palmitoyl-2-oleoyl-*sn*-glycero-3-phosphoethanolamine (POPE), N-(lissamine rhodamine B sulfonyl)-1,2-dipalmitoyl-*sn*-glycero-3-phosphatidylethanolamine (Rho-PE) and N-NBD-1,2-dipalmitoyl-*sn*-glycero-3-phosphatidylethanolamine (NBD-PE), cholesterol (Ch), L- $\alpha$ -phosphatidylinositol-4,5-bisphosphate (PIP<sub>2</sub>), 1-palmitoyl-2-oleoyl-*sn*-glycerol (DAG) (Avanti Polar Lipids) 1,1'-Dioctadecyl-

3,3,3',3'-Tetramethylindodicarbocyanine Perchlorate (DiD), (Invitrogen) in chloroform were mixed in a glass test tube in a desired ratio, and chloroform was evaporated using dry nitrogen stream, while immersing test tubes in 35 °C water bath. The lipids were placed in a vacuum chamber overnight for complete removal of the organic solvent.

For direct method, lipid films were hydrated with reconstitution buffer (25 mM Hepes pH: 7.4, 150 mM KCl and 10 % glycerol) in an appropriate volume yielding 10 mM lipids. Lipids were vortexed for 5 minutes then frozen and thawed five times. Large unilamellar vesicles were prepared by extruding the hydrated lipid solution through 0.08- $\mu$ m polycarbonate membranes 23 times using an Avanti Mini-Extruder. The homogeneity of the vesicle size distribution was confirmed by dynamic light scattering was centered around a diameter of 80 nm.

For standard method, lipid films were dissolved with reconstitution buffer + 2 % octyl- $\beta$ -D-glucopyranoside ( $\beta$ -OG) in an appropriate volume yielding 10 mM lipids. Large unilamellar vesicles were prepared by dialyzing the lipid solution through a 10 kDa dialysis cassette (Pierce). The homogeneity of the vesicle size distribution was confirmed by dynamic light scattering was centered around a diameter of 100 nm.

#### **4.4.3 Reconstitution of SNAREs**

For synaptobrevin containing liposomes, synaptobrevin: lipids (M/M); 1: 600 protein to lipid ratio is used. In lipid mixing experiments, POPC: DOPS: POPE: Rho-PE: NBD-PE: Ch; 40: 20: 17: 1.5: 1.5: 20 lipid ratio was used. In content mixing experiments, POPC: DOPS:

POPE: DiD: Ch; 39.5: 20: 17: 3.5: 20 lipid ratio was used and lipids are hydrated with reconstitution buffer containing 40 mM sulforhodamine B (Acros Organics).

For syntaxin-1/SNAP-25 containing liposomes, syntaxin-1: SNAP-25: lipids (M/M/M); 1: 5: 800 protein to lipid ratio was used. In both of the lipid and content mixing experiments, POPE: DOPS: POPE: PIP<sub>2</sub>: DAG: Ch; 38: 18: 20: 2: 2: 20 lipid ratio was used.

For direct method, syntaxin-1 and SNAP-25 were incubated on room temperature for 20 minutes. Syntaxin-1/SNAP-25 or synaptobrevin solubilized in reconstitution buffer containing 1%  $\beta$ -OG + 1mM TCEP were slowly titrated to the preformed liposomes, while vortexing the liposomes. Volume of the protein was adjusted to keep the final concentration of  $\beta$ -OG below the solubilization concentration of the proteoliposomes. Proteoliposomes were incubated at room temperature for 20 minutes and dialyzed 3 times against 1 L reconstitution buffer containing 1 g BioBeads (BioRad) or Amberlite XAD-2 (Sigma-Aldrich) through a 10 kDa dialysis cassette for 1 hour, 2 hours and 16 hours at 4 °C. For content mixing assays, proteoliposomes were purified from excess sulforhodamine B with PD-10 (G-25) column (GE Healthcare) according to manufacturer protocol before dialysis.

For standard method, syntaxin-1 and SNAP-25 were incubated on room temperature for 20 minutes. Syntaxin-1/SNAP-25 or synaptobrevin solubilized in reconstitution buffer containing 1%  $\beta$ -OG + 1mM TCEP was mixed with detergent solubilized lipids to yield 3.75 mM lipids for Syntaxin-1/SNAP-25 liposomes and 2.5 mM lipids for synaptobrevin liposomes. Protein-lipid solutions were incubated at room temperature for 20 minutes and dialyzed 3 times against 1 L reconstitution buffer containing 1 g BioBeads (BioRad) or

Amberlite XAD-2 (Sigma-Aldrich) through a 10 kDa dialysis cassette for 1 hour, 2 hours and 16 hours at 4 °C.

#### **4.4.4 Lipid mixing assays**

The syntaxin-1/SNAP-25 containing liposomes (0.25 mM-lipid concentration) were first incubated with 4 mM ATP, 2 μM of α-SNAP, 0.8 μM NSF, 5 mM MgCl<sub>2</sub> and 2 μM of Munc18-1 as a 100 μl reaction using reconstitution buffer with 0.5 mM TCEP and 0.1 mM EGTA for 20 minutes at 37 °C. The synaptobrevin containing liposomes (0.125 mM-lipid concentration), 0.5 μM C<sub>1</sub>C<sub>2</sub>BMun, 1 μM SNAP-25 and 1 μM C<sub>2</sub>AB were added to the reaction after incubation. Final volume of the reaction is adjusted to 200 μl, which brings the concentration of pre-incubation molecules to the half. The combination of the proteins used in each reaction is indicated in the figures. NBD fluorescence emission experiments at 538 nm were performed on a Photon Technology International spectrophotometer with a 3 nm slit width and 460 nm excitation at 37 °C. The lipid mixing experiments were repeated at least three times, and standard deviations were calculated. Microsquare cuvettes with 5 mm interior width were used. Ca<sup>2+</sup> (0.5 mM) was added after 5 minutes of data acquisition and 1 % β-OG was added at the end of the reaction to reach maximum NBD fluorescence intensity.

#### **4.4.5 Content Mixing Assays**

Samples were treated similar to the samples in lipid mixing assays. The lipid concentration for synaptobrevin containing liposomes was determined by UV absorbance of DiD. Lipid

and content mixing were monitored simultaneously by measuring dequenching of DiD at 675 nm (excitation at 650 nm) and sulforhodamine B at 587 nm (excitation at 565 nm) at 30 °C.

#### **4.4.6 Co-Flootation Assays**

Liposomes were prepared with the same lipid compositions as the syntaxin-1/SNAP-25 containing liposomes without proteins and the lipid molecules stated in Figure 4.4 C. C<sub>1</sub>C<sub>2</sub>BMUN (1 μM) was mixed with the liposomes (0.5 mM) and incubated at room temperature for 30 minutes . The incubated samples were mixed with an equal volume of 80 % histodenz to make a 40 % layer of histodenz in a 5 × 41 mm ultraclear Bechman centrifuge tube. This layer was overlaid sequentially with 35 and 30 % of histodenz and buffer. The samples in histodenz gradient were centrifuged in a SW55Ti rotor (Beckman) at 40,000 rpm for 4 hours at 4 °C. Liposomes with proteins collected from top of the histodenz gradient and analyzed with SDS-PAGE and Coomassie blue staining.

#### **4.4.7 Dynamic Light Scattering**

Samples were analyzed with a Protein Solutions DynaPro instrument from Wyatt Technology equipped with a temperature-controlled microsampler. Data were acquired for each sample with 10 % laser power and 10 seconds acquisition time for 30 times. The samples were prepared in reconstitution buffer and diluted to a final lipid concentration of 30 μM or 100 μM lipids and centrifuged at 14,000 x g for 10 minutes before each acquisition.

The results were analyzed with the Dynamics V6 software to calculate the size distribution of the macromolecules in the samples.

## 5 References:

1. Chen, E.H., et al., *Cell-cell fusion*. FEBS Lett, 2007. **581**(11): p. 2181-93.
2. Duelli, D. and Y. Lazebnik, *Cell-to-cell fusion as a link between viruses and cancer*. Nat Rev Cancer, 2007. **7**(12): p. 968-76.
3. Earp, L.J., et al., *The many mechanisms of viral membrane fusion proteins*. Curr Top Microbiol Immunol, 2005. **285**: p. 25-66.
4. Hoppins, S., L. Lackner, and J. Nunnari, *The machines that divide and fuse mitochondria*. Annu Rev Biochem, 2007. **76**: p. 751-80.
5. Jahn, R. and R.H. Scheller, *SNAREs--engines for membrane fusion*. Nat Rev Mol Cell Biol, 2006. **7**(9): p. 631-43.
6. Kielian, M. and F.A. Rey, *Virus membrane-fusion proteins: more than one way to make a hairpin*. Nat Rev Microbiol, 2006. **4**(1): p. 67-76.
7. Martens, S. and H.T. McMahon, *Mechanisms of membrane fusion: disparate players and common principles*. Nat Rev Mol Cell Biol, 2008. **9**(7): p. 543-56.
8. McNeil, P.L. and R.A. Steinhardt, *Plasma membrane disruption: repair, prevention, adaptation*. Annu Rev Cell Dev Biol, 2003. **19**: p. 697-731.
9. Sapir, A., et al., *Viral and developmental cell fusion mechanisms: conservation and divergence*. Dev Cell, 2008. **14**(1): p. 11-21.
10. Weissenhorn, W., A. Hinz, and Y. Gaudin, *Virus membrane fusion*. FEBS Lett, 2007. **581**(11): p. 2150-5.
11. Chernomordik, L.V. and M.M. Kozlov, *Mechanics of membrane fusion*. Nat Struct Mol Biol, 2008. **15**(7): p. 675-83.

12. Otter-Nilsson, M., et al., *Cytosolic ATPases, p97 and NSF, are sufficient to mediate rapid membrane fusion*. EMBO J, 1999. **18**(8): p. 2074-83.
13. Chernomordik, L.V. and M.M. Kozlov, *Protein-lipid interplay in fusion and fission of biological membranes*. Annu Rev Biochem, 2003. **72**: p. 175-207.
14. Lentz, B.R., et al., *Protein machines and lipid assemblies: current views of cell membrane fusion*. Curr Opin Struct Biol, 2000. **10**(5): p. 607-15.
15. Chanturiya, A., L.V. Chernomordik, and J. Zimmerberg, *Flickering fusion pores comparable with initial exocytotic pores occur in protein-free phospholipid bilayers*. Proc Natl Acad Sci U S A, 1997. **94**(26): p. 14423-8.
16. Jahn, R., T. Lang, and T.C. Sudhof, *Membrane fusion*. Cell, 2003. **112**(4): p. 519-33.
17. Chernomordik, L.V., G.B. Melikyan, and Y.A. Chizmadzhev, *Biomembrane fusion: a new concept derived from model studies using two interacting planar lipid bilayers*. Biochim Biophys Acta, 1987. **906**(3): p. 309-52.
18. Kozlov, M.M. and V.S. Markin, [*Possible mechanism of membrane fusion*]. Biofizika, 1983. **28**(2): p. 242-7.
19. Blasi, J., et al., *BOTULINUM NEUROTOXIN-A SELECTIVELY CLEAVES THE SYNAPTIC PROTEIN SNAP-25*. Nature, 1993. **365**(6442): p. 160-163.
20. Blasi, J., et al., *BOTULINUM NEUROTOXIN-C1 BLOCKS NEUROTRANSMITTER RELEASE BY MEANS OF CLEAVING HPC-1/SYNTAXIN*. Embo Journal, 1993. **12**(12): p. 4821-4828.
21. Link, E., et al., *TETANUS TOXIN ACTION - INHIBITION OF NEUROTRANSMITTER RELEASE LINKED TO SYNAPTOBREVIN PROTEOLYSIS*. Biochemical and Biophysical Research Communications, 1992. **189**(2): p. 1017-1023.

22. Schiavo, G., et al., *TETANUS AND BOTULINUM-B NEUROTOXINS BLOCK NEUROTRANSMITTER RELEASE BY PROTEOLYTIC CLEAVAGE OF SYNAPTOBREVIN*. Nature, 1992. **359**(6398): p. 832-835.
23. Hanson, P.I., et al., *Structure and conformational changes in NSF and its membrane receptor complexes visualized by quick-freeze/deep-etch electron microscopy*. Cell, 1997. **90**(3): p. 523-535.
24. Poirier, M.A., et al., *The synaptic SNARE complex is a parallel four-stranded helical bundle*. Nature Structural Biology, 1998. **5**(9): p. 765-769.
25. Sollner, T., et al., *A PROTEIN ASSEMBLY-DISASSEMBLY PATHWAY IN-VITRO THAT MAY CORRESPOND TO SEQUENTIAL STEPS OF SYNAPTIC VESICLE DOCKING, ACTIVATION, AND FUSION*. Cell, 1993. **75**(3): p. 409-418.
26. Sutton, R.B., et al., *Crystal structure of a SNARE complex involved in synaptic exocytosis at 2.4 angstrom resolution*. Nature, 1998. **395**(6700): p. 347-353.
27. Sutton, R.B., et al., *Crystal structure of a SNARE complex involved in synaptic exocytosis at 2.4 A resolution*. Nature, 1998. **395**(6700): p. 347-53.
28. Fernandez, I., et al., *Three-dimensional structure of an evolutionarily conserved N-terminal domain of syntaxin 1A*. Cell, 1998. **94**(6): p. 841-9.
29. Burkhardt, P., et al., *Munc18a controls SNARE assembly through its interaction with the syntaxin N-peptide*. EMBO J, 2008. **27**(7): p. 923-33.
30. Fasshauer, D., et al., *Conserved structural features of the synaptic fusion complex: SNARE proteins reclassified as Q- and R-SNAREs*. Proceedings of the National Academy of Sciences of the United States of America, 1998. **95**(26): p. 15781-15786.
31. Antonin, W., et al., *Crystal structure of the endosomal SNARE complex reveals common structural principles of all SNAREs*. Nature Structural Biology, 2002. **9**(2): p. 107-111.

32. Sollner, T., et al., *SNAP RECEPTORS IMPLICATED IN VESICLE TARGETING AND FUSION*. Nature, 1993. **362**(6418): p. 318-324.
33. Weber, T., et al., *SNAREpins: minimal machinery for membrane fusion*. Cell, 1998. **92**(6): p. 759-72.
34. Rizo, J., X. Chen, and D. Arac, *Unraveling the mechanisms of synaptotagmin and SNARE function in neurotransmitter release*. Trends Cell Biol, 2006. **16**(7): p. 339-50.
35. Brunger, A.T., *Structure and function of SNARE and SNARE-interacting proteins*. Quarterly Reviews of Biophysics, 2005. **38**(1): p. 1-47.
36. Jahn, R., T. Lang, and T.C. Sudhof, *Membrane fusion*. Cell, 2003. **112**(4): p. 519-533.
37. Rizo, J., X.C. Chen, and D. Arac, *Unraveling the mechanisms of synaptotagmin and SNARE function in neurotransmitter release*. Trends in Cell Biology, 2006. **16**(7): p. 339-350.
38. Banerjee, A., et al., *N-ethylmaleimide-sensitive factor acts at a profusion ATP-dependent step in Ca<sup>2+</sup>-activated exocytosis*. Journal of Biological Chemistry, 1996. **271**(34): p. 20223-20226.
39. Mayer, A., W. Wickner, and A. Haas, *Sec18p (NSF)-driven release of sec17p (alpha-SNAP) can precede docking and fusion of yeast vacuoles*. Cell, 1996. **85**(1): p. 83-94.
40. Fernandez, I., et al., *Three-dimensional structure of an evolutionarily conserved N-terminal domain of syntaxin 1A*. Cell, 1998. **94**(6): p. 841-849.
41. Dulubova, I., et al., *A conformational switch in syntaxin during exocytosis: role of munc18*. Embo Journal, 1999. **18**(16): p. 4372-4382.
42. Misura, K.M.S., R.H. Scheller, and W.I. Weis, *Three-dimensional structure of the neuronal-Sec1-syntaxin 1a complex*. Nature, 2000. **404**(6776): p. 355-362.
43. Dulubova, I., et al., *How Tlg2p/syntaxin 16 'snares' Vps45*. Embo Journal, 2002. **21**(14): p. 3620-3631.

44. Dulubova, I., et al., *Vam3p structure reveals conserved and divergent properties of syntaxins*. Nature Structural Biology, 2001. **8**(3): p. 258-264.
45. Fiebig, K.M., et al., *Folding intermediates of SNARE complex assembly*. Nature Structural Biology, 1999. **6**(2): p. 117-123.
46. Nicholson, K.L., et al., *Regulation of SNARE complex assembly by an N-terminal domain of the t-SNARE Sso1p*. Nature Structural Biology, 1998. **5**(9): p. 793-802.
47. Yamaguchi, T., et al., *Sly1 binds to Golgi and ER syntaxins via a conserved N-terminal peptide motif*. Developmental Cell, 2002. **2**(3): p. 295-305.
48. Antonin, W., et al., *The N-terminal domains of syntaxin 7 and vti1b form three-helix bundles that differ in their ability to regulate SNARE complex assembly*. Journal of Biological Chemistry, 2002. **277**(39): p. 36449-36456.
49. Lu, J., et al., *Solution structure of the Vam7p PX domain*. Biochemistry, 2002. **41**(19): p. 5956-5962.
50. Tochio, H., et al., *An autoinhibitory mechanism for nonsyntaxin SNARE proteins revealed by the structure of Ykt6p*. Science, 2001. **293**(5530): p. 698-702.
51. Vivona, S., et al., *The Longin SNARE VAMP7/TI-VAMP Adopts a Closed Conformation*. Journal of Biological Chemistry, 2010. **285**(23): p. 17965-17973.
52. Bracher, A. and W. Weissenhorn, *Structural basis for the Golgi membrane recruitment of Sly1p by Sed5p*. Embo Journal, 2002. **21**(22): p. 6114-6124.
53. Dulubova, I., et al., *Munc18-1 binds directly to the neuronal SNARE complex*. Proceedings of the National Academy of Sciences of the United States of America, 2007. **104**(8): p. 2697-2702.

54. Hu, S.H., et al., *Structure of the Munc18c/Syntaxin4 N-peptide complex defines universal features of the N-peptide binding mode of Sec1/Munc18 proteins*. Proceedings of the National Academy of Sciences of the United States of America, 2007. **104**(21): p. 8773-8778.
55. Khvotchev, M., et al., *Dual modes of Munc18-1/SNARE interactions are coupled by functionally critical binding to syntaxin-1 n terminus*. Journal of Neuroscience, 2007. **27**(45): p. 12147-12155.
56. Latham, C.F., et al., *Molecular dissection of the Munc18c/syntaxin4 interaction: Implications for regulation of membrane trafficking*. Traffic, 2006. **7**(10): p. 1408-1419.
57. Shen, J.S., et al., *Selective activation of cognate SNAREpins by Sec1/Munc18 proteins*. Cell, 2007. **128**(1): p. 183-195.
58. Rizo, J. and T.C. Sudhof, *The Membrane Fusion Enigma: SNAREs, Sec1/Munc18 Proteins, and Their Accomplices-Guilty as Charged?* Annual Review of Cell and Developmental Biology, Vol 28, 2012. **28**: p. 279-308.
59. Fasshauer, D., et al., *Mixed and non-cognate SNARE complexes - Characterization of assembly and biophysical properties*. Journal of Biological Chemistry, 1999. **274**(22): p. 15440-15446.
60. Grosshans, B.L., D. Ortiz, and P. Novick, *Rabs and their effectors: Achieving specificity in membrane traffic*. Proceedings of the National Academy of Sciences of the United States of America, 2006. **103**(32): p. 11821-11827.
61. Yang, B., et al., *SNARE interactions are not selective - Implications for membrane fusion specificity*. Journal of Biological Chemistry, 1999. **274**(9): p. 5649-5653.
62. Misura, K.M.S., et al., *Crystal structure and biophysical properties of a complex between the N-terminal SNARE region of SNAP25 and syntaxin 1a*. Journal of Biological Chemistry, 2001. **276**(44): p. 41301-41309.

63. Misura, K.M.S., R.H. Scheller, and W.I. Weis, *Self-association of the H3 region of syntaxin 1A - Implications for intermediates in snare complex assembly*. Journal of Biological Chemistry, 2001. **276**(16): p. 13273-13282.
64. Xiao, W.Z., et al., *The neuronal t-SNARE complex is a parallel four-helix bundle*. Nature Structural Biology, 2001. **8**(4): p. 308-311.
65. Mima, J. and W. Wickner, *Phosphoinositides and SNARE chaperones synergistically assemble and remodel SNARE complexes for membrane fusion*. Proceedings of the National Academy of Sciences of the United States of America, 2009. **106**(38): p. 16191-16196.
66. Ma, C., et al., *Reconstitution of the vital functions of Munc18 and Munc13 in neurotransmitter release*. Science, 2013. **339**(6118): p. 421-5.
67. Zimmerberg, J. and L.V. Chernomordik, *Membrane fusion*. Advanced Drug Delivery Reviews, 1999. **38**(3): p. 197-205.
68. Markin, V.S. and J.P. Albanesi, *Membrane fusion: stalk model revisited*. Biophys J, 2002. **82**(2): p. 693-712.
69. Cohen, F.S. and G.B. Melikyan, *The energetics of membrane fusion from binding, through hemifusion, pore formation, and pore enlargement*. Journal of Membrane Biology, 2004. **199**(1): p. 1-14.
70. Li, F., et al., *Energetics and dynamics of SNAREpin folding across lipid bilayers*. Nature Structural & Molecular Biology, 2007. **14**(10): p. 890-896.
71. Liu, W., et al., *Single Molecule Measurements of Interaction Free Energies Between the Proteins Within Binary and Ternary SNARE Complexes*. J Nanoneurosci, 2009. **1**(2): p. 120-129.
72. Gao, Y., et al., *Single reconstituted neuronal SNARE complexes zipper in three distinct stages*. Science, 2012. **337**(6100): p. 1340-3.

73. Mohrmann, R., et al., *Fast Vesicle Fusion in Living Cells Requires at Least Three SNARE Complexes*. Science, 2010. **330**(6003): p. 502-505.
74. Sinha, R., et al., *Two synaptobrevin molecules are sufficient for vesicle fusion in central nervous system synapses*. Proceedings of the National Academy of Sciences of the United States of America, 2011. **108**(34): p. 14318-14323.
75. Hanson, P.I., J.E. Heuser, and R. Jahn, *Neurotransmitter release - four years of SNARE complexes*. Current Opinion in Neurobiology, 1997. **7**(3): p. 310-315.
76. Hanson, P.I., et al., *Structure and conformational changes in NSF and its membrane receptor complexes visualized by quick-freeze/deep-etch electron microscopy*. Cell, 1997. **90**(3): p. 523-35.
77. Stein, A., et al., *Helical extension of the neuronal SNARE complex into the membrane*. Nature, 2009. **460**(7254): p. 525-8.
78. Kim, C.S., D.H. Kweon, and Y.K. Shin, *Membrane topologies of neuronal SNARE folding intermediates*. Biochemistry, 2002. **41**(36): p. 10928-10933.
79. Carr, C.M. and J. Rizo, *At the junction of SNARE and SM protein function*. Current Opinion in Cell Biology, 2010. **22**(4): p. 488-495.
80. Sudhof, T.C. and J.E. Rothman, *Membrane Fusion: Grappling with SNARE and SM Proteins*. Science, 2009. **323**(5913): p. 474-477.
81. Toonen, R.F.G. and M. Verhage, *Munc18=1 in secretion: lonely Munc joins SNARE team and takes control*. Trends in Neurosciences, 2007. **30**(11): p. 564-572.
82. Verhage, M., et al., *Synaptic assembly of the brain in the absence of neurotransmitter secretion*. Science, 2000. **287**(5454): p. 864-869.

83. Hata, Y., C.A. Slaughter, and T.C. Sudhof, *SYNAPTIC VESICLE FUSION COMPLEX CONTAINS UNC-18 HOMOLOG BOUND TO SYNTAXIN*. *Nature*, 1993. **366**(6453): p. 347-351.
84. Carr, C.M., et al., *Sec1p binds to SNARE complexes and concentrates at sites of secretion*. *Journal of Cell Biology*, 1999. **146**(2): p. 333-344.
85. Carpp, L.N., et al., *The Sec1p/Munc18 protein Vps45p binds its cognate SNARE proteins via two distinct modes*. *Journal of Cell Biology*, 2006. **173**(6): p. 927-936.
86. Collins, K.M., et al., *Sec17p and HOPS, in distinct SNARE complexes, mediate SNARE complex disruption or assembly for fusion*. *Embo Journal*, 2005. **24**(10): p. 1775-1786.
87. Peng, R.W. and D. Gallwitz, *Sly1 protein bound to Golgi syntaxin Sed5p allows assembly and contributes to specificity of SNARE fusion complexes*. *Journal of Cell Biology*, 2002. **157**(4): p. 645-655.
88. Aravamudan, B., et al., *Drosophila Unc-13 is essential for synaptic transmission*. *Nature Neuroscience*, 1999. **2**(11): p. 965-971.
89. Augustin, I., et al., *Munc13-1 is essential for fusion competence of glutamatergic synaptic vesicles*. *Nature*, 1999. **400**(6743): p. 457-461.
90. Richmond, J.E., W.S. Davis, and E.M. Jorgensen, *UNC-13 is required for synaptic vesicle fusion in C-elegans*. *Nature Neuroscience*, 1999. **2**(11): p. 959-964.
91. Varoqueaux, F., et al., *Total arrest of spontaneous and evoked synaptic transmission but normal synaptogenesis in the absence of Munc13-mediated vesicle priming*. *Proceedings of the National Academy of Sciences of the United States of America*, 2002. **99**(13): p. 9037-9042.

92. Brose, N., et al., *MAMMALIAN HOMOLOGS OF CAENORHABDITIS-ELEGANS UNC-13 GENE DEFINE NOVEL FAMILY OF C-2-DOMAIN PROTEINS*. Journal of Biological Chemistry, 1995. **270**(42): p. 25273-25280.
93. Hammarlund, M., et al., *Open syntaxin docks synaptic vesicles*. Plos Biology, 2007. **5**(8): p. 1695-1711.
94. Siksou, L., et al., *A common molecular basis for membrane docking and functional priming of synaptic vesicles*. European Journal of Neuroscience, 2009. **30**(1): p. 49-56.
95. Weimer, R.M., et al., *UNC-13 and UNC-10/Rim localize synaptic vesicles to specific membrane domains*. Journal of Neuroscience, 2006. **26**(31): p. 8040-8047.
96. Lu, J., et al., *Structural basis for a Munc13-1 homodimer to Munc13-1/RIM heterodimer switch*. Plos Biology, 2006. **4**(7): p. 1159-1172.
97. Rizo, J. and T.C. Südhof, *C-2-domains, structure and function of a universal Ca<sup>2+</sup>-binding domain*. Journal of Biological Chemistry, 1998. **273**(26): p. 15879-15882.
98. Shin, O.H., et al., *Munc13 C2B domain is an activity-dependent Ca<sup>2+</sup> regulator of synaptic exocytosis*. Nature Structural & Molecular Biology, 2010. **17**(3): p. 280-U42.
99. Junge, H.J., et al., *Calmodulin and Munc13 form a Ca<sup>2+</sup> sensor/effector complex that controls short-term synaptic plasticity*. Cell, 2004. **118**(3): p. 389-401.
100. Basu, J., et al., *A minimal domain responsible for Munc13 activity*. Nature Structural & Molecular Biology, 2005. **12**(11): p. 1017-1018.
101. Madison, J.M., S. Nurrish, and J.M. Kaplan, *UNC-13 interaction with syntaxin is required for synaptic transmission*. Current Biology, 2005. **15**(24): p. 2236-2242.
102. Stevens, D.R., et al., *Identification of the minimal protein domain required for priming activity of Munc13-1*. Curr Biol, 2005. **15**(24): p. 2243-8.

103. Rosenmund, C., J. Rettig, and N. Brose, *Molecular mechanisms of active zone function*. *Curr Opin Neurobiol*, 2003. **13**(5): p. 509-19.
104. Basu, J., et al., *A minimal domain responsible for Munc13 activity*. *Nat Struct Mol Biol*, 2005. **12**(11): p. 1017-8.
105. Richmond, J.E., R.M. Weimer, and E.M. Jorgensen, *An open form of syntaxin bypasses the requirement for UNC-13 in vesicle priming*. *Nature*, 2001. **412**(6844): p. 338-341.
106. Gerber, S.H., et al., *Conformational switch of syntaxin-1 controls synaptic vesicle fusion*. *Science*, 2008. **321**(5895): p. 1507-10.
107. Li, W., et al., *The crystal structure of a Munc13 C-terminal module exhibits a remarkable similarity to vesicle tethering factors*. *Structure*, 2011. **19**(10): p. 1443-55.
108. Sivaram, M.V., et al., *The structure of the exocyst subunit Sec6p defines a conserved architecture with diverse roles*. *Nat Struct Mol Biol*, 2006. **13**(6): p. 555-6.
109. Shen, N., O. Guryev, and J. Rizo, *Intramolecular occlusion of the diacylglycerol-binding site in the C1 domain of munc13-1*. *Biochemistry*, 2005. **44**(4): p. 1089-96.
110. Shin, O.H., et al., *Munc13 C2B domain is an activity-dependent Ca<sup>2+</sup> regulator of synaptic exocytosis*. *Nat Struct Mol Biol*, 2010. **17**(3): p. 280-8.
111. Rodriguez-Castaneda, F., et al., *Modular architecture of Munc13/calmodulin complexes: dual regulation by Ca<sup>2+</sup> and possible function in short-term synaptic plasticity*. *EMBO J*, 2010. **29**(3): p. 680-91.
112. Lu, J., et al., *Structural basis for a Munc13-1 homodimer to Munc13-1/RIM heterodimer switch*. *PLoS Biol*, 2006. **4**(7): p. e192.
113. Guan, R., H. Dai, and J. Rizo, *Binding of the Munc13-1 MUN domain to membrane-anchored SNARE complexes*. *Biochemistry*, 2008. **47**(6): p. 1474-81.

114. Weninger, K., et al., *Accessory proteins stabilize the acceptor complex for synaptobrevin, the 1 : 1 syntaxin/SNAP-25 complex*. Structure, 2008. **16**(2): p. 308-320.
115. Ma, C., et al., *Munc13 mediates the transition from the closed syntaxin-Munc18 complex to the SNARE complex*. Nature Structural & Molecular Biology, 2011. **18**(5): p. 542-U206.
116. Ma, C., et al., *Munc13 mediates the transition from the closed syntaxin-Munc18 complex to the SNARE complex*. Nat Struct Mol Biol, 2011. **18**(5): p. 542-9.
117. Sabatini, B.L. and W.G. Regehr, *Timing of neurotransmission at fast synapses in the mammalian brain*. Nature, 1996. **384**(6605): p. 170-2.
118. Pang, Z.P. and T.C. Sudhof, *Cell biology of Ca<sup>2+</sup>-triggered exocytosis*. Curr Opin Cell Biol, 2010. **22**(4): p. 496-505.
119. Fatt, P. and B. Katz, *Spontaneous subthreshold activity at motor nerve endings*. J Physiol, 1952. **117**(1): p. 109-28.
120. Sudhof, T.C., *Calcium control of neurotransmitter release*. Cold Spring Harb Perspect Biol, 2012. **4**(1): p. a011353.
121. Geppert, M., et al., *Synaptotagmin I: a major Ca<sup>2+</sup> sensor for transmitter release at a central synapse*. Cell, 1994. **79**(4): p. 717-27.
122. Maximov, A., et al., *Genetic analysis of synaptotagmin-7 function in synaptic vesicle exocytosis*. Proc Natl Acad Sci U S A, 2008. **105**(10): p. 3986-91.
123. Xu, W., et al., *Distinct neuronal coding schemes in memory revealed by selective erasure of fast synchronous synaptic transmission*. Neuron, 2012. **73**(5): p. 990-1001.
124. Yoshihara, M. and J.T. Littleton, *Synaptotagmin I functions as a calcium sensor to synchronize neurotransmitter release*. Neuron, 2002. **36**(5): p. 897-908.

125. Matthew, W.D., L. Tsavaler, and L.F. Reichardt, *Identification of a synaptic vesicle-specific membrane protein with a wide distribution in neuronal and neurosecretory tissue*. J Cell Biol, 1981. **91**(1): p. 257-69.
126. Sudhof, T.C., *Synaptotagmins: why so many?* J Biol Chem, 2002. **277**(10): p. 7629-32.
127. Craxton, M., *Synaptotagmin gene content of the sequenced genomes*. BMC Genomics, 2004. **5**(1): p. 43.
128. Gustavsson, N. and W. Han, *Calcium-sensing beyond neurotransmitters: functions of synaptotagmins in neuroendocrine and endocrine secretion*. Biosci Rep, 2009. **29**(4): p. 245-59.
129. Shao, X., et al., *Solution structures of the Ca<sup>2+</sup>-free and Ca<sup>2+</sup>-bound C2A domain of synaptotagmin I: does Ca<sup>2+</sup> induce a conformational change?* Biochemistry, 1998. **37**(46): p. 16106-15.
130. Fernandez, I., et al., *Three-dimensional structure of the synaptotagmin 1 C2B-domain: synaptotagmin 1 as a phospholipid binding machine*. Neuron, 2001. **32**(6): p. 1057-69.
131. Dai, H., et al., *A quaternary SNARE-synaptotagmin-Ca<sup>2+</sup>-phospholipid complex in neurotransmitter release*. J Mol Biol, 2007. **367**(3): p. 848-63.
132. von Poser, C. and T.C. Sudhof, *Synaptotagmin 13: structure and expression of a novel synaptotagmin*. Eur J Cell Biol, 2001. **80**(1): p. 41-7.
133. von Poser, C., et al., *The evolutionary pressure to inactivate. A subclass of synaptotagmins with an amino acid substitution that abolishes Ca<sup>2+</sup> binding*. J Biol Chem, 1997. **272**(22): p. 14314-9.
134. Dai, H., et al., *Structural basis for the evolutionary inactivation of Ca<sup>2+</sup> binding to synaptotagmin 4*. Nat Struct Mol Biol, 2004. **11**(9): p. 844-9.

135. Fernandez-Chacon, R., et al., *Synaptotagmin I functions as a calcium regulator of release probability*. Nature, 2001. **410**(6824): p. 41-9.
136. Perin, M.S., et al., *Phospholipid binding by a synaptic vesicle protein homologous to the regulatory region of protein kinase C*. Nature, 1990. **345**(6272): p. 260-3.
137. Sugita, S., et al., *Synaptotagmins form a hierarchy of exocytotic Ca(2+) sensors with distinct Ca(2+) affinities*. EMBO J, 2002. **21**(3): p. 270-80.
138. Geppert, M., B.T. Archer, 3rd, and T.C. Sudhof, *Synaptotagmin II. A novel differentially distributed form of synaptotagmin*. J Biol Chem, 1991. **266**(21): p. 13548-52.
139. Li, C., et al., *Ca(2+)-dependent and -independent activities of neural and non-neural synaptotagmins*. Nature, 1995. **375**(6532): p. 594-9.
140. Li, C., B.A. Davletov, and T.C. Sudhof, *Distinct Ca<sup>2+</sup> and Sr<sup>2+</sup> binding properties of synaptotagmins. Definition of candidate Ca<sup>2+</sup> sensors for the fast and slow components of neurotransmitter release*. J Biol Chem, 1995. **270**(42): p. 24898-902.
141. Shin, O.H., et al., *Unexpected Ca<sup>2+</sup>-binding properties of synaptotagmin 9*. Proc Natl Acad Sci U S A, 2004. **101**(8): p. 2554-9.
142. Brose, N., et al., *Synaptotagmin: a calcium sensor on the synaptic vesicle surface*. Science, 1992. **256**(5059): p. 1021-5.
143. Littleton, J.T., et al., *Mutational analysis of Drosophila synaptotagmin demonstrates its essential role in Ca(2+)-activated neurotransmitter release*. Cell, 1993. **74**(6): p. 1125-34.
144. Pang, Z.P., et al., *Synaptotagmin-2 is essential for survival and contributes to Ca<sup>2+</sup> triggering of neurotransmitter release in central and neuromuscular synapses*. J Neurosci, 2006. **26**(52): p. 13493-504.
145. Sorensen, J.B., et al., *Examining synaptotagmin I function in dense core vesicle exocytosis under direct control of Ca<sup>2+</sup>*. J Gen Physiol, 2003. **122**(3): p. 265-76.

146. Sun, J., et al., *A dual-Ca<sup>2+</sup>-sensor model for neurotransmitter release in a central synapse*. Nature, 2007. **450**(7170): p. 676-82.
147. Andrews, N.W. and S. Chakrabarti, *There's more to life than neurotransmission: the regulation of exocytosis by synaptotagmin VII*. Trends Cell Biol, 2005. **15**(11): p. 626-31.
148. Cao, P., A. Maximov, and T.C. Sudhof, *Activity-dependent IGF-1 exocytosis is controlled by the Ca<sup>2+</sup>-sensor synaptotagmin-10*. Cell, 2011. **145**(2): p. 300-11.
149. Sudhof, T.C., *The synaptic vesicle cycle*. Annu Rev Neurosci, 2004. **27**: p. 509-47.
150. Butz, S., et al., *The subcellular localizations of atypical synaptotagmins III and VI. Synaptotagmin III is enriched in synapses and synaptic plasma membranes but not in synaptic vesicles*. J Biol Chem, 1999. **274**(26): p. 18290-6.
151. Davletov, B.A. and T.C. Sudhof, *A single C2 domain from synaptotagmin I is sufficient for high affinity Ca<sup>2+</sup>/phospholipid binding*. J Biol Chem, 1993. **268**(35): p. 26386-90.
152. Bennett, M.K., N. Calakos, and R.H. Scheller, *Syntaxin: a synaptic protein implicated in docking of synaptic vesicles at presynaptic active zones*. Science, 1992. **257**(5067): p. 255-9.
153. Chapman, E.R., et al., *Ca<sup>2+</sup> regulates the interaction between synaptotagmin and syntaxin I*. J Biol Chem, 1995. **270**(40): p. 23667-71.
154. Pang, Z.P., et al., *A gain-of-function mutation in synaptotagmin-1 reveals a critical role of Ca<sup>2+</sup>-dependent soluble N-ethylmaleimide-sensitive factor attachment protein receptor complex binding in synaptic exocytosis*. J Neurosci, 2006. **26**(48): p. 12556-65.
155. Bollmann, J.H. and B. Sakmann, *Control of synaptic strength and timing by the release-site Ca<sup>2+</sup> signal*. Nat Neurosci, 2005. **8**(4): p. 426-34.
156. Schneggenburger, R. and E. Neher, *Intracellular calcium dependence of transmitter release rates at a fast central synapse*. Nature, 2000. **406**(6798): p. 889-93.

157. Meinrenken, C.J., J.G. Borst, and B. Sakmann, *Local routes revisited: the space and time dependence of the Ca<sup>2+</sup> signal for phasic transmitter release at the rat calyx of Held*. *J Physiol*, 2003. **547**(Pt 3): p. 665-89.
158. Bollmann, J.H., B. Sakmann, and J.G. Borst, *Calcium sensitivity of glutamate release in a calyx-type terminal*. *Science*, 2000. **289**(5481): p. 953-7.
159. Sutton, R.B., J.A. Ernst, and A.T. Brunger, *Crystal structure of the cytosolic C2A-C2B domains of synaptotagmin III. Implications for Ca(+2)-independent snare complex interaction*. *J Cell Biol*, 1999. **147**(3): p. 589-98.
160. Hui, E., et al., *Three distinct kinetic groupings of the synaptotagmin family: candidate sensors for rapid and delayed exocytosis*. *Proc Natl Acad Sci U S A*, 2005. **102**(14): p. 5210-4.
161. Maximov, A., et al., *Synaptotagmin-12, a synaptic vesicle phosphoprotein that modulates spontaneous neurotransmitter release*. *J Cell Biol*, 2007. **176**(1): p. 113-24.
162. McMahon, H.T., et al., *Complexins: cytosolic proteins that regulate SNAP receptor function*. *Cell*, 1995. **83**(1): p. 111-9.
163. Pabst, S., et al., *Selective interaction of complexin with the neuronal SNARE complex. Determination of the binding regions*. *J Biol Chem*, 2000. **275**(26): p. 19808-18.
164. Chen, X., et al., *Three-dimensional structure of the complexin/SNARE complex*. *Neuron*, 2002. **33**(3): p. 397-409.
165. Reim, K., et al., *Structurally and functionally unique complexins at retinal ribbon synapses*. *J Cell Biol*, 2005. **169**(4): p. 669-80.
166. Reim, K., et al., *Complexins regulate a late step in Ca<sup>2+</sup>-dependent neurotransmitter release*. *Cell*, 2001. **104**(1): p. 71-81.

167. Maximov, A., et al., *Complexin controls the force transfer from SNARE complexes to membranes in fusion*. Science, 2009. **323**(5913): p. 516-21.
168. Yang, X., et al., *Complexin clamps asynchronous release by blocking a secondary Ca(2+) sensor via its accessory alpha helix*. Neuron, 2010. **68**(5): p. 907-20.
169. Xue, M., et al., *Distinct domains of complexin I differentially regulate neurotransmitter release*. Nat Struct Mol Biol, 2007. **14**(10): p. 949-58.
170. Zimmerberg, J., S.S. Vogel, and L.V. Chernomordik, *Mechanisms of membrane fusion*. Annu Rev Biophys Biomol Struct, 1993. **22**: p. 433-66.
171. Cohen, F.S. and G.B. Melikyan, *The energetics of membrane fusion from binding, through hemifusion, pore formation, and pore enlargement*. J Membr Biol, 2004. **199**(1): p. 1-14.
172. Harrison, S.C., *Viral membrane fusion*. Nat Struct Mol Biol, 2008. **15**(7): p. 690-8.
173. Wickner, W. and R. Schekman, *Membrane fusion*. Nat Struct Mol Biol, 2008. **15**(7): p. 658-64.
174. Rizo, J. and C. Rosenmund, *Synaptic vesicle fusion*. Nat Struct Mol Biol, 2008. **15**(7): p. 665-74.
175. Carr, C.M. and J. Rizo, *At the junction of SNARE and SM protein function*. Curr Opin Cell Biol, 2010. **22**(4): p. 488-95.
176. Pei, J., et al., *Remote homology between Munc13 MUN domain and vesicle tethering complexes*. J Mol Biol, 2009. **391**(3): p. 509-17.
177. Poirier, M.A., et al., *The synaptic SNARE complex is a parallel four-stranded helical bundle*. Nat Struct Biol, 1998. **5**(9): p. 765-9.
178. van den Bogaart, G., et al., *One SNARE complex is sufficient for membrane fusion*. Nat Struct Mol Biol, 2010. **17**(3): p. 358-64.

179. Chen, X., et al., *SNARE-mediated lipid mixing depends on the physical state of the vesicles*. Biophys J, 2006. **90**(6): p. 2062-74.
180. Bowen, M.E., et al., *Single molecule observation of liposome-bilayer fusion thermally induced by soluble N-ethyl maleimide sensitive-factor attachment protein receptors (SNAREs)*. Biophys J, 2004. **87**(5): p. 3569-84.
181. Dennison, S.M., et al., *Neuronal SNAREs do not trigger fusion between synthetic membranes but do promote PEG-mediated membrane fusion*. Biophys J, 2006. **90**(5): p. 1661-75.
182. Hu, K., et al., *Vesicular restriction of synaptobrevin suggests a role for calcium in membrane fusion*. Nature, 2002. **415**(6872): p. 646-50.
183. Ji, H., et al., *Protein determinants of SNARE-mediated lipid mixing*. Biophys J, 2010. **99**(2): p. 553-60.
184. Kweon, D.H., C.S. Kim, and Y.K. Shin, *Regulation of neuronal SNARE assembly by the membrane*. Nat Struct Biol, 2003. **10**(6): p. 440-7.
185. Liu, T., et al., *SNARE-driven, 25-millisecond vesicle fusion in vitro*. Biophys J, 2005. **89**(4): p. 2458-72.
186. Sudhof, T.C. and J.E. Rothman, *Membrane fusion: grappling with SNARE and SM proteins*. Science, 2009. **323**(5913): p. 474-7.
187. Toonen, R.F. and M. Verhage, *Munc18-1 in secretion: lonely Munc joins SNARE team and takes control*. Trends Neurosci, 2007. **30**(11): p. 564-72.
188. Verhage, M., et al., *Synaptic assembly of the brain in the absence of neurotransmitter secretion*. Science, 2000. **287**(5454): p. 864-9.
189. Misura, K.M., R.H. Scheller, and W.I. Weis, *Three-dimensional structure of the neuronal-Sec1-syntaxin 1a complex*. Nature, 2000. **404**(6776): p. 355-62.

190. Dulubova, I., et al., *A conformational switch in syntaxin during exocytosis: role of munc18*. EMBO J, 1999. **18**(16): p. 4372-82.
191. Chen, X., et al., *NMR analysis of the closed conformation of syntaxin-1*. J Biomol NMR, 2008. **41**(1): p. 43-54.
192. Shen, J., et al., *Selective activation of cognate SNAREpins by Sec1/Munc18 proteins*. Cell, 2007. **128**(1): p. 183-95.
193. Dulubova, I., et al., *Munc18-1 binds directly to the neuronal SNARE complex*. Proc Natl Acad Sci U S A, 2007. **104**(8): p. 2697-702.
194. Khvotchev, M., et al., *Dual modes of Munc18-1/SNARE interactions are coupled by functionally critical binding to syntaxin-1 N terminus*. J Neurosci, 2007. **27**(45): p. 12147-55.
195. Deak, F., et al., *Munc18-1 binding to the neuronal SNARE complex controls synaptic vesicle priming*. J Cell Biol, 2009. **184**(5): p. 751-64.
196. Rodkey, T.L., et al., *Munc18a scaffolds SNARE assembly to promote membrane fusion*. Mol Biol Cell, 2008. **19**(12): p. 5422-34.
197. Tareste, D., et al., *SNAREpin/Munc18 promotes adhesion and fusion of large vesicles to giant membranes*. Proc Natl Acad Sci U S A, 2008. **105**(7): p. 2380-5.
198. Diao, J., et al., *Single-Vesicle Fusion Assay Reveals Munc18-1 Binding to the SNARE Core Is Sufficient for Stimulating Membrane Fusion*. ACS Chem Neurosci, 2010. **1**(3): p. 168-174.
199. Rathore, S.S., et al., *Syntaxin N-terminal peptide motif is an initiation factor for the assembly of the SNARE-Sec1/Munc18 membrane fusion complex*. Proc Natl Acad Sci U S A, 2010. **107**(52): p. 22399-406.
200. Xu, Y., L. Su, and J. Rizo, *Binding of Munc18-1 to synaptobrevin and to the SNARE four-helix bundle*. Biochemistry, 2010. **49**(8): p. 1568-76.

201. Rigaud, J.L., B. Pitard, and D. Levy, *Reconstitution of membrane proteins into liposomes: application to energy-transducing membrane proteins*. *Biochim Biophys Acta*, 1995. **1231**(3): p. 223-46.
202. Arac, D., et al., *Close membrane-membrane proximity induced by Ca(2+)-dependent multivalent binding of synaptotagmin-1 to phospholipids*. *Nat Struct Mol Biol*, 2006. **13**(3): p. 209-17.
203. Arac, D., T. Murphy, and J. Rizo, *Facile detection of protein-protein interactions by one-dimensional NMR spectroscopy*. *Biochemistry*, 2003. **42**(10): p. 2774-80.
204. Bracher, A. and W. Weissenhorn, *Crystal structures of neuronal squid Sec1 implicate inter-domain hinge movement in the release of t-SNAREs*. *J Mol Biol*, 2001. **306**(1): p. 7-13.
205. Kim, J. and H. Kim, *Fusion of phospholipid vesicles induced by alpha-lactalbumin at acidic pH*. *Biochemistry*, 1986. **25**(24): p. 7867-74.
206. Grote, E., C.M. Carr, and P.J. Novick, *Ordering the final events in yeast exocytosis*. *J Cell Biol*, 2000. **151**(2): p. 439-52.
207. Takamori, S., et al., *Molecular anatomy of a trafficking organelle*. *Cell*, 2006. **127**(4): p. 831-46.
208. Wang, L., et al., *Vacuole fusion at a ring of vertex docking sites leaves membrane fragments within the organelle*. *Cell*, 2002. **108**(3): p. 357-69.
209. Chan, Y.H., B. van Lengerich, and S.G. Boxer, *Effects of linker sequences on vesicle fusion mediated by lipid-anchored DNA oligonucleotides*. *Proc Natl Acad Sci U S A*, 2009. **106**(4): p. 979-84.
210. Delaglio, F., et al., *NMRPipe: a multidimensional spectral processing system based on UNIX pipes*. *J Biomol NMR*, 1995. **6**(3): p. 277-93.

211. Johnson, B.A. and R.A. Blevins, *NMR View: A computer program for the visualization and analysis of NMR data*. J Biomol NMR, 1994. **4**(5): p. 603-14.
212. Rizo, J. and T.C. Sudhof, *The membrane fusion enigma: SNAREs, Sec1/Munc18 proteins, and their accomplices--guilty as charged?* Annu Rev Cell Dev Biol, 2012. **28**: p. 279-308.
213. Brunger, A.T., et al., *Single-molecule studies of the neuronal SNARE fusion machinery*. Annu Rev Biochem, 2009. **78**: p. 903-28.
214. Chapman, E.R., *How does synaptotagmin trigger neurotransmitter release?* Annu Rev Biochem, 2008. **77**: p. 615-41.
215. Jahn, R. and D. Fasshauer, *Molecular machines governing exocytosis of synaptic vesicles*. Nature, 2012. **490**(7419): p. 201-7.
216. Sutton, R.B., et al., *Structure of the first C2 domain of synaptotagmin I: a novel Ca<sup>2+</sup>/phospholipid-binding fold*. Cell, 1995. **80**(6): p. 929-38.
217. Ubach, J., et al., *Ca<sup>2+</sup> binding to synaptotagmin: how many Ca<sup>2+</sup> ions bind to the tip of a C2-domain?* EMBO J, 1998. **17**(14): p. 3921-30.
218. Xue, M., et al., *The Janus-faced nature of the C(2)B domain is fundamental for synaptotagmin-1 function*. Nat Struct Mol Biol, 2008. **15**(11): p. 1160-8.
219. Bhalla, A., et al., *Ca(2+)-synaptotagmin directly regulates t-SNARE function during reconstituted membrane fusion*. Nat Struct Mol Biol, 2006. **13**(4): p. 323-30.
220. Rhee, J.S., et al., *Augmenting neurotransmitter release by enhancing the apparent Ca<sup>2+</sup> affinity of synaptotagmin I*. Proc Natl Acad Sci U S A, 2005. **102**(51): p. 18664-9.
221. Giraudo, C.G., et al., *A clamping mechanism involved in SNARE-dependent exocytosis*. Science, 2006. **313**(5787): p. 676-80.
222. Schaub, J.R., et al., *Hemifusion arrest by complexin is relieved by Ca<sup>2+</sup>-synaptotagmin I*. Nat Struct Mol Biol, 2006. **13**(8): p. 748-50.

223. Tang, J., et al., *A complexin/synaptotagmin I switch controls fast synaptic vesicle exocytosis*. Cell, 2006. **126**(6): p. 1175-87.
224. Parisotto, D., et al., *SNAREpin assembly by Munc18-1 requires previous vesicle docking by synaptotagmin I*. J Biol Chem, 2012. **287**(37): p. 31041-9.
225. Damer, C.K. and C.E. Creutz, *Synergistic membrane interactions of the two C2 domains of synaptotagmin*. J Biol Chem, 1994. **269**(49): p. 31115-23.
226. Diao, J., et al., *C2AB: a molecular glue for lipid vesicles with a negatively charged surface*. Langmuir, 2009. **25**(13): p. 7177-80.
227. Vennekate, W., et al., *Cis- and trans-membrane interactions of synaptotagmin-1*. Proc Natl Acad Sci U S A, 2012. **109**(27): p. 11037-42.
228. Park, Y., et al., *Controlling synaptotagmin activity by electrostatic screening*. Nat Struct Mol Biol, 2012. **19**(10): p. 991-7.
229. Connell, E., et al., *Cross-linking of phospholipid membranes is a conserved property of calcium-sensitive synaptotagmins*. J Mol Biol, 2008. **380**(1): p. 42-50.
230. Hui, E., et al., *Mechanism and function of synaptotagmin-mediated membrane apposition*. Nat Struct Mol Biol, 2011. **18**(7): p. 813-21.
231. Herrick, D.Z., et al., *Solution and membrane-bound conformations of the tandem C2A and C2B domains of synaptotagmin I: Evidence for bilayer bridging*. J Mol Biol, 2009. **390**(5): p. 913-23.
232. Diao, J., et al., *Synaptic proteins promote calcium-triggered fast transition from point contact to full fusion*. Elife, 2012. **1**: p. e00109.
233. van den Bogaart, G., et al., *Synaptotagmin-1 may be a distance regulator acting upstream of SNARE nucleation*. Nat Struct Mol Biol, 2011. **18**(7): p. 805-12.

234. Ubach, J., et al., *The C2B domain of synaptotagmin I is a Ca<sup>2+</sup>-binding module*. *Biochemistry*, 2001. **40**(20): p. 5854-60.
235. Zhou, A., K.D. Brewer, and J. Rizo, *Analysis of SNARE complex/synaptotagmin-I interactions by one-dimensional NMR spectroscopy*. *Biochemistry*, 2013. **52**(20): p. 3446-56.
236. Sun, J. and H. Li, *How to operate a cryo-electron microscope*. *Methods Enzymol*, 2010. **481**: p. 231-49.
237. Crowley, K.S., G.D. Reinhart, and A.E. Johnson, *The signal sequence moves through a ribosomal tunnel into a noncytoplasmic aqueous environment at the ER membrane early in translocation*. *Cell*, 1993. **73**(6): p. 1101-15.
238. Zhang, X., J. Rizo, and T.C. Sudhof, *Mechanism of phospholipid binding by the C2A-domain of synaptotagmin I*. *Biochemistry*, 1998. **37**(36): p. 12395-403.
239. Chapman, E.R. and A.F. Davis, *Direct interaction of a Ca<sup>2+</sup>-binding loop of synaptotagmin with lipid bilayers*. *J Biol Chem*, 1998. **273**(22): p. 13995-4001.
240. Wu, Y., et al., *Visualization of synaptotagmin I oligomers assembled onto lipid monolayers*. *Proc Natl Acad Sci U S A*, 2003. **100**(4): p. 2082-7.
241. Denisov, I.G., et al., *Directed self-assembly of monodisperse phospholipid bilayer Nanodiscs with controlled size*. *J Am Chem Soc*, 2004. **126**(11): p. 3477-87.
242. Ruschak, A.M. and L.E. Kay, *Methyl groups as probes of supra-molecular structure, dynamics and function*. *J Biomol NMR*, 2010. **46**(1): p. 75-87.
243. Battiste, J.L. and G. Wagner, *Utilization of site-directed spin labeling and high-resolution heteronuclear nuclear magnetic resonance for global fold determination of large proteins with limited nuclear overhauser effect data*. *Biochemistry*, 2000. **39**(18): p. 5355-65.

244. Clore, G.M. and J. Iwahara, *Theory, practice, and applications of paramagnetic relaxation enhancement for the characterization of transient low-population states of biological macromolecules and their complexes*. Chem Rev, 2009. **109**(9): p. 4108-39.
245. Choi, U.B., et al., *Single-molecule FRET-derived model of the synaptotagmin I-SNARE fusion complex*. Nat Struct Mol Biol, 2010. **17**(3): p. 318-24.
246. Vrljic, M., et al., *Molecular mechanism of the synaptotagmin-SNARE interaction in Ca<sup>2+</sup>-triggered vesicle fusion*. Nat Struct Mol Biol, 2010. **17**(3): p. 325-31.
247. Chicka, M.C., et al., *Synaptotagmin arrests the SNARE complex before triggering fast, efficient membrane fusion in response to Ca<sup>2+</sup>*. Nat Struct Mol Biol, 2008. **15**(8): p. 827-35.
248. Honigsmann, A., et al., *Phosphatidylinositol 4,5-bisphosphate clusters act as molecular beacons for vesicle recruitment*. Nat Struct Mol Biol, 2013. **20**(6): p. 679-86.
249. Wang, P., et al., *Mutations in the effector binding loops in the C2A and C2B domains of synaptotagmin I disrupt exocytosis in a nonadditive manner*. J Biol Chem, 2003. **278**(47): p. 47030-7.
250. Banerjee, S., T. Huber, and T.P. Sakmar, *Rapid incorporation of functional rhodopsin into nanoscale apolipoprotein bound bilayer (NABB) particles*. J Mol Biol, 2008. **377**(4): p. 1067-81.
251. Brewer, K.D., et al., *Reluctance to membrane binding enables accessibility of the synaptobrevin SNARE motif for SNARE complex formation*. Proc Natl Acad Sci U S A, 2011. **108**(31): p. 12723-8.
252. Augustin, I., et al., *Munc13-1 is essential for fusion competence of glutamatergic synaptic vesicles*. Nature, 1999. **400**(6743): p. 457-61.

253. Rodriguez-Castaneda, F., et al., *Modular architecture of Munc13/calmodulin complexes: dual regulation by Ca<sup>2+</sup> and possible function in short-term synaptic plasticity*. *Embo Journal*, 2010. **29**(3): p. 680-691.
254. Shin, O.H., et al., *Differential but convergent functions of Ca<sup>2+</sup> binding to synaptotagmin-1 C2 domains mediate neurotransmitter release*. *Proc Natl Acad Sci U S A*, 2009. **106**(38): p. 16469-74.
255. Boswell, K.L., et al., *Munc13-4 reconstitutes calcium-dependent SNARE-mediated membrane fusion*. *J Cell Biol*, 2012. **197**(2): p. 301-12.
256. Rhee, J.S., et al., *Beta phorbol ester- and diacylglycerol-induced augmentation of transmitter release is mediated by Munc13s and not by PKCs*. *Cell*, 2002. **108**(1): p. 121-33.
257. Kabachinski, G., et al., *CAPS and Munc13 utilize distinct PIP2-linked mechanisms to promote vesicle exocytosis*. *Mol Biol Cell*, 2014. **25**(4): p. 508-21.
258. Hernandez, J.M., et al., *Membrane fusion intermediates via directional and full assembly of the SNARE complex*. *Science*, 2012. **336**(6088): p. 1581-4.
259. Pei, J.M., et al., *Remote Homology between Munc13 MUN Domain and Vesicle Tethering Complexes*. *Journal of Molecular Biology*, 2009. **391**(3): p. 509-517.
260. Li, W., et al., *The Crystal Structure of a Munc13 C-terminal Module Exhibits a Remarkable Similarity to Vesicle Tethering Factors*. *Structure*, 2011. **19**(10): p. 1443-1455.
261. Bacaj, T., et al., *Synaptotagmin-1 and synaptotagmin-7 trigger synchronous and asynchronous phases of neurotransmitter release*. *Neuron*, 2013. **80**(4): p. 947-59.
262. Kyoung, M., et al., *In vitro system capable of differentiating fast Ca<sup>2+</sup>-triggered content mixing from lipid exchange for mechanistic studies of neurotransmitter release*. *Proc Natl Acad Sci U S A*, 2011. **108**(29): p. E304-13.

263. van den Bogaart, G., et al., *Synaptotagmin-1 may be a distance regulator acting upstream of SNARE nucleation*. Nat Struct Mol Biol, 2011. **18**(7): p. 805-812.